NAVAL POSTGRADUATE SCHOOL

MONTEREY, CALIFORNIA

DISSERTATION

ADAPTIVE RECEPTION FOR UNDERWATER COMMUNICATIONS

by

Spyridon Dessalermos

June 2011

Dissertation Supervisor: Roberto Cristi

Approved for public release; distribution is unlimited

THIS PAGE INTENTIONALLY LEFT BLANK

REPORT DOCUMENTATION PAGE			Form Approved OMB No. 0704-0188
Public reporting burden for this collection of information is estimated to average 1 hour per response, including the time for reviewing instruction, searching existing data sources, gathering and maintaining the data needed, and completing and reviewing the collection of information. Send comments regarding this burden estimate or any other aspect of this collection of information, including suggestions for reducing this burden, to Washington headquarters Services, Directorate for Information Operations and Reports, 1215 Jefferson Davis Highway, Suite 1204, Arlington, VA 22202-4302, and to the Office of Management and Budget, Paperwork Reduction Project (0704-0188) Washington DC 20503.			
1. AGENCY USE ONLY ***(Leave blank)***	**2. REPORT DATE** June 2011	**3. REPORT TYPE AND DATES COVERED** Dissertation	
4. TITLE AND SUBTITLE: Adaptive Reception for Underwater Communications		**5. FUNDING NUMBERS**	
6. AUTHOR(S): Spyridon Dessalermos			
7. PERFORMING ORGANIZATION NAME(S) AND ADDRESS(ES) Naval Postgraduate School Monterey, CA 93943-5000		**8. PERFORMING ORGANIZATION REPORT NUMBER**	
9. SPONSORING / MONITORING AGENCY NAME(S) AND ADDRESS(ES) N/A		**10. SPONSORING / MONITORING AGENCY REPORT NUMBER**	
11. SUPPLEMENTARY NOTES The views expressed in this thesis are those of the author and do not reflect the official policy or position of the Department of Defense or the U.S. Government. IRB Protocol number N/A.			
12a. DISTRIBUTION / AVAILABILITY STATEMENT Approved for public release; distribution is unlimited		**12b. DISTRIBUTION CODE** A	

13. ABSTRACT

This research concerns the development of an adaptive receiver for underwater communication. In this type of wireless link, the radio channel is replaced by an underwater acoustic channel, which is strongly dependent on the physical properties of the ocean medium and its boundaries, the link geometry and the ambient noise. Traditional acoustic communications have involved a priori matching of the signaling parameters to the expected characteristics of the channel. To achieve more robust communications, as well as high quality of service, it is necessary to develop a type of adaptive receiver for the acoustic link. This process involves estimating the channel scattering function by processing the received Direct Sequence Spread Spectrum (DSSS) acoustic signal. This information is used by an innovative receiver introduced for usage in the underwater environment. The research also involves the development of a robust acquisition system for the acoustic communication signal. The major design goal is the receiver's robustness on a Doppler distorted fast varying multipath fading channel, for applications in multiuser environments. Another important design goal is low complexity in signal processing. The proposed receiver is able to adapt in the acoustic channel variations. Experimental results prove the effectiveness of the receiver.

14. SUBJECT TERMS Underwater acoustic communications, adaptive algorithms, Kalman filter, spatial processing, signal acquisition, channel identification, Doppler correction, interference cancelation			**15. NUMBER OF PAGES** 186 **16. PRICE CODE**
17. SECURITY CLASSIFICATION OF REPORT Unclassified	**18. SECURITY CLASSIFICATION OF THIS PAGE** Unclassified	**19. SECURITY CLASSIFICATION OF ABSTRACT** Unclassified	**20. LIMITATION OF ABSTRACT** UU

NSN 7540-01-280-5500 Standard Form 298 (Rev. 2-89)
Prescribed by ANSI Std. 239-18

THIS PAGE INTENTIONALLY LEFT BLANK

Approved for public release; distribution is unlimited

ADAPTIVE RECEPTION FOR UNDERWATER COMMUNICATIONS

Spyridon Dessalermos
Lieutenant, Hellenic Navy
B.S., Hellenic Naval Academy, 1998
M.S., Naval Postgraduate School, 2005

Submitted in partial fulfillment of the
requirements for the degree of

DOCTOR OF PHILOSOPHY IN ENGINEERING ACOUSTICS

from the
NAVAL POSTGRADUATE SCHOOL
June 2011

Author: _____
Spyridon Dessalermos

Approved by:

_____ Roberto Cristi, Professor of Electrical and Computer Engineering Dissertation Supervisor and Committee Chairman	_____ Murali Tummala, Professor of Electrical and Computer Engineering
_____ Kevin B. Smith, Professor of Physics	_____ Steven R. Baker, Professor of Physics
_____ John G. Proakis, Professor of Electrical and Computer Engineering Northeastern University, Boston, MA	_____ Joseph Rice, Research Professor of Physics

Approved by: _____
Andres Larraza, Chair, Department of Physics

Approved by: _____
R. Clark Robertson, Chair, Department of
Electrical and Computer Engineering

Approved by: _____
Douglas Moses, Vice Provost for Academic Affairs

THIS PAGE INTENTIONALLY LEFT BLANK

ABSTRACT

This research concerns the development of an adaptive receiver for underwater communication. In this type of wireless link, the radio channel is replaced by an underwater acoustic channel, which is strongly dependent on the physical properties of the ocean medium and its boundaries, the link geometry and the ambient noise. Traditional acoustic communications have involved a priori matching of the signaling parameters to the expected characteristics of the channel. To achieve more robust communications, as well as high quality of service, it is necessary to develop a type of adaptive receiver for the acoustic link. This process involves estimating the channel scattering function by processing the received Direct Sequence Spread Spectrum (DSSS) acoustic signal. This information is used by an innovative receiver introduced for usage in the underwater environment. The research also involves the development of a robust acquisition system for the acoustic communication signal. The major design goal is the receiver's robustness on a Doppler distorted fast varying multipath fading channel, for applications in multiuser environments. Another important design goal is low complexity in signal processing. The proposed receiver is able to adapt in the acoustic channel variations. Experimental results prove the effectiveness of the receiver.

THIS PAGE INTENTIONALLY LEFT BLANK

TABLE OF CONTENTS

THIS PAGE INTENTIONALLY LEFT BLANK

LIST OF FIGURES

LIST OF TABLES

THIS PAGE INTENTIONALLY LEFT BLANK

LIST OF ACRONYMS AND ABBREVIATIONS

AUV	Autonomous Underwater Vehicles
AWGN	Additive White Gaussian Noise
BER	Bit Error Rate
BPSK	Binary Phase Shift Keying
BW	Bandwidth
CDMA	Code Division Multiple Access
DATS	Digital Acoustic Telemetry System
DFE	Decision Feedback Equalizer
DFT	Discrete Fourier Transform
DPSK	Differential Phase Shift Keying
DS	Direct Sequence
DS/CDMA	Direct Sequence Code Division Multiple Access
DSSS	Direct Sequence Spread Spectrum
FIR	Finite Impulse Response
FSK	Frequency Shift Keying
ISI	Inter-Symbol Interference
ISO/OSI	International Standards Organization's Open System Interconnection
LMS	Least Mean Squares
MC	Multi-Carrier
MFSK	Multitone Frequency Shift Keying
MI/DFE	Multiple Input Decision Feedback Equalizer MIMO Multiple Input Multiple Output

MIP	Multipath Intensity Profile
MMSE	Minimum Mean Squared Error
MSE	Mean Squared Error
MSK	Minimum Shift Keying
NC	Noncoherent
OFDM	Orthogonal Frequency Division Multiplexing
OOK	On Off Keying
PLL	Phase Locked Loop
PN	Pseudonoise
PSK	Phase Shift Keying
QAM	Quadrature Amplitude Modulation
QDPSK	Quadrature Differential Phase Shift Keying
QPSK	Quadrature Phase Shift Keying
RBF	Radial Basis Function
RLS	Recursive Least Squares
SIMO	Single Input Multiple Output
SINR	Signal to Interference and Noise Ratio
SISO	Single Input Single Output
SNR	Signal to Noise Ratio
SVD	Singular Value Decomposition
TL	Transmission Loss
UUV	Unmanned Underwater Vehicle
WHOI	Woods Hole Oceanographic Institution
WSSUS	Wide Sense Stationarity and Uncorrelated Scattering

EXECUTIVE SUMMARY

Underwater communication is vital for a number of military and commercial applications. The central idea for military applications is to develop wireless networks covering wide areas of littoral waters, extending net-centric operations to the underwater environment. Acoustic pressure waves provide the only option for communications through water across useful distances.

The underwater acoustic environment is a particularly challenging communications medium. In order to effectively design underwater communications systems, it is necessary to have a deep understanding of the nature of the physical barriers constraining performance in the underwater channel.

This dissertation addresses the problem of designing a robust and reliable coherent receiver which will be able to operate in a multiuser environment. The proposed scheme is based on Direct Sequence Spread Spectrum (DSSS) modulation. The DSSS signal can also be used for channel identification, which is a vital task for estimating the time-varying characteristics of the communication medium and adjusting the receiver parameters for optimum detection.

The developed receiver is based on an array of hydrophones, thus exploiting the advantages of spatial diversity. The signals received from the hydrophones are processed in such a way that the principal multipath arrival is amplified, whereas environmental noise and weaker multipath arrivals are suppressed. The spatial combiner is designed based on array processing theory and processes the received signals before equalization.

The receiver includes a dual input equalizer based on a Kalman filter estimator, which has a relatively low computational complexity. With multiple receivers, the transmitted signal can be viewed as the state of a dynamic system with the received signals as inputs and outputs. As a consequence, a Kalman estimator can be used. Furthermore, in order to ensure the reliability of the

equalizer, a method was developed for choosing the multipath components to be used as inputs of the equalizer based on the channel consistency of those components. Additionally, an adaptive mechanism is developed on the equalizer in order to track the channel changes and ensure the filter's convergence. Incorporated into the equalizer is also an algorithm for dynamically tracking and correcting the Doppler shift on each of the multipath arrivals. Since the Doppler shift is strongly time-varying, dynamically tracking it and correcting it for best performance of the acoustic receiver is crucial.

Finally, an external interference and noise canceller mechanism was developed, intended for use in the multiuser underwater environment. The outcome of this dissertation is a robust receiver able to operate in a fast time-varying, multipath fading, multiuser environment. Experimental results prove the effectiveness of the receiver.

ACKNOWLEDGMENTS

First and foremost, I must acknowledge the constant and unconditional support I received from my supervisor, Roberto Cristi. I would like to express my sincere gratitude for his supervision and his patience. His explanations and guidance led me to the completion of this dissertation.

I would also like to thank my committee, Professors Murali Tummala, Kevin Smith, Steven Baker and John Proakis, for their suggestions, ideas, and advice during the development of this dissertation.

I also wish to thank Joseph Rice, a member of my committee, for his motivation and inspiration. I would also like to express my gratitude to Paul Hursky and Mike Porter for tolerating the transmission of my acoustic waveforms during the Makai 2005 experiment and for providing me with the received data of the SignalEx-B and Makai 2005 experiments.

I dedicate this thesis to my thoughtful and supportive father and brothers, and especially to the sweet memory of my mother. I would like also to express my sincere appreciation to my fiancée, Lora, for her help and support, as well as to my friends and my colleagues in HS HYDRA for their support.

Finally, I would like to express my gratefulness to the Hellenic Navy for giving me the opportunity to start and complete this research.

THIS PAGE INTENTIONALLY LEFT BLANK

I. INTRODUCTION

A. MOTIVATION AND BACKGROUND

1. Underwater Networks

Underwater communication is vital for a number of military and commercial applications. Since electromagnetic waves cannot propagate over long distances in seawater, acoustic pressure waves provide the only wireless option to enable underwater communications.

In the late 1990s, the U.S. Navy started showing an interest in developing underwater acoustic communication networks in littoral waters. The central idea was to develop wireless networks covering wide areas of littoral waters, extending net-centric operations to the underwater environment. Such a network is composed of a number of fixed and mobile battery-powered nodes. The stationary nodes are the backbone of the network, operating as repeaters, surveillance sensors and gateways, and exchanging information with manned command centers or mobile nodes. Mobile nodes can be unmanned underwater vehicles (UUVs), swimmers or submarines. These types of networks are able to accomplish multiple missions, such as undersea surveillance of littoral waters, submerged submarines' digital connectivity with command centers, wireless net-centric command and control, and navigation of UUVs.

The product of this development is Seaweb, an organized network of battery-operated acoustic modem nodes deployed on the seabed [1]. A general illustration of Seaweb is depicted in Figure 1.1. This network provides physical, network, and link layers, as represented in the International Standards Organization's Open Systems Interconnection (ISO/OSI) model. The focus in this dissertation is at the physical layer [1].

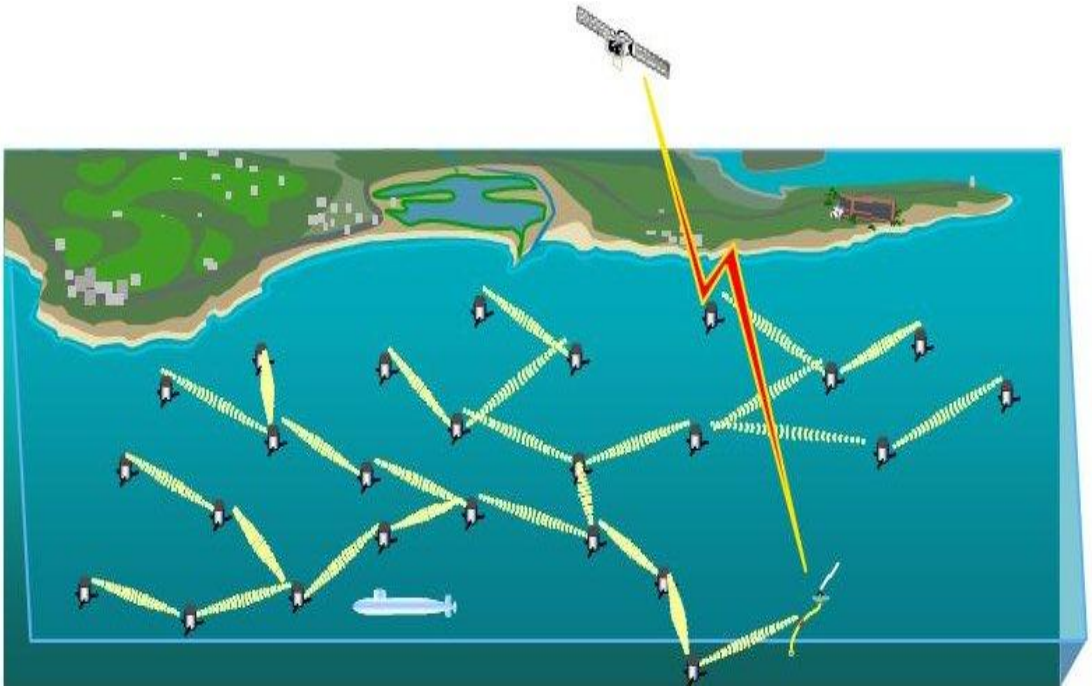

Figure 1. Seaweb illustration. From [1]

2. Challenges for the Physical Layer of Underwater Networks

The basic challenge of wireless communications systems is to yield high data rates and low error probability in the presence of poorly known channel characteristics. Key developments of digital communications techniques such as Code Division Multiple Access (CDMA) and Multi-Carrier (MC) modulation or Orthogonal Frequency Division Multiplexing (OFDM) have been the basis of reliable wireless systems in the air.

The underwater acoustic environment is a particularly challenging communication medium. In order to effectively design underwater communications systems, a deep understanding of the nature of the physical barriers constraining the communication performance in the underwater channel is necessary.

Propagation of sound waves in the sea greatly affects the reliability and efficiency of the communication link. In particular, the following issues have to be taken into account:

- Since wave attenuation is highly frequency dependent, only a limited spectral bandwidth is available for communications. This limits the channel capacity in terms of data rates achievable and number of users;
- Noise characteristics are in general non-Gaussian and non-stationary due to a number of factors, including noise generated by marine life and ship traffic;
- There is almost always a considerable multipath effect to be taken into account;
- Finally, Doppler shift of acoustic signals induced by transmitter-receiver relative motion and wave motion can be significant due to the relatively low speed of sound propagation. In addition, its fast time-varying nature can also set an obstacle toward reliable communications [2].

Major advances in signal processing of underwater acoustic communications were made when the physical nature of propagation was taken into account. Therefore, this dissertation makes an effort to address all the physical barriers in order to construct a robust communication link.

B. UNDERWATER ACOUSTIC COMMUNICATIONS: AN OVERVIEW

Early attempts to design reliable acoustic communications systems are based on noncoherent (NC) methods, which only require coarse synchronization, and are relatively insensitive to channel variations. One such scheme [3] dates as far back as 1978, and based on a Multitone On Off Keying (OOK) or a Multitone Frequency Shift Keying (MFSK) system with noncoherent reception, with use of guard bands and guard intervals. Frequency Shift Keying (FSK) systems use distinct tone pulses to send information and detect incoming energy in narrow frequency bands at the receiver. By simple energy detection independent of the signal's phase, as well as by the use of guard periods and/or bands in between the symbols, the proposed noncoherent systems overcome the variability of the channel and the resulting Inter-Symbol Interference (ISI). The idea of applying an OOK communication scheme was not further investigated due to the difficulty of setting a threshold for reliable symbol decision because of large amplitude fluctuations in the underwater environment [4].

The first actual designs and implementations of digital acoustic modems were made in the early 1980s. The main approach was based on MFSK modulation and noncoherent receivers as well as error correction coding [5, 6]. The data rates of those systems were very low (<200 bps), mainly because of the limited signal processing capabilities and the limited bandwidth, due to the low center frequency of the order of 10 KHz. A few years later an improved system (Digital Acoustic Telemetry System – DATS) was demonstrated and tested, applying higher data rates up to 1200 bps [7, 8]. This system used the same modulation scheme (MFSK), but with a higher center frequency and more advanced computer hardware, allowing more real time data processing [9].

Eventually, other acoustic modems using NC MFSK were implemented for commercial purposes. In [10], a reliable, extremely low bit rate (2 bps) system is described for monitoring and controlling oil wellheads, while in [11] a very low bit rate system is introduced for transmission of sensor data from a platform buried in sediment on the ocean floor.

In the early 1990s, the development of more efficient processors led to the construction of more reliable underwater communication systems. At Woods Hole Oceanographic Institution (WHOI), a robust telemetry system was developed and tested in shallow and deep water environments. The operation frequency band was divided into 16 sub-bands, in each of which a 4-FSK signal was transmitted [12]. The system was successfully tested at 1200 bps over a 3000 meters vertical path in [13] and at 5000 bps over a 750 meters very shallow water channel [14]. The first long-term autonomous operation was tested in a WHOI experiment described in [15], where data was transmitted at 600 bps over a 3000 meters vertical channel. Also in [16], the author uses a NC/MFSK system with directional transducers and controlled operating geometries in order to achieve higher data rates (up to 4800 bps) over longer distances (up to 10 km).

A different approach has been presented in [17] based on the OFDM principle, implemented by means of the DFT. The reception of the proposed

system was still noncoherent in the sense that it did not use phase information. The system transmitted successfully at a 250 bps data rate over a 2000-meter shallow water channel.

In [18], a system has been presented based on FSK modulation using 128 bands and employing coding operating at 2400 bps. The error correction is based on [19] with a Hadamard code to select tones for each word and a convolutional code to select a hopping pattern for the tonal alphabet. This algorithm builds upon the work in [20]. The most recent development in [21] presents a frequency-hopped M-ary FSK modulation combined with advanced signal processing.

Noncoherent receivers have been developed during the last 25 years, and they demonstrate a very robust tolerance to time and frequency spreading of the channel, making them suitable for littoral areas. The inefficient use of the already limited bandwidth, however, combined with the use of guard periods and frequency bands, makes the noncoherent systems inadequate for high data rate applications. Also, none of these noncoherent systems attempt to adapt to the specific channel characteristics to improve the data rate, since they are designed to fit the worst environment, thus sacrificing performance. Consequently, in the last two decades the scientific community has been developing coherent systems for underwater acoustic communications.

1. Acoustic Modems Based on Phase Coherent Communications

A considerable gain in data rate can be obtained by making use of both amplitude and phase information. Since phase is relative, either between transmitter and receiver or between received symbols, precise synchronization between transmitter and receiver is necessary, thus increasing the receiver's complexity.

Phase coherent systems, depending on the method of coherent synchronization, can be separated into two categories: differentially coherent and purely phase coherent. Although the relative bit-rate capacity of differentially

coherent systems is inferior to that of fully coherent ones [22], the advantage of simple carrier recovery in comparison with the estimation of the absolute phase needed in the fully coherent systems made the Differential Phase Shift Keying (DPSK) methods easier to implement.

The first developed coherent systems were intended for vertical underwater channels and used DPSK modulation schemes operating at data rates of 2000–5000 bps [16, 23, 24]. A vertical channel system operating at a very high data rate (500 Kbps) is described in [25]; the system used 16-QAM modulation with decision directed equalization and was operated at 1MHz carrier acoustic frequency. It was limited to very short range vertical channel communications (60 meters).

Another system, intended for vertical underwater channels, was developed in Japan and is described in [26]. Using Quadrature Differential Phase Shift Keying (QDPSK) and a 20 KHz carrier frequency, it transmitted at 16 Kbps over a distance of 6500 meters. A similar system for vertical transmission, developed in France, achieved a data rate of 19.2 Kbps over a distance of 2000 meters [27].

The first coherent system operating in a very shallow water horizontal channel, presented in [28], was based on binary DPSK modulation. In this scheme, reliable data rates of the order of 10 Kbps over a distance of 100 meters have been reported. The first implementation of spread spectrum techniques for the underwater environment was presented in [29], where each bit consists of 16 “chips,” resulting in a 625 bps link over a 1000 meter range (simulated).

C. RECENT DEVELOPMENTS IN UNDERWATER COMMUNICATIONS SYSTEMS

In order to better exploit channel capacity and allow for multiuser communications, a number of signal processing techniques have been introduced in the past decade. A number of important areas of research have been addressed and are listed below.

1. Channel Equalization

To mitigate the effects of multipath and channel variation, the channel characteristics must be estimated and tracked in real time. Technological advances in the areas of wireless communications and digital signal processing drove researchers to design and implement a large variety of receiver structures with channel equalization. The equalizers are employed to undo the effect of the channel.

In [30], Proakis offers a theoretical analysis of the adaptive equalization techniques that can be used to combat the time-varying multipath fading of the underwater channel. The techniques described belong to two main categories: linear equalization techniques, such as the adaptive linear Finite Impulse Response (FIR) equalizer with Least Mean Squares (LMS) or Recursive Least Squares (RLS) estimation algorithms, and nonlinear equalization techniques such as Decision Feedback Equalizer (DFE) with LMS or RLS. He concludes that block processing algorithms appear to be more suitable than sequential processing algorithms for acoustic channels with severe channel variation. Additionally, he notes that nonlinear DFE techniques are appropriate due to spectral nulls.

Following this report, in [31, 32], Stojanovic, Catipovic, and Proakis designed and implemented the first phase-coherent acoustic modem with channel equalization. The receiver jointly performed carrier synchronization and fractionally spaced decision feedback equalization of the received signal. Its parameters are adaptively adjusted using a combination of the RLS algorithm and a second order digital phase locked loop. The performance during the experiments was outstanding since the system achieved a 660 bps data rate over 110 nautical miles in the deep water channel and 1000 bps over 48 nautical miles in the shallow water.

In [33], the same group of researchers noted that in strongly fluctuating shallow water channels, higher transmission rates allow for higher sampling rates of the time-varying channel, resulting in a better tracking capability of the receiver. They explain this phenomenon by the fact that increasing the signaling rate effectively decreases the normalized Doppler spread of the channel, thereby reducing the penalty induced by imperfect channel tracking. Later, other researchers successfully developed receivers with similar structures based on DFE and Phase Locked Loop (PLL), and they also compared the filter coefficient update algorithms [34, 35, 36]. The performance of a linear equalizer was evaluated by Capellano et al. in [37], where the update algorithm design and the value of the spatial diversity are addressed. In this research, an adaptive multichannel equalizer made up of a bank of transversal filters was tested over a 50 km range in deep water.

The equalizers have a number of parameters that can influence dramatically the performance of the receiver and which need to be set according to the channel. In [38, 39], the authors try to overcome this problem, designing a system based on DFE/PLL where, during initialization, a block of data is processed repeatedly to provide a mean squared error (MSE) estimate for different sets of equalizer settings and to choose those settings that lead to the smallest output MSE. While this receiver is considered to be an efficient structure, a problem to be addressed is the interaction between the DFE and the PLL. Eggen, in [40], shows that under some circumstances this could result in an unstable system. Also, the same research reveals that the RLS update algorithm is not adequate to track severely time-varying channels with high Doppler distortion. In order to overcome this problem, the authors of [41] suggested a method of estimating the mean Doppler shift from a training sequence and then compensating for it while decoding the data.

A key issue regarding the implementation of coherent receivers is the increased computational complexity. In [42, 43], a reduced complexity equalizer is presented which takes full advantage of the sparse profile in time domain of the channel impulse response in the design of the equalizer.

All techniques presented so far rely on the transmission of training sequences to estimate the channel dynamics. A different approach to channel equalization is blind equalization, which relies on redundant information in the structure of the signal, without relying on training sequences and correct symbol detection.

In [44], Gomes and Barroso introduced a radial basis function (RBF) neural network used for blind adaptive equalization of the underwater channel. The system successfully demodulates data at 120 bps over a 1000 m shallow water range, but is sensitive to high Doppler distortion. A different approach is presented in [45, 46]. The system has two modes: in the starting mode, the equalizer operates blindly and can be viewed as a linear cascade of a recursive whitening filter, a gain control device, a transversal filter and a PLL. When the MSE of the receiver is low enough, the equalizer goes to the tracking mode, which is the usual DFE/PLL. The authors note that, except for the successful tests of the receiver, an important advantage is that if the MSE gets large again while in the tracking mode, the equalizer is switched back to the starting mode, avoiding the error propagation problem of the DFE/PLL. A more recent approach of that receiver is described in [47], where the receiver has multiple inputs from the channel and is compared to the multiple input decision feedback equalizer (MI/DFE) structure. The experimental results showed that the introduced multiple input receiver outperforms the MI/DFE receiver.

In related research, two methods of blind equalization of multiple-channel data were considered [48], based on Minimum Shift Keying (MSK). The first method combines a constant modulus algorithm equalizer with a PLL, and the

second a blind decision directed equalizer with a PLL. The results are satisfactory for both implementations, but the second approach seems to have better performance.

Although the performance of the blind equalizers seems comparable to that of the methods using training sequences, it is the opinion of a number of authors that they are not reliable in actual applications [9].

2. Multiple-Input Multiple-Output (MIMO)

In recent years, there has been interest in designing multiple-input/multiple-output (MIMO) communication systems for underwater acoustic communications. These systems make use of multiple receivers and take advantage of the diversity of multiple channels. Information theoretical studies have shown that the capacity of a channel increases linearly with $\min\{N_R, N_T\}$ where N_R, N_T the numbers of antennas at the receiver and transmitter respectively. This increase in capacity translates to a corresponding increase in achievable data rate on MIMO systems.

The first MIMO underwater communication experimental results were reported in the early 2000s by Kilfoyle et al., who studied the number and nature of the available degrees of freedom of a MIMO system on a shallow water channel [49, 50]. The arrays used were a 16-element receive array and a six-element projector array. The experiments demonstrated that the proposed spatial modulation scheme offered increased bandwidth and power efficiency compared to signals constrained to temporal modulation only [51].

Song et al. studied the MIMO data rate using active and passive time reversal methods [52]. The principle behind time reversal systems is based on the reciprocity of the linear wave Equation, so that the sound transmitted from one location, received, reversed and retransmitted, focuses back at the original source location. The more transmitters there are, the better the focus [51]. The transmitter and receiver arrays had 29 and 32 elements, respectively, and their

experimental results were satisfactory. In another MIMO experiment Song et al found that continuous channel updates and Doppler shift tracking is required before time reversal in order to achieve acceptable performance in the presence of ocean variability due to surface movement [52, 53]. Rapidly changing channels due to moving communication nodes may pose a challenge to the use of phase conjugation in mobile applications [51].

More and more researchers are interested in MIMO systems for underwater communications and they are trying to take advantage of the full multiplicity and diversity gain of MIMO systems. In this direction, Yang, using experimental data, studies how multi antenna systems improve both data rate and Signal to Interference and Noise Ratio (SINR) [49]. He concludes that an 8x8 MIMO system in an underwater acoustic channel can support a full multiplicity gain of order 8, where multiplicity gain is defined as the ratio of the capacity of a MIMO system over that of a SISO system.

3. Modulation: Direct Sequence Spread Spectrum and OFDM

While underwater communications were evolving, the first underwater networks started developing. The requirement for multiple accesses and the desire for low probability of intercept have drawn attention to Direct Sequence Spread Spectrum (DSSS) techniques. In DSSS, each transmitted symbol modulates a pseudorandom code, unique to each user. A noise-like signal is generated which can be decoded only by the intended user, thus making it attractive for secure environments.

One of the first approaches is analyzed in [29], where a DPSK system uses a DSSS method to resolve a transmitted signal in a shallow water multipath environment. The interfering reception is rejected and only the principal arrival is used for decoding. Since the multipath reception is neglected at the receiver, the performance is poor. An improved method is presented in [54], which takes advantage of all the information contained in the multipath arrivals. The proposed receiver is based on a rake filter which includes threshold devices at each tap to

reduce the amount of noise in the combiner. The channel impulse response is estimated from a probe signal and it is used to set the filter parameters.

A different approach for DSSS signaling is the hypothesis-feedback DSSS technique developed by Stojanovic and Freitag in [55]. Based on a parallel set of adaptive chip rate DFEs, each is tuned for a different hypothesis of the transmitted symbol. The one which yields the smallest error is chosen. This system is particularly suited to communications through a rapidly varying multipath fading channel with multiple access interference, at the expense of increased computational complexity.

In [56], the last two techniques presented are compared. It is shown that the hypothesis-feedback DSSS receiver outperforms the RAKE receiver, especially in highly time-varying channels, due to its ability to track the channel on a chip-by-chip basis, at the price of increased computational complexity. If, however, Doppler shift correction can be performed, the RAKE receiver can offer good performance with lower complexity.

Recently OFDM has gained considerable attention due to its ease of implementation and high data rate. A MIMO implementation of OFDM is particularly suitable to high data rate implementation in uncertain and time-varying environments.

The most important challenge, however, related to underwater acoustic OFDM communications is the non-uniform Doppler shift across the sub-carriers, which degrades the orthogonality of the subcarriers [57]. In [58], Stojanovic introduces a successful MIMO-OFDM structure which dynamically compensates for the non-uniform Doppler shifts and adaptively estimates the acoustic channel's characteristics. Doppler shift correction is achieved through a two-step approach: non-uniform Doppler effect compensation via resampling, followed by high resolution uniform compensation on the residual Doppler shift. Experimental results demonstrate successful operation of a 3x12 MIMO system, using 4–PSK and 8–PSK with 1024 carriers in a 10 kHz acoustic bandwidth over 1 km in

shallow water [58]. OFDM, however, is very sensitive to time and frequency synchronization errors and its effectiveness in the underwater acoustic communications is still under investigation.

4. Design Considerations and Solutions

In line with the considerations mentioned above, this dissertation addresses the problem of designing a robust and reliable coherent receiver which will be able to operate in a multi-user environment.

The proposed scheme is based on DSSS modulation, which is particularly suitable to multi-user communications in the presence of time-varying channels with multipath propagation. The DSSS signal can also be used for channel-scattering function measurement, which is a vital task for estimating the time-varying characteristics of the communication medium, and adjusting the receiver parameters for optimum detection.

Initially, a robust method based on DSSS signals for acquisition and synchronization of the receiver is developed and a significant fraction of the Doppler shift is detected and corrected.

The receiver, based on an array of hydrophones, exploits the advantages of spatial diversity. The received signals from the hydrophones are processed in such a way that the principal multipath arrival is amplified, whereas environmental noise and weaker multipath arrivals are suppressed. The spatial combiner, designed based on array processing theory, processes the received signals before being processed by the equalizer.

The heart of the receiver is a dual-input equalizer, which is based on a Kalman filter estimator and has a relatively low computational complexity. With multiple receivers, the transmitted signal can be viewed as the state of a dynamic system, with the received signals as inputs and outputs. Consequently, a Kalman estimator can be used. Furthermore, in order to ensure the reliability of the

equalizer, a method was developed for choosing the multipath components to be used as inputs of the equalizer based on the channel consistency of those components.

Also, an adaptive mechanism is developed for the equalizer, in order to track the channel changes and ensure the filter's convergence. Incorporated into the equalizer is an algorithm for dynamically tracking and correcting the Doppler shift of each of the multipath arrivals. Since the Doppler shift is heavily time-varying, it is crucial to dynamically track and correct it for best performance of the acoustic receiver.

Finally, an external interference and noise canceller mechanism was developed, intended for use in the multiuser underwater environment. The outcome of this dissertation is a robust receiver able to operate in a fast time-varying, Doppler-distorted, multipath-fading, multiuser environment.

D. RESEARCH GOALS

After introducing the theoretical background of how an underwater acoustic channel influences acoustic communications, a robust communication scheme is developed based on theory, simulations and experimental results.

The objectives of this research are:

- Develop a reliable mechanism for channel identification and validate its performance though simulations and experiments;
- Develop a reliable method for the precise acquisition and synchronization of the communication signal. A particular feature of this objective is that it has to be robust in the presence of a highly Doppler distorted underwater channel;
- Develop an innovative coherent receiver/equalizer for multiple input signals, robust to a fast-varying highly distorted communication channel;
- Design a Doppler shift tracking mechanism operating independently of the receiver in an attempt to eliminate most of the Doppler effect before the received signals are processed by the receiver/equalizer; and
    - Develop an algorithm for interference cancelation in a multiuser environment.

E. DISSERTATION ORGANIZATION

This dissertation is organized as follows: Chapter II analyzes the basic characteristics of the underwater channel. Starting from basic acoustics and ray propagation, the signal distortion effects in the acoustic communication channel are discussed in terms of their time and frequency spread. Finally, the various types of fading channels are defined illustrating the usual mathematical models describing their behavior.

Chapter III describes a method of channel estimation based on DSSS/PSK. The performance of a channel identification algorithm is tested first on an artificial channel and then the method is applied and validated to two real underwater channels (New England Shelf 2000 and Makai 2005 experiments [75, 82]).

Chapter IV addresses the problem of initial synchronization, i.e., determining the starting time of the data packet in a multiuser environment using code-division multiple-access. A robust synchronization method will be presented, compared with other methods and tested using simulations and experimental results.

Chapter V discusses several receiver-equalizer designs used for the accurate demodulation of the DSSS acoustic signal. In the first part of the chapter, some well known methods will be mentioned and analyzed. In the latter parts, the approaches of combining a number of received signals using Kalman Filtering and then array focusing will be presented and tested on simulated channels.

Chapter VI addresses the development of an innovative multiple input equalizer/receiver for the accurate demodulation of the DSSS acoustic signal. This chapter also introduces an adaptive receiver to track variations of the acoustic communication channel. In particular issues related to dynamic Doppler compensation and interference cancelation in a multiuser environment will be

addressed The receiver's performance, using data from Makai 2005 experiment, will be presented and compared to other reception schemes.

Finally, Chapter VII of this dissertation presents conclusions and further research.

II. UNDERWATER CHANNEL AND ACOUSTIC COMMUNICATIONS

This chapter analyzes the basic characteristics of underwater acoustic communications. Starting from basic acoustics and ray propagation, the underwater acoustic communication channel is described and the signal distortion effects in time and in the frequency domain are discussed. The impulse response is then defined and how it influences the received signal is demonstrated. Finally, the various types of fading channels are defined and the usual mathematical models describing their behavior are illustrated.

A. SOUND PROPAGATION IN THE OCEAN

The ocean is an acoustic waveguide, limited above by the sea surface and below by the sea floor. The sea surface can be modeled as a pressure release boundary and the sea floor as a second fluid medium (Pekeris Waveguide) [59]. The result is no loss of acoustic energy to the air, but almost always a loss of energy to the sea floor. The degree of this loss depends on the characteristics of the bottom—sound speed and density—and on the incident angle of the acoustic wave to the bottom. Accordingly, each time the acoustic wave impinges the bottom, it suffers a loss in strength.

The propagation of sound in the ocean can be described in various ways, but for the purposes of this dissertation, ray theory is followed, an approach borrowed from optics. This theory is based on the assumption that energy travels along reasonably well defined paths through the medium. Rays, however, are not exact representations of waves, but only approximations that are valid under certain rather restrictive conditions [60]. The ocean water column is not a homogeneous medium and the sound speed varies as a function of depth. The acoustic “rays” in the ocean refract according to Snell’s law. Snell’s law provides

a simple formula for calculating the ray declination angle at any depth z based only on the declination angle $\theta(z)$ at any other depth and knowledge of the sound speed:

$$c\ z_o\ \cos\ \theta\ z\ = c\ z\ \cos\ \theta\ z_o \tag{2.1}$$

where $c(z)$ is the sound speed at depth z. A general rule for ray propagation is that a ray always bends toward the neighboring region of lower sound speed. If the sound speed profile of the water column is known, the sound propagation in this environment can be modeled.

An example of ray tracing is presented in Figure 2. This example involves sound propagation in a 120-meter deep sea. The transmitter is located at a depth of 30 meters, and the receiver at a depth of 73 meters, at a distance of 12800 meters from the transmitter. In the left plot, the sound speed profile is illustrated. In the right plot, the dominant eigenrays are shown. Eigenrays are the rays that start from the transmitter and pass though the position of the receiver. In this case there are three dominant eigenrays, each one with different values of attenuation, phase shift, and propagation delay. The red eigenray arrives at the receiver first and experiences the least attenuation. Its phase shift will be close to zero. Approximately 0.11 milliseconds later, the yellow eigenray reaches the receiver with a phase shift close to π radians. The green eigenray reaches the receiver 0.55 milliseconds after the red one with a phase shift close to π as well.

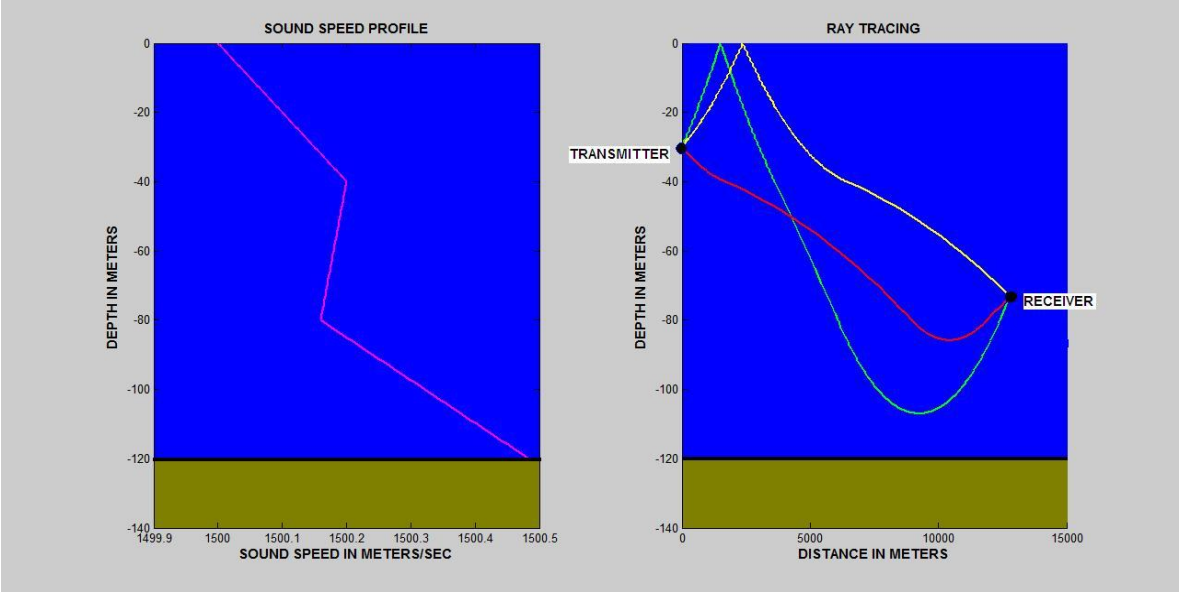

Figure 2. Ray Tracing example, for source depth at 30 meters

The intensity of the propagating sound in the ocean attenuates as a function of the distance r between the transmitter and the receiver. The term transmission loss (TL) describes this attenuation and is determined by combining the signal loss from source to receiver due to a combination of geometric spreading and sound absorption.

Geometric spreading from the transmitter is in the form of spherical spreading up to a range approximately equal to the water depth of the channel. Spherical spreading loss is proportional to $1/r^2$. Beyond this range, cylindrical spreading (intensity) approximates the propagation. Cylindrical spreading loss is proportional to $1/r$ [61].

The absorption of sound in seawater depends on numerous factors, such as temperature, salinity, depth, pH, and frequency. A general rule is that, as frequency increases, the absorption of sound in the ocean is stronger. Figure 3 illustrates the absorption coefficient as a function of frequency for $T = 0^o$ C and $T = 20^o$ C, for a depth of 0 meters, $\mathrm{pH} = 8$ and $S = 35$ ppt (parts per thousand) [59].

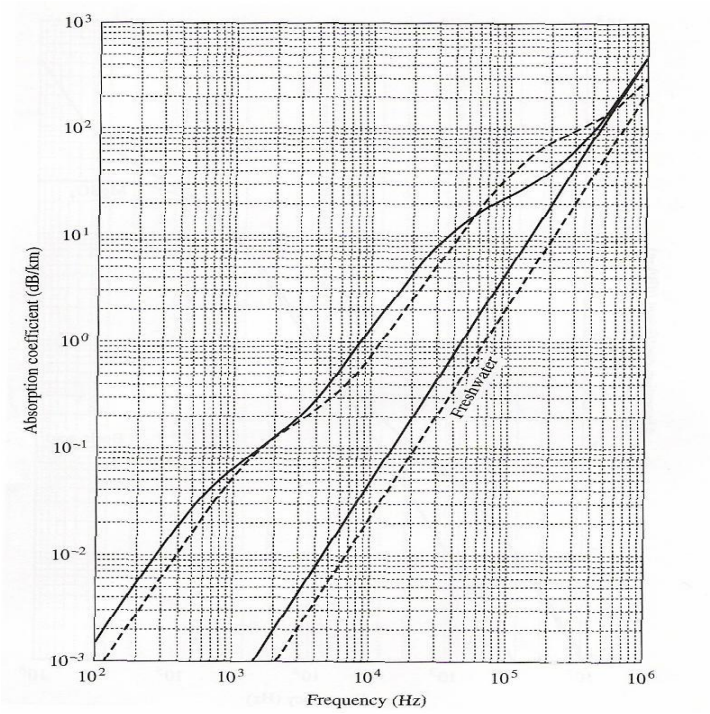

Figure 3. Absorption in seawater. Solid line for $T = 0^o$,dashed line for $T = 20^o$ From [59]

The spectral bandwidth of an acoustic communication link is limited for two reasons. First, with higher acoustic frequencies the absorption increases (as seen in Figure 3), thus limiting the effective distance of the communication link. The second problem is the non-uniform frequency response of underwater sound projectors. A relatively flat frequency response over a wide frequency band would be ideal; however, due to physical constraints, at typical communications frequencies between 15 and 30 kHz, it turns out that at best we can have a relatively flat response over a bandwidth of about 15 kHz.

B. NOISE IN THE UNDERWATER CHANNEL

The ambient noise of the ocean is not Gaussian and is “colored.” Below 500 Hz the major contribution to ambient noise is from distant shipping and biological noise. From 500 Hz to 50 kHz the local sea surface is the strongest source of noise. This is the frequency band of interest for most acoustic modems

and, as a result, the channel noise varies depending on surface conditions (sea state, wind), as illustrated in Figure 4. Above 50 kHz ocean turbulence and the thermal agitation of the water molecules are the predominant noise source [62].

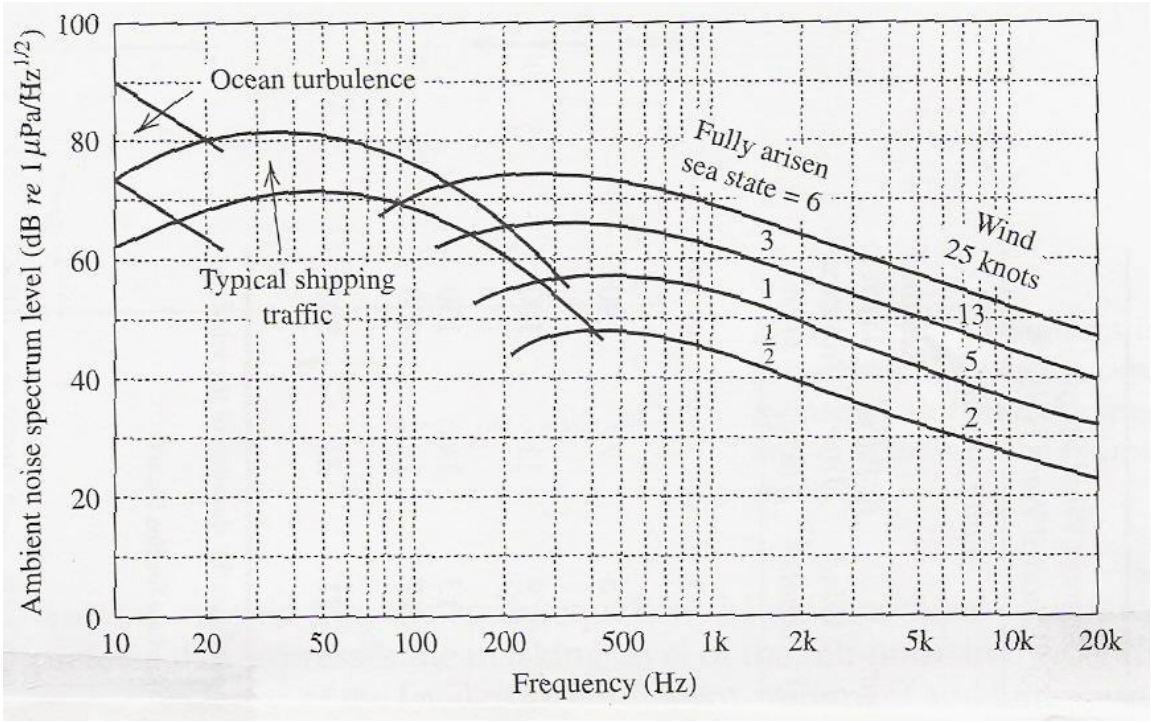

Figure 4. Deep water ambient noise. From [59]

Traditionally the theory of communications assumes Additive White Gaussian Noise (AWGN). AWGN's power spectral density is the same for all frequencies of interest, while also consisting of a Gaussian random process. AWGN, however, is not representative of the acoustic channel and as a result, the underwater acoustic communications performance is worse than the performance of wireless electromagnetic communications. Finally, the estimation of the acoustic communication channel is harder when the noise is not white.

C. SIGNAL DISTORTION DUE TO MULTIPATH PROPAGATION

In the case of underwater acoustic communications, the signal is carried by acoustic pressure waves. Some interesting effects take place in the underwater channel, which put severe limitations on the reliability of the communication link. The first effect is illustrated in Figure 5, which shows that for the geometry shown, the acoustic waves reach the receiver following three different paths. Destructive interference, the result of the multipath propagation, creates severe fading in the channel [63, 64].

Fading is caused by interference of two or more replicas of the transmitted signal arriving at the receiver at slightly different times, following different paths. They combine at the receiver to give a resultant signal, which may vary widely in amplitude and phase, depending on the distribution of the intensity and relative propagation time of the waves and the bandwidth of the transmitted signal.

The effect of multipath on the spectrum of the signal is frequency dependent so that the frequency response of the channel is not flat over the bandwidth of the signal.

Another important characteristic of the multipath propagation is the time variation in the structure of the acoustic medium (waves, wind, current) and the motion of either the receiver or the transmitter. As a result, the signal passing through the underwater channel is distorted both in the time and frequency domains.

1. Energy Time Spread

Consider the simplified case of Figure 5. A sinusoidal signal with a transmit duration of one millisecond is assumed. The acoustic wave follows three different paths. Each path has some attenuation, some phase shift and some propagation delay. The transmitted pulse is illustrated on the left side of Figure 5, and the received pulse on the right side. As seen, the received pulse is distorted and its energy is spread in time.

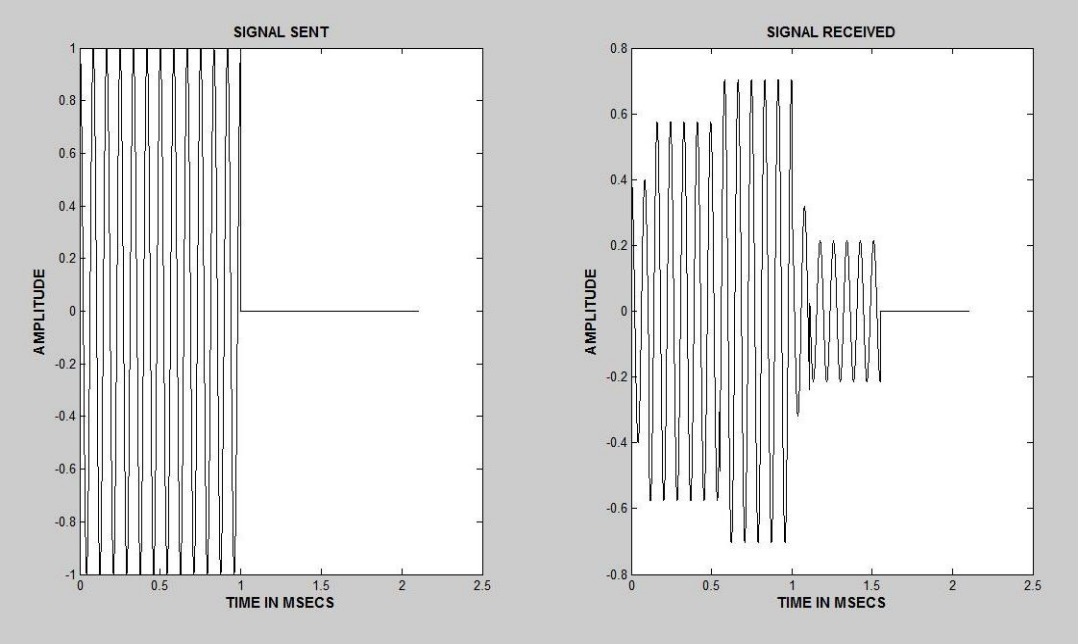

Figure 5. Multipath effect on a sinusoidal pulse

2. Doppler Spread

In addition to time spread of the propagating energy, another important phenomenon is the distortion of the signal in the frequency domain. This is caused by the time variations in the structure of the acoustic medium and the relative motion of the receiver and the transmitter.

The motion of the receiver or transmitter gives the well-known Doppler shift effect wherein the center frequency of the carrier is shifted. The shift is positive if the receiver and transmitter are coming closer to each other, and negative if they are moving away from each other. The amount of shift is given by the following equation:

$$f_d = \frac{f}{c} v \cos\ \theta\ . \qquad (2.2)$$

which depends on the frequency f, the speed of sound c, the relative speed between the receiver and transmitter v, and the spatial angle θ between the

direction of motion and the direction of arrival. Since for each path the wave arrives from a different angle (in general), there is a different Doppler shift associated with each path.

The time variations of the structure of the acoustic medium create a relative phenomenon, which is called Doppler spread. Assume that a pure tone is sent through the channel. If the channel is time invariant, no spectral broadening is noticed in the received tone. Time variations of a channel, however, result in a broadening of the spectral line. This effect is called Doppler spread. The Doppler spread, just like the Doppler shift, has a different value for each path [65].

D. IMPULSE RESPONSE PROFILE CHARACTERISTICS

As discussed earlier, each path has a different attenuation, phase shift and delay. Therefore, if a real bandpass signal $s\ t$ is sent through the channel, the received signal can be expressed as

$$r\ t\ =\sum_{n=0}^{N} a_n\ t\ \ s\ t-\tau_n\ t\ \ . \tag{2.3}$$

In this equation, N is the total number of paths comprising the underwater channel, $a_n\ t$ is the gain of the n-th path, which is a function of time, and $\tau_n\ t$ is the time delay associated with the n-th signal path, which is a function of time as well, with $\tau_0 = 0$. If this signal is expressed in baseband form as

$$\tilde{r}\ t\ =\sum_{n=0}^{N} |\ a_n\ t\ |\tilde{s}\ t-\tau_n\ t\ \ \exp\left[\ i\ \omega_c\times\tau_n\ t\ +\varphi_n\ t\ \ \right] \tag{2.4}$$

with ω_c the carrier frequency, $\tilde{s}\ t-\tau_n\ t$ the baseband form of the transmitted signal and $\varphi_n\ t$ is the time-varying phase shift of the n-th path. The complex baseband impulse response of the multipath propagation channel is defined as: [22]

$$h\ \tau,t\ =\sum_{n=0}^{N} |\ a_n\ t\ |\exp\left[\ i\ \omega_c\tau_n\ t\ +\varphi_n\ t\ \ \right]\delta\ \tau-\tau_n\ t\ \ . \tag{2.5}$$

From the last relation, it can be seen that the impulse response of the channel is the superposition of the impulse responses of the individual paths. This is a very important quantity for analysis since, after determining its form, all other characteristic parameters of the channel can be derived using this result. More specifically, the time and frequency effects of the underwater multipath fading channel on the signal can be determined.

E. UNDERWATER CHANNEL CHARACTERISTIC PARAMETERS

The underwater channel can be characterized by at least two parameters associated to the time and the frequency variations of the channel.

The Fourier transform of the impulse response $h\ \tau,t$ with respect to the time delay, is given by the relation

$$H\ \ t,f\ \ = \int_{-\infty}^{+\infty} h\ \ \tau,t\ \ e^{-i2\pi f\tau} d\tau. \tag{2.6}$$

and its autocorrelation is defined as:

$$S_H(t,t_1;\, f\,,\, f_1) = \frac{1}{2}\mathrm{E}\{H(t,\, f)H^*(t_1,\, f_1)\}, \tag{2.7}$$

where $E\{\bullet\}$ stands for the expected value of the function inside the brackets.

It is shown in numerous sources (see, for example, Proakis' book [22]) that the assumption of Wide Sense Stationarity and Uncorrelated Scattering (WSSUS) yields stationarity in both the time and frequency domains. In this way, (2.7) can be written as

$$S_H(\Delta t;\Delta f) = \frac{1}{2}\mathrm{E}\{H(t,\, f)H^*(t+\Delta t,\, f+\Delta f)\}, \tag{2.8}$$

By taking the inverse Fourier transform of $S_H\ \ \Delta t;\Delta f$ with respect to Δf, we obtain:

$$P_h\ \ \Delta t;\tau\ \ = \int_{-\infty}^{+\infty} S_H\ \ \Delta t;\Delta f\ \ e^{i2\pi\tau\Delta f} d\ \ \Delta f\ \ . \tag{2.9}$$

In the case of $\Delta t = 0$, we define $P_h(\tau) = P_h(0, \tau)$ to be the average power out of the channel as a function of the time delay. It is called the power delay profile or multipath intensity profile [22, 65].

The range of τ over which the power delay profile is nonzero is the multipath spread T_m of the channel. The multipath spread is the first of the two important parameters and describes the time dispersive nature of the channel. Some typical values of the multipath spread for an underwater channel are 10-20 msec, compared to the cellular wireless communication channel, where they are 1-10 μsecs [22, 66]. The greater the multipath spread, the more dispersive the channel will be.

Now consider $S_H(\Delta t; \Delta f)$ in the case when $\Delta t = 0$, $S_H(\Delta f)$ is the frequency correlation function. The range of Δf over which the frequency correlation function is greater than some defined value is the coherence bandwidth of the channel B_c. Since $S_H(\Delta f)$ and $P_h(\tau)$ are a Fourier transform pair, the relation $B_c \approx 1/T_m$ holds. Consequently, both parameters describe the time dispersive nature of the channel. The coherence bandwidth is a measure of the range of frequencies over which the channel can be considered flat, which means that the channel will pass all spectral components with approximately equal gain and linear phase.

Again, consider $S_H(\Delta t; \Delta f)$ in the case when $\Delta f = 0$, $S_H(\Delta t)$ is the space-time correlation function, which represents the correlation of a single sine wave with itself over time Δt. The time over which $S_H(\Delta t)$ is essentially unity is defined as the coherence time of the channel Δt_c. Coherence time, the parameter that describes the time-varying nature of the channel, is a measure of the time duration over which the channel attenuation and delay are essentially

constant, so the received amplitude and phase are constant over a period of Δt_c seconds. If we take the Fourier transform of $S_H(\Delta t;\Delta f)$ with respect to Δt, we obtain

$$P_h(\nu;\Delta f) = \int_{-\infty}^{+\infty} S_H(\Delta t;\Delta f)\, e^{-i2\pi\nu\Delta t} d(\Delta t) \,. \tag{2.10}$$

In the case when $\Delta f = 0$, we define $P_h(\nu)$ to be the Doppler power spectrum of the channel. The range of ν over which $P_h(\nu)$ is essentially nonzero is the Doppler spread B_d of the channel. The Doppler spread, as discussed before, is a measure of the spectral broadening caused by the time rate of change of the underwater channel. Since $S_H(\Delta t)$ and $P_h(\nu)$ are a Fourier transform pair, the relation $B_d \approx 1/\Delta t_c$ will be true. As a result, both parameters describe the time-varying nature of the channel. [22]

F. TYPES OF FADING CHANNELS

A multipath fading channel can be characterized by comparing the parameters of the channel to the characteristics of the communication signal, specifically, the signal's bandwidth and symbol period.

Time dispersion due to multipath effect causes the transmitted signal to experience either flat or frequency selective fading. If the channel has a constant gain and linear phase response over a bandwidth which is greater than the bandwidth of the transmitted signal (i.e., B_c is large in comparison to the BW), the channel is said to be frequency-nonselective or flat fading. In the time domain this means that all of the multipath components arrive within the symbol duration. On the other hand, if B_c is small in comparison with the BW, significant distortion of the signal occurs and the channel is said to be frequency-selective. In this case successive pulses interfere with each other. Figure 6 illustrates the concept of flat and frequency selective fading. Typical values of coherence bandwidth, observed during experiments, are on the order of several tens of Hz.

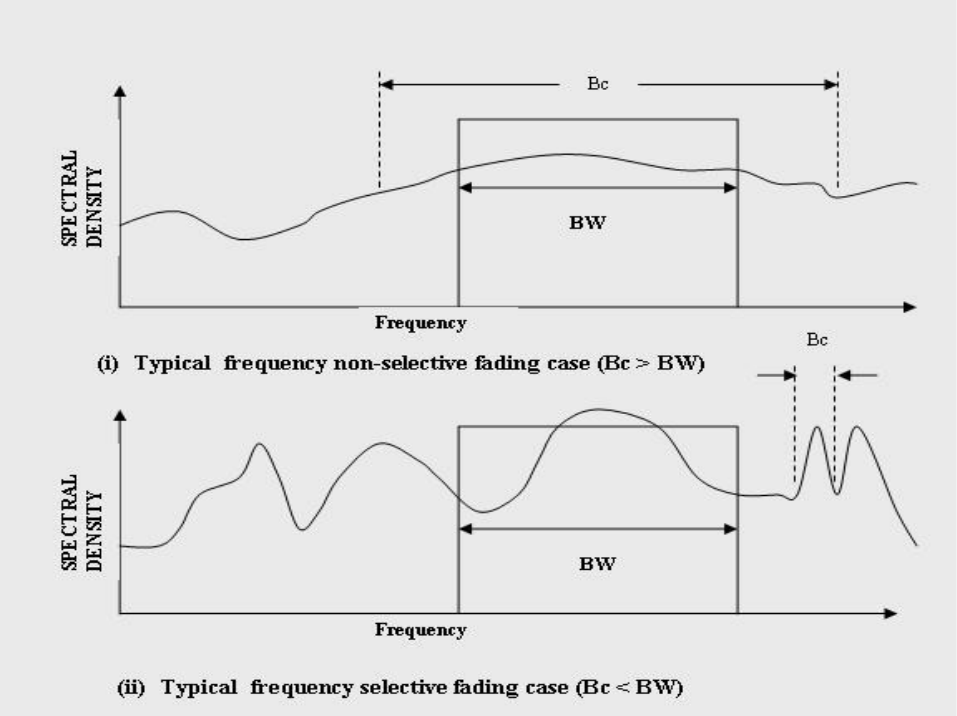

Figure 6. Examples of frequency non-selective/selective fading channels

Depending on how rapidly the transmitted signal changes compared to the rate of change of the channel, a channel may be classified as either a fast fading or slow fading channel. If the symbol duration is smaller than the coherence time, then the received amplitude and phase are effectively constant for the duration of at least one symbol and the channel is said to be slowly fading. If the received amplitude and phase fluctuate over time periods that are short compared to the duration of a symbol, the channel is said to be fast fading. During experiments, values of channel coherence time below 100msec have been observed, but not often [67].

The underwater channel is always strongly frequency selective, with the large multipath effect time spread likely to cause Inter-Symbol Interference—depending on the signaling rate—of up to several tens of symbol intervals. Depending on the conditions and its geometry, the channel can be slow or fast fading with the worst-case scenario being in shallow waters and under rough weather [62].

G. STATISTICAL CHARACTERIZATION OF AN UNDERWATER CHANNEL

Since the time variations of the multipath propagation channel appear to be unpredictable to the user, it is reasonable to characterize this time variant channel statistically. When the impulse response $h\ \tau,t$ is modeled as a zero mean complex valued Gaussian process, the envelope of $\left|h\ \tau,t\ \right|$ at any instant t is Rayleigh-distributed. The Rayleigh distributed case describes a channel in which there is no line-of-sight direct path. This type of channel is referred to as a Rayleigh fading channel. If there are fixed scatterers or signal reflectors in the medium in addition to randomly moving scatterers, $h\ \tau,t$ can no longer be modeled as having zero mean. In this case, the envelope of $h\ \tau,t$ at any instant t is Ricean-distributed, and the channel is characterized as a Ricean fading channel. Communication performance is better in the Ricean fading channel, than in the Rayleigh case.

At a first glance, the underwater channel would seem to be Ricean fading, since the sea surface and sea floor represent fixed scatterers in the acoustic medium; however, experiments show that the behavior of the channel, depending on the conditions, resembles either a Ricean or a Rayleigh channel. In deep waters when the wind is feeble, the underwater channel behaves as a Ricean fading channel. Alternatively, in shallow waters with strong winds, the channel behaves as a Rayleigh fading channel. Performance is poorer in the second case [22].

During the shallow waters experiments presented in the next chapters of the dissertation, the channel behaves mostly as a Rayleigh fading channel.

THIS PAGE INTENTIONALLY LEFT BLANK

III. CHANNEL IDENTIFICATION WITH USE OF DSSS/PSK

In this chapter, a method of channel estimation based on a Direct Sequence Spread Spectrum with Phase Shift keying (DSSS/PSK) is presented. The performance of a channel identification algorithm is tested first on an artificial channel and then the method is applied to two different underwater channels. The results obtained will be at the basis of the arguments presented in the following chapters.

A. THEORETICAL DEVELOPMENT OF THE PROPOSED METHOD

In high speed wireless communications, whether over a water column or in the air, one of the major issues is modeling and estimation of the effects of the channel. In particular, the presence of a multipath effect due to reflections, and Doppler shift due to non-stationarity has to be accounted for by the demodulator for reliable communications. As shown in previous chapters, a typical channel is parameterized as a linear system with time-varying coefficients, as

$$y(t) = \sum_i h_i(t)x(t-\tau_i) + w(t) \tag{3.1}$$

with $x(t)$ and $y(t)$ the transmitted and received signals while $w(t)$ is additive white noise. The effects of channel's parameters $h_i(t)$ and τ_i are in terms of a spread in time by multiple receptions and in frequency by Doppler shift [22].

Although this is a well-known standard problem in wireless communications, the underwater communications are made more challenging because the effects of Doppler spread can be particularly severe and need to be taken into account for reliable demodulation [67, 68].

1. Probe Signal for Channel Estimation

In order to estimate the effect of the acoustic channel, a signal known to the receiver has to be transmitted. Referred to as a probe, this signal is spread both in time and frequency, as seen in Section C of Chapter II.

The transmitted probe signal must be suitable for estimating the dynamics of the underwater channel. A wideband probe signal will provide high resolution in time and frequency. This type of probe is often used in practical systems to measure the channel characteristics. A typical wideband signal for this purpose can be a pseudorandom-noise-spread signal (such as a Direct Sequence Spread Spectrum signal—DSSS) [69].

DSSS signals achieve band spreading by modulating the information bit sequence with a chip sequence at a higher rate. The “chip” is the fundamental unit of transmission in DSSS, and in the binary case it is typically a rectangular pulse. The chip sequences that are employed to spread the signal usually belong to the class of pseudorandom noise sequences. Typical examples are maximum length sequences (m-sequence) [70, 71], or Gold sequences [22].

The generation of a DSSS bandpass signal in the time domain using a binary information sequence is illustrated in Figure 7. In this example, each bit of duration T_b (in this example, $T_b = 0.75\ \text{msec}$) is spread into multiple chips of duration T_c (in this example $T_c = 0.05\ \text{msec}$) by an m-sequence of length N, with $N = T_b / T_c$. The factor N is called the “spreading factor” or “processing gain.” It is well-known [22, 70] that the null-to-null bandwidth of the resulting DSSS/BPSK signal is N times larger than that of a typical (unspread) BPSK signal, thus making it suitable for the goal, the channel identification.

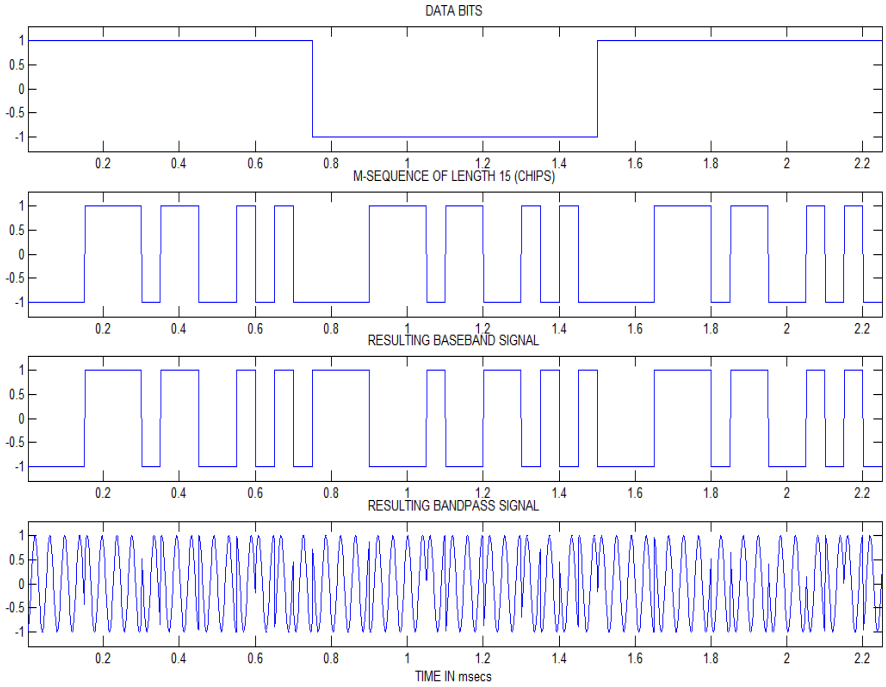

Figure 7. Direct Sequence Spread Spectrum Signal Generation

DSSS modulation offers many advantages, such as suppressing both multi-user interference and channel-induced ISI due to multipath arrivals at different times. In particular, DSSS systems are the basis of multiple user communication as in code division multiple access (CDMA) and secure communications, by spreading the signal power under the noise floor. The DSSS signal, which will be designed for the task of channel identification, needs to have some specific characteristics so that accurate channel recognition can take place. These characteristics deal with the chip duration T_c and the number of chips per bit N, and are based on the expected channel aspects. They will be analyzed after the description of the channel's identification algorithm.

2. Channel Identification Method Based on DSSS Signals

The underwater acoustic channel spreads the transmitted signal in both time and frequency. The temporal spread is associated with multipath effects and the frequency spread (Doppler effect) with scatterer motion and changes in the medium propagation characteristics. Assuming wide sense stationary and uncorrelated scattering conditions, the channel can be completely described through the well-known scattering function. This function $S(\tau, f)$ can be viewed as a density function giving the average power modulation as a function of time delay τ and Doppler shift f. Consequently, the goal in the channel identification is to develop a method to estimate $S(\tau, f)$.

The estimate of the scattering function $S_{est}(\tau, f)$ can be computed by processing the channel's impulse response estimate $h_{est}\ \tau, t$. The first step is to compute the autocorrelation function of the estimated impulse response using the following equation:

$$\phi_h\ \tau, \Delta t\ = \frac{1}{N}\sum_{n=0}^{N}\{h_{est}\ \tau, n\Delta t\ \ h_{est}^{*}\ \tau, n\Delta t + \Delta t\ \}. \tag{3.2}$$

In order to compute the scattering function estimate, the Fourier transform must be taken with respect to Δt of the autocorrelation function of the estimated impulse response $\phi_h\ \tau, \Delta t$ using the following Equation:

$$S\ \tau, f\ = \mathbb{F}_{\Delta t}\{\phi_h\ \tau, \Delta t\ \} \tag{3.3}$$

As mentioned in Chapter II, the knowledge of the estimate of $S\ \tau, f$ by itself is enough to provide all the characteristics of the channel, that is, its multipath spread, Doppler shift and Doppler spread for all signal arrivals [72].

From Equations 3.2 and 3.3, it is evident that the estimation of $S\ \tau, f$ is based on prior knowledge of the channel's impulse response estimate $h_{est}\ \tau, t$. As a consequence, it is essential to estimate the channel impulse response

which can be easily accomplished by probing the channel with a DSSS signal. Consider a DSSS signal $x(t)$ that is sent through the underwater channel. In baseband this signal has the following form

$$x\ t\ = d\ t\ \ p_1\ t\ + jp_2\ t \tag{3.4}$$

where p_1 and p_2 are two different pseudonoise (PN) Gold sequences [22] of the same length N, modulated by the same data bit $d(t)$. The multipath fading channel is represented as a tapped delay line with L taps. The delay between the taps is set equal to the inverse of the sampling rate, as $T_s = \frac{1}{R_{sample}}$. Then the total length L of the tapped delay line has to correspond identically to the multipath spread of the channel T_m, that is $T_m = T_s \times L$.

The received signal at time t is the result of the summation of the L different contributions of delayed versions of the transmitted signal, weighted by the appropriate channel coefficients, given by:

$$r\ t\ = \sum_{l=0}^{L-1} h\ lT_s, t\ \ d\ \ t - lT_s\ \ \ p_1\ t - lT_s\ + jp_2\ t - lT_s \tag{3.5}$$

The receiver correlates the received signal with the known spreading sequence delayed by kT_s, and this process is repeated L times for each time delay from 0 to $L-1\ T_s$ seconds. For example, the result for a time delay of kT_s will be:

$$h_{est}\ \ kT_s, t\ = \sum_{n=0}^{N-1} \frac{1}{2L} r\ \ t + nT_s\ \ \ p_1\ \ t + nT_s - kT_s\ \ - jp_2\ \ t + nT_s - kT_s\ \ d\ \ t + nT_s - kT_s \tag{3.6}$$

and replacing $r(t + nT_s)$ in (3.6) using equality (3.5) we obtain:

$$h_{est}(kT_s, t) = \sum_{n=0}^{N-1} \frac{1}{2L} h\ \ nT_s, t\ \{L\ \ p_1\ \ nT_s - kT_s\ \ ^2 + L\ \ p_2\ \ nT_s - kT_s\ \ ^2\} \delta\ \ nT_s - kT_s \tag{3.7}$$

This implies

$$h_{est}(kT_s, t) = \sum_{n=0}^{N-1} \delta(nT_s - kT_s) h\ \ nT_s, t\ = h\ \ kT_s, t \tag{3.8}$$

where $\delta\ \ nT_s - kT_s$ is the discrete time impulse.

The result of Equations 3.7 and 3.8 shows that, at least in the ideal case, an estimate of the impulse response of the channel $h_{est}\ \tau,t$ can be computed by cross-correlating the transmitted and the received sequences. The assumptions are that the two sequences, $p_1\ t$ and $p_2(t)$, have ideal autocorrelations and that there is no noise in the receiver. In practice, the result will be degraded due to the noise and the non-ideal correlation properties of the Gold sequence [69].

3. Design Considerations on Channel's Probe DSSS Signal

The first consideration in the design of the signal is the bandwidth of the received acoustic signal, which is always limited by the non-uniform frequency response of the underwater sound projectors. Although a relatively flat frequency response along a wide frequency band would be ideal, this is usually not the case due to the limited bandwidth and the non-ideal frequency response of the transducers. As a consequence, the signal's bandwidth is determined by the frequency response of the transducer used [67, 73].

The form of the transmitted DSSS signal in baseband is given by Equation 3.4, where $p_1\ t$ and $p_2(t)$ are two different pseudonoise sequences of the same length, modulated by the same data bit $d\ t$. The characteristics of the PN sequence have to be like those of a true random white binary sequence as described by its autocorrelation function. The greater the number of chips N in the PN sequences, the closer the autocorrelation is to the ideal. A usual set of PN sequences used in communications are the Gold sequences.

The spreading sequence $p(t)$ is defined by two parameters, namely its period and its chip duration. These two parameters have to be set according to the expected spread in time and frequency of the channel.

In particular, the period T_{sym} of the PN sequence has to be longer than the multipath spread of the channel. The symbol rate has to be shorter than the inverse of the multipath spread:

$$R_{sym} < 1/T_m \simeq (\Delta f)_c \tag{3.9}$$

In case that inequality (3.9) holds, the channel is frequency nonselective.

Additionally, the period T_{sym} of the PN sequence has to be shorter than the channel's coherence time $(\Delta t)_c$:

$$T_{sym} < (\Delta t)_c \tag{3.10}$$

In case that inequality 3.10 holds, channel attenuation and phase shift are basically fixed for the duration of one symbol and the channel is slowly fading. The typical value for the coherence time is larger than 100 msecs [2], therefore, the symbol duration T_{sym} must be shorter than this value, a task that can be easily achieved.

By combining Equations 3.9 and 3.10, and since $B_d \approx 1/\Delta t_c$, it can be deduced that in case of a slowly fading frequency non-selective channel, the following inequality will hold:

$$T_m B_d < 1 \tag{3.11}$$

The product of Equation 3.11 is called the spread factor. If the spreading factor is smaller than unity the channel is characterized as underspread, an important condition for a reliable channel measurement.

The minimum time resolution in determining the impulse response of the channel will be T_{chip} seconds. Furthermore, in order to get accurate estimates of the Doppler effect on the acoustic signal from the scattering function and to avoid aliasing (sampling theorem), the symbol rate should be at least two times larger than the Doppler shift of the channel:

$$R_{sym} > 2 f_d \tag{3.12}$$

Therefore, there is a trade-off in the channel estimation in the presence of multipath and Doppler effects: a long symbol period T_{sym} is well suited to estimate multipath arrivals but is degraded in the presence of Doppler effects, while a shorter period T_{sym} is more suitable to estimate the Doppler effect rather

than the multipath effect. A compromise is needed between the multipath and Doppler effect. As a consequence, the probe used for channel estimation has to be designed for the particular environment where it will be applied. Another solution is to design and transmit multiple types of probes with different symbol periods, compute multiple channel estimates and choose the most accurate. In this solution the entire probe's duration will be fairly longer.

Experimental work in this field [2] reveals that a typical value for the multipath spread in a shallow water environment is on the order of a few tens of milliseconds (~30 msecs). By using Equation 3.9, the value of the symbol rate has to be smaller than 35 Hz. In the same time, for a typical UUV application and using a 12000 Hz center frequency, the typical Doppler shift will be on the order of 18 Hz [2] (for a UUV speed of 5 knots). Then by using Equation 3.12, the value of the symbol rate has to be larger than 36 Hz. Then, for a typical UUV application in a shallow water environment, a suitable symbol rate of the DSSS signal is 35 symbols per second.

It is difficult to set a priori value of the symbol rate to cover all underwater channels. The only solution for this concern is to design the signal for the purpose of its installation on the site where it is going to be used. For example, in a UUVs' operation in shallow waters there usually are short multipath spreads and a high Doppler effect, while in a stationary underwater network environment in deep waters there usually are a low Doppler effect and long multipath spreads.

B. ESTIMATION OF A SIMULATED CHANNEL

1. Setting Up the Simulation

After the completion of the channel identification algorithm description, a validation of the performance of the algorithm is presented. Toward this goal, an artificial time-varying channel is created. The artificial channel assumed to have three discrete paths for the eigenrays. It is also assumed that the transmitter and

receiver are stationary, which implies that there is no Doppler shift due to relative motion. Nevertheless, the channel is assumed to be time-varying due to the changes of the medium in the water column.

The artificial channel is developed so that each path has a different time-varying nature and hence a different Doppler spread. The first path (the direct path) is assumed to have zero time delay and the smallest Doppler spread. The other two paths correspond to the surface and bottom reflected eigenrays, having time delays of about 10 and 50 milliseconds respectively. The amplitudes of the three components of the impulse response are time-varying, resembling a real underwater channel with time-varying channel coefficients. The average multipath intensity profile of the artificial channel as a function of the time delay is illustrated in Figure 8; clearly, the multipath spread T_m of the artificial channel is 50 milliseconds.

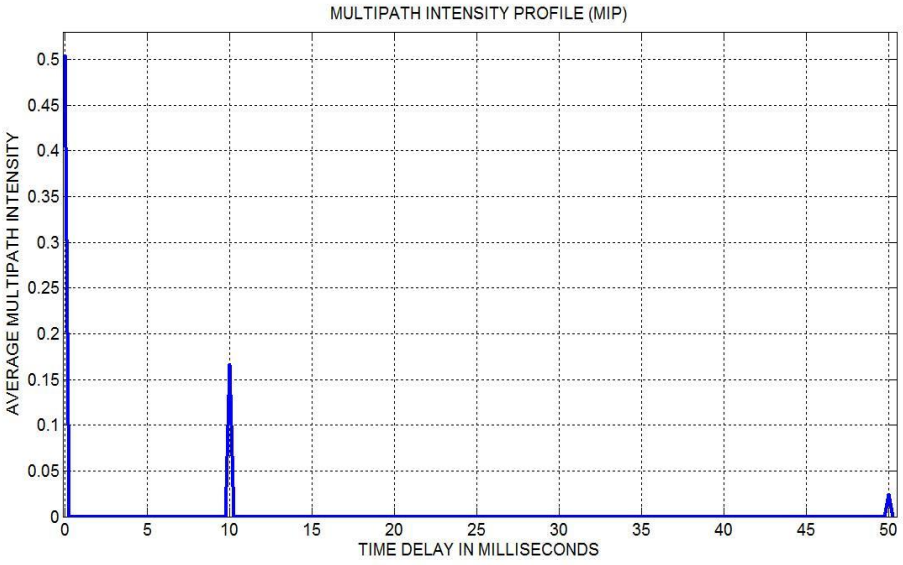

Figure 8. Multipath intensity profile of artificial signal (in time delay)

In order to evaluate the Doppler spread of the artificial channel, the space-time correlation function of the known artificial channel is used, as discussed in Chapter II. This function is expressed as the autocorrelation of each component of the impulse response:

$$S_{hk}\ \Delta t\ = \frac{\mathrm{E}\{|\ h_k^*\ t\ h_k\ t+\Delta t\ |^2\}}{\mathrm{E}\{|\ h_k^*\ t\ h_k\ t\ |^2\}} \quad k=1,2,3... \tag{3.13}$$

In this case, the impulse response has only three nonzero components, so there are three autocorrelation functions, which are illustrated in Figure 9. According to the previous discussion, the period of time over which this function is approximately constant is the coherence time of the specific path.

In this example, consider that the coherence time corresponds to the period Δt over which $S_{hk}(\Delta t)$ is greater than 0.5. Assume the coherence time for the direct path case to be 1.8 seconds, for the second path 1.6 seconds and for the third path 1.16 seconds, which are realistic values for a slowly time-varying acoustic communication channel. Since the Doppler spread B_d is equal to the inverse of the coherence time, the corresponding spreads for the three paths are 0.55 Hz, 0.86 Hz and 0.63 Hz, respectively.

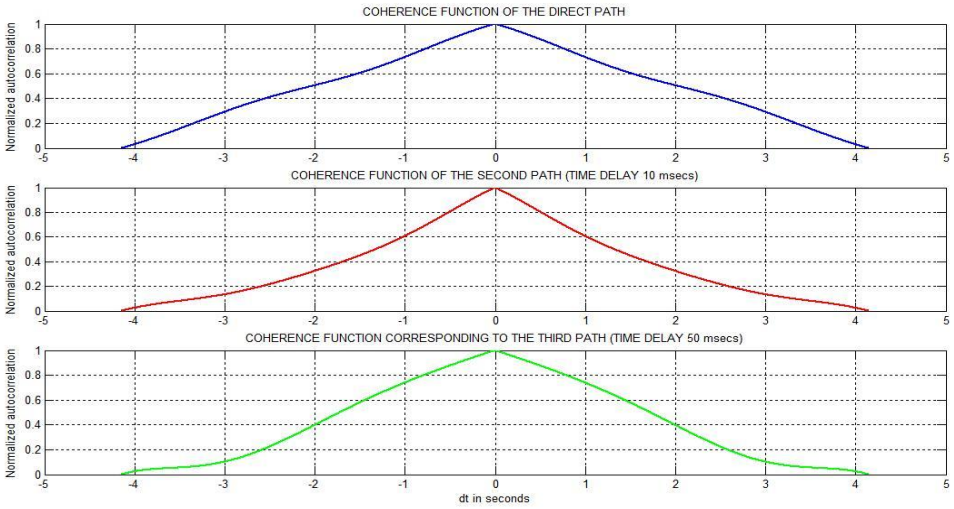

Figure 9. Coherence function of the three components of the impulse response

The transmitted signal in the artificial channel is a DSSS baseband signal like the one described before. It uses PN sequences defined by two different Gold codes of length 2047, one on the in-phase and the other on the quadrature

component, modulating the same data bit. The chipping rate used in the simulation is 4000 chips/second. In what follows, an information sequence of 8 bits is sent, so the duration of the entire information sequence is 4.094 seconds. The signal is corrupted by the presence of additive white Gaussian noise, resulting in a 7 dB SNR.

2. Results of the Simulation

The channel identification method that was previously analyzed seems to have robust performance for this simulation. The estimated multipath intensity profile (MIP) is almost the same as the original MIP illustrated in Figure 10. Also, the algorithm's estimates for the impulse response coefficients follow the variability of the original ones.

The most significant function in this analysis is the scattering function $S(\tau,\nu)$ of the channel, introduced in the previous chapters, which combines information about both the frequency and time spread of the channel. In Figure 10, the artificial channel's normalized scattering function is illustrated. By inspecting the plot, a few conclusions can be drawn. First, information about the channel is revealed showing that it has three dominant paths with time delays 0, 10 and 50 milliseconds respectively. Even if it seems that the second path is stronger than the other two, this is not the case. The apparent discrepancy is because the DC component of the impulse response was deleted before processing. Another important observation is that the Doppler spread of the second path is by far the largest. Finally, since the functions are centered on the zero frequency, then the Doppler shift of the underwater channel must be zero, which is consistent with a fixed transmitter-receiver geometry.

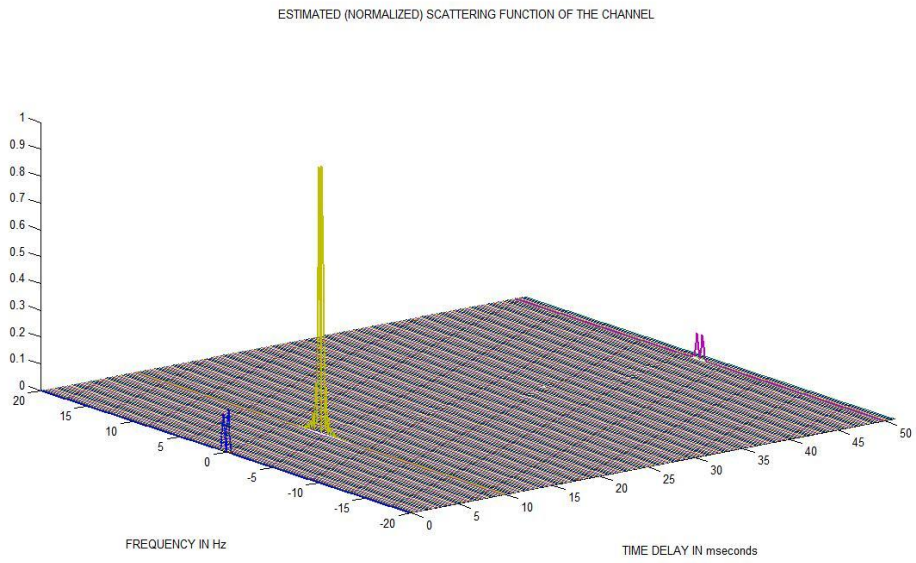

Figure 10. Estimated normalized scattering function of the artificial channel

The analytical estimation of the Doppler spread of the dominant paths is accomplished by finding the bandwidths of the scattering functions $S(\tau,\nu)$ corresponding to those paths. In order to determine the bandwidth, we follow the definition of rms bandwidth:

$$B_{d,\tau} = \sqrt{\frac{\int_{-\infty}^{+\infty} f^2 \,|S_\tau(f)|\,df}{\int_{-\infty}^{+\infty} |S_\tau(f)|\,df}} \tag{3.14}$$

The resulting estimated values, as well as the values calculated earlier from the coherence times $(\Delta t)_c$ of Doppler spreads, are summarized in Table 1. The result shows that the values of the Doppler spread estimated two different ways are close to each other.

Path	Calculated Doppler spread from coherence time of the channel	Estimated Doppler spread using the algorithm
Direct path	0.55 Hz	0.46 Hz
2nd path (*10* ms delay)	0.86 Hz	1.04 Hz
3rd path (*50* ms delay)	0.63 Hz	0.74 Hz

Table 1. Doppler spreads of the dominant paths of the underwater channel

C. CHANNEL ESTIMATION ON NEW ENGLAND SHELF EXPERIMENT

1. Description of Experimental Setup

After the theoretical description and the verification of the channel's identification algorithm through a simulation, the next task is to validate its performance with the use of experimental data from two different experiments. In the first case, data were collected during April 2000 in the Forefront-2 experiment over the New England shelf area [74, 75, 76].

The experimental setup was as follows: the receiver was deployed on the ocean bottom at a depth of about 30 meters in a stationary position while the transmitter was an over-the-side projector deployed at a depth of about 20 meters, and probe signals were transmitted from the R/V Connecticut as it was drifting away from the receiver. The received waveforms were taken at ten transmitter-to-receiver ranges starting at 700 meters and increasing to 6550 meters. The scope of these multiple ranges was to examine in more detail the behavior of the underwater channel as the distance grew [74].

Figure 11 provides a plot of the bottom topography (bathymetry) and source track. The position of the stationary receiver is indicated with the letter R while the position of the transmitter for the ten different cases (corresponding to ten different distances from the receiver) is indicated by the letters T1 to T10.

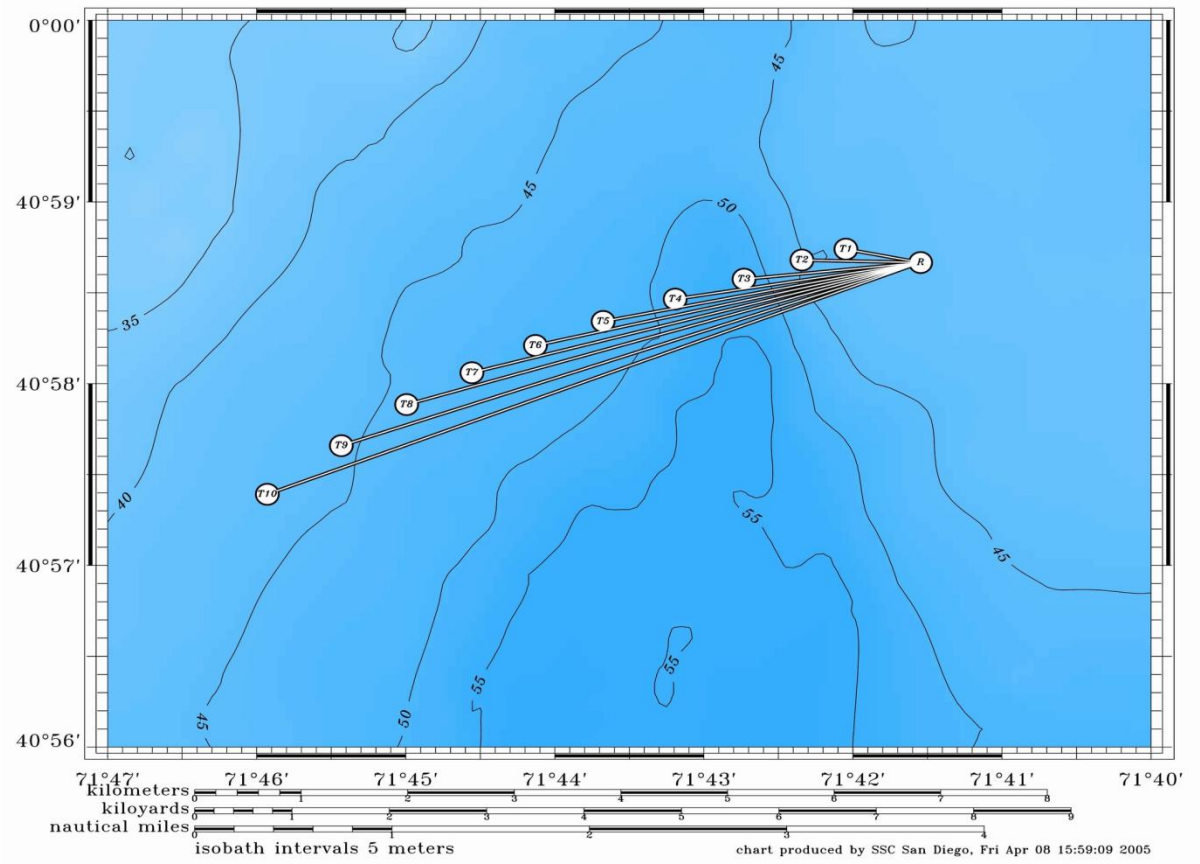

Figure 11. Bathymetry, Transmitter–Receiver positions

In order to determine the sound speed profile in the underwater channel, prior to the experiment, measurements from a CTD instrument were used, which measures Conductivity, Temperature and Depth (thus the name CTD). All theoretical impulse response plots and results were developed based on this measured sound speed profile, which is illustrated in Figure 12.

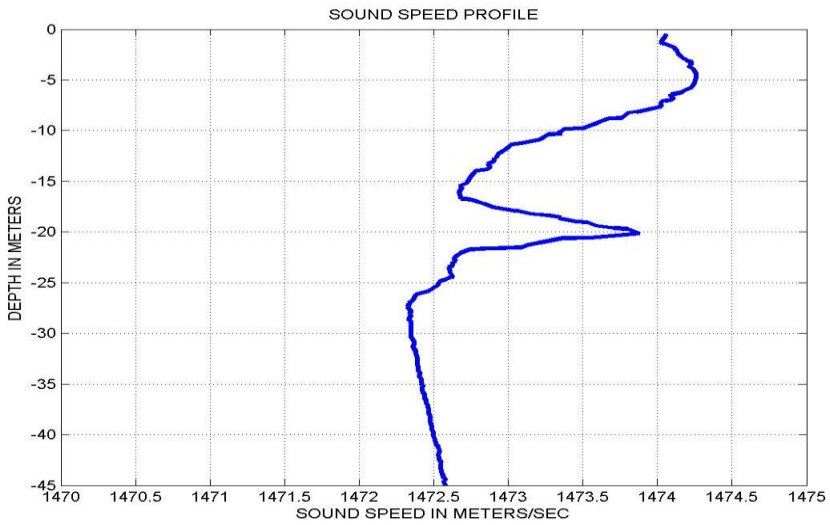

Figure 12. New England shelf experiment's sound speed profile

2. Description of DSSS Signal Used for Channel Identification

The direct sequence spread spectrum signal used for channel identification has almost the same format as the DSSS signal used previously for the artificial acoustic communication channel. It is a bandpass direct-sequence spread spectrum signal with center frequency of 12 kHz, a chip rate of 2000 chips/second and a sampling rate of 48000 samples/second [75, 76].

In this experimental setup, six different DSSS probes are sent through the underwater channel. In all six cases, the same number of four hundred information bits was transmitted. Two different Gold sequences were used as spreading sequences; a different PN sequence is used for the in-phase and quadrature data, although the same information bit is modulated by each component, leading to a DSSS/BPSK scheme. The six different probes correspond to six different bit rates of 10, 20, 50, 100, 200 and 400 bps. In all cases, the chip rate and length of the Gold sequence are kept constant. For example, in the first case about 400 chips are modulated by one data bit, in the second case 200 chips are modulated by one data bit, etc. Intuitively, this implementation would result in greater correlation noise than in the ideal

simulated case previously considered, in which the entire length of the Gold sequence was modulated by one data bit. In order to minimize this problem, the lower bit rate probe (first probe with 10 bps) will be used for the channel estimation, so a portion of the Gold code is used and not the entire sequence [75, 76].

The signal train is transmitted from a single projector and is received from a single hydrophone as well. The signal train is transmitted repetitively 10 times during the experiment for 10 different distances and resulting signals to noise ratio (SNRs).

3. Experimental Results

In this paragraph, the results of the channel estimation algorithm using real data from the New England shelf experiment will be presented. From a total of ten different channel cases, only one characteristic example will be discussed in detail. In this example the distance between transmitter and receiver is 1100 meters and the signal to noise ratio in the receiver is approximately 35 dB.

The first plot illustrates the MIP $P_h\ \tau$ of the channel as a function of the time delay τ. $P_h\ \tau$ is the average power out of the channel and a function of the time delay τ. The estimated multipath intensity or power delay profile of the channel is illustrated in Figure 13.

In order to validate the accuracy of the estimate, the eigenrays characterizing the acoustic propagation channel were traced using a numerical model called Bellhop [77] (see Figure 13). The estimate of the MIP from the Bellhop model is presented in Figure 13. Note that the Bellhop channel modeling neglects boundary losses and shows arrivals with artificially high intensity. Comparison of Figures 14 and 15 shows a consistency between the theoretically estimated MIP and the one estimated from the actual data. From Figure 14, the multipath spread of the channel using real data is determined to be about 11.5 milliseconds, whereas from Figure 13 using Bellhop channel modeling it is

determined to be about 11 milliseconds. Finally, from both Figures 14 and 15, it is deduced that there are nine dominant paths in this underwater channel.

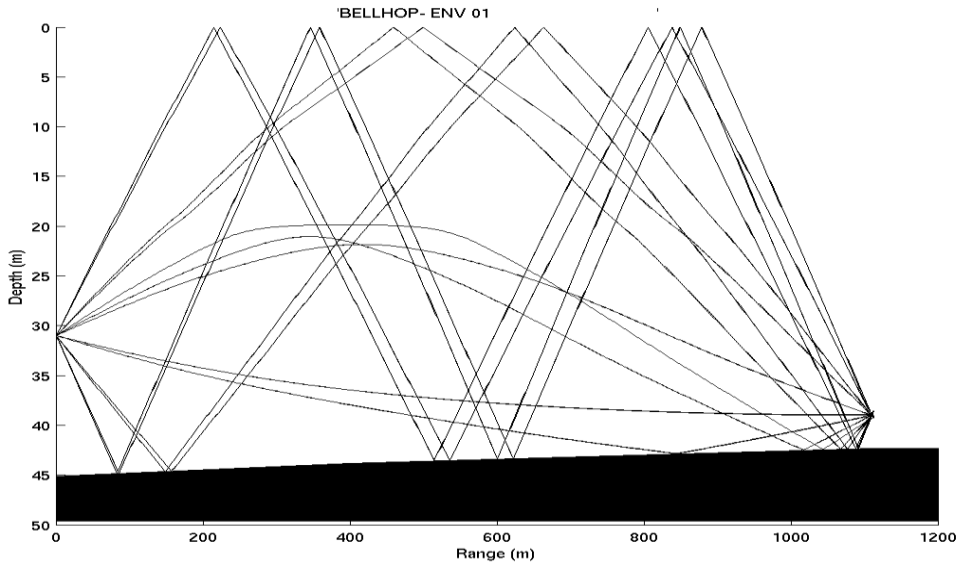

Figure 13. Eigenrays plot for distance of 1100 meters

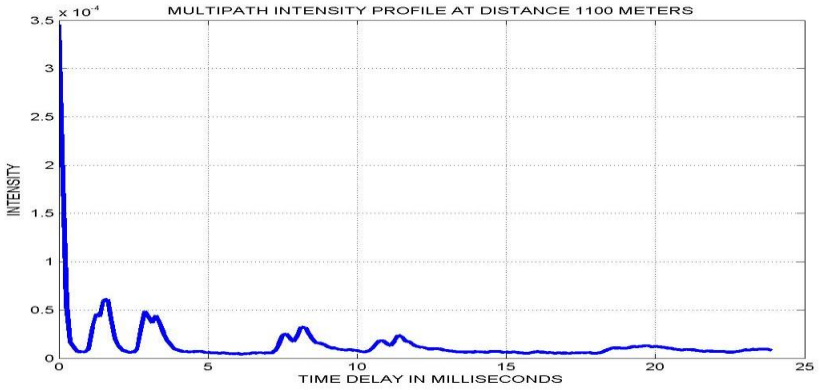

Figure 14. Multipath Intensity Profile for SNR=35dB using DSSS signal

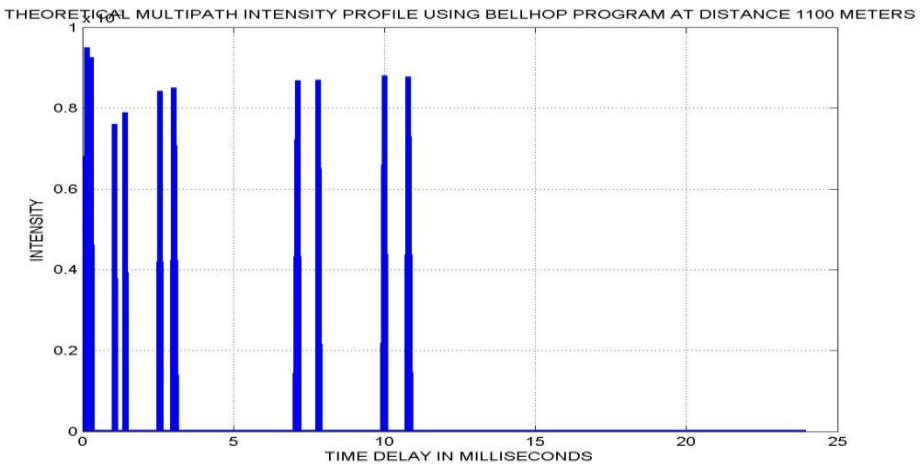

Figure 15. Multipath Intensity Profile for SNR=35dB – numerical model estimate

Following the method developed earlier and using the DSSS signal in baseband, the scattering function of the underwater channel is determined as shown in Figure 16. The Doppler spread of the dominant paths is estimated by finding the bandwidths of the scattering functions $S(\tau,\nu)$ corresponding to those paths, while the Doppler shift is determined by finding the center frequency for each path. A point of special interest in the result of Figure 16 is that from a possibly noisy impulse response estimate an unambiguous scattering function plot is obtained. Inspection of the plot shows that there is a negative Doppler shift, consistent with the opening range of the source-receiver geometry, and a Doppler spread that is different for each path.

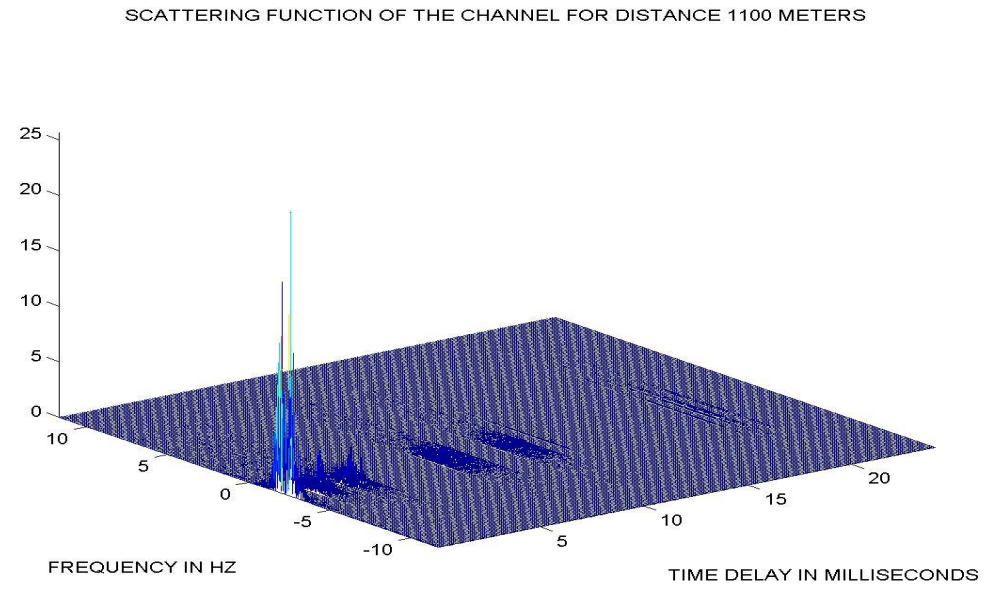

Figure 16. Estimated Scattering function of the channel for SNR=35dB

The estimated values of the Doppler shift and the Doppler spread for the eight dominant paths of this underwater channel are presented in Table 2. In order to validate the estimated Doppler shift values, some tone probes transmitted prior to the DSSS signal were used. The tone probe method resulted in a Doppler shift value of -2.3Hz. The value of the Doppler shift corresponding to the first path, estimated from the scattering function is -2.25 Hz, which agrees with the result obtained from the probes. The stronger paths have relatively smaller Doppler spreads of 0.8 to 1.8 Hz while the weaker paths have larger spreads of 2.2 to 2.6 Hz. Because the weaker paths are subject to faster varying fluctuations due to the greater number of reflections at the non-stationary sea surface compared to the stronger paths, a higher Doppler spread is expected. This high variability of the weaker paths can possibly cause a DFE to fail in a coherent reception communication scheme [56, 78, 79, 80].

PATH WITH TIME DELAY (in msec):	DOPPLER SHIFT (HZ)	DOPPLER SPREAD (HZ)
0	−2.25	0.83
1.5	−2.15	1.50
2.875	−2.05	1.70
3.25	−2.1	1.84
7.625	−1.8	2.25
8.125	−1.8	2.13
10.75	−1.65	2.62
11.375	−1.6	2.40

Table 2. Doppler spreads and shifts of the dominant paths for SNR=35dB

D. CHANNEL ESTIMATION ON MAKAI 2005 EXPERIMENT

1. Description of Experimental Setup

The second experiment (MAKAI 2005) was conducted in September 2005 in Kauai, Hawaii. The experimental setup was as follows: there were two arrays, the receive array consisting of eight hydrophones separated by about 25 centimeters and the transmit array consisting of ten projectors separated by 2 meters. The 10 element source array was deployed over the side of the drifting Kilo Moana vessel with its deepest hydrophone in 26 meters depth. The 8-element receiving aperture was drifting as well and its deepest element was located in 5 meters depth. While the two arrays were both drifting freely, the distance between them stayed almost unvarying in a value of about 2200 meters for all the duration of the experiment (for about 30 minutes) [81, 82].

A plot of the bathymetry between the transmit and receive arrays is provided in Figure 17. Following this figure, for each time instant (y-axis) the position of the transmit array is located at the origin, while the position of the receive array is located on the white line. Different depths are indicated by different colors. The simultaneous drifting of the two arrays can be easily realized since, even if the shape of the seabed in between the transmit and receive arrays changes, their distance stays almost constant through time.

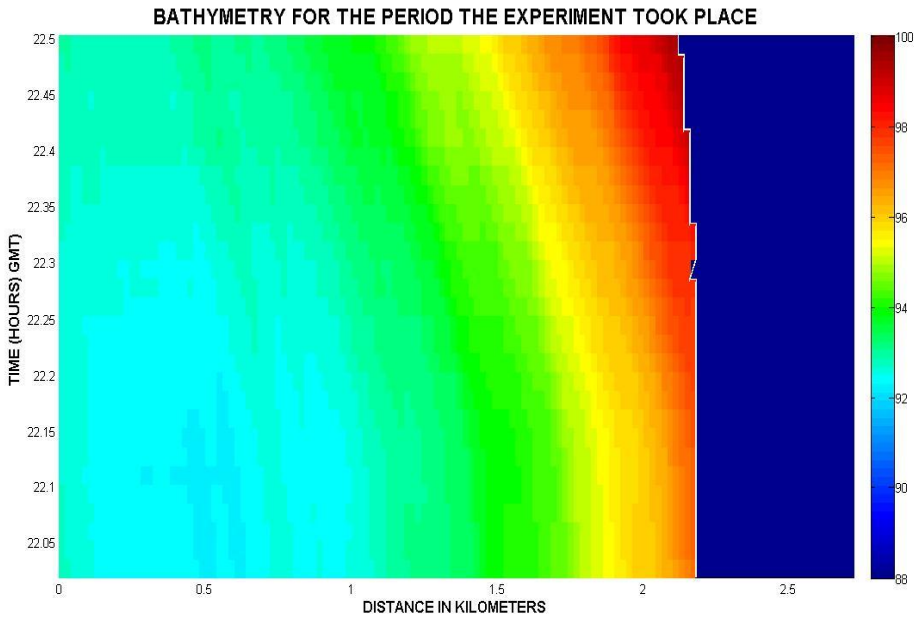

Figure 17. Bathymetry between transmitter and receiver

Figure 18 illustrates a plot of the measured sound speed profile. For this measurement a CTD instrument was used prior to the experiment. As in the New England shelf experiment, all the following theoretical impulse response plots and results are based on this measured sound speed profile.

Figure 18. MAKAI 2005 experiment's sound speed profile

2. Description of DSSS Signal Used for Channel Identification

The signal used for channel identification in the MAKAI 2005 experiment is a bandpass direct-sequence spread spectrum signal with center frequency of 35 kHz, a chip rate of 20000 chips/second and a sampling rate of 160000 samples/second.

In this experimental setup, five different DSSS probes were sent through the underwater channel. In all five cases, the same number of 144 information bits was transmitted. Two different Gold sequences were used as spreading sequences; a different PN sequence was used for the in-phase and quadrature data, although the same information bit is modulated by each component, leading to a DSSS/BPSK scheme. The six different probes correspond to six different code lengths, keeping the chip rate constant. The Gold code lengths used in the experiment were: 63 chips/bit, 127 chips/bit, 511 chips/bit, 1023 chips/bit and 2047 chips/bit. Different code lengths and invariant chip rate lead to different bit rates for each case. The lowest bit rate (for code length 2047) is approximately 10 bps, while the highest bit rate (for code length 63) is approximately 318 bps.

The signal train is transmitted from a single projector and received from an array of 8 different hydrophones with a separation between them of about 6 wavelengths (related to the center frequency). As will be clarified in the next paragraphs, different code length signals will be used for different tasks. Therefore, longer code length signals will be used for channel identification and RAKE receiver implementation schemes, while short code length signals will be used for more advanced types of receivers. Finally, the signal train is transmitted repetitively twelve times during the experiment.

3. Experimental Results

In this paragraph, the results of the application of the algorithm to real data of the MAKAI 2005 experiment will be presented. From the twelve distinct repetitions of the experiment, only one characteristic example will be presented.

In this example the distance between the transmitter and receiver is about 2200 meters and the signal to noise ratio in the receiver is very low, between 1 and 2.5 dB, depending on the receiving hydrophone in the array. For each repetition there are eight distinct acoustic channels (one for each receiving hydrophone). In this channel recognition example, two channels will be analyzed.

a. Channel Identification for Receiving Hydrophone in 3 Meters Depth

The first example concerns a situation where the transmitting projector is situated in 8 meters depth and the receiving hydrophone is situated in 3 meters depth, 2200 meters from each other. The SNR at the input of the receiver is approximately 2 dB (direct sequence processing gain is not included in the value of SNR). For the channel identification, in this example, the DSSS/BPSK signal with code length 511 chips will be used. The resulting symbol duration in this case will be 25.5 milliseconds. As stated before, in order to have accurate channel identification, the DSSS symbol duration must be greater than the multipath spread of the channel.

The plot in Figure 19 shows the eigenrays characterizing the propagation channel, traced using the Bellhop numerical model. The estimated MIP $P_h\ \tau$ of the channel as a function of the time delay τ is illustrated in Figure 19. In order to validate the accuracy of the estimate, the Bellhop numerical model was again used and an MIP theoretical estimate was obtained. The Bellhop numerical method estimate of the MIP is presented in Figure 19. Comparison of Figures 20 and 21 shows a consistency between the theoretically estimated MIP and the one estimated from the actual data. The multipath spread resulted from the theoretical model is 7.3 msecs while the multipath spread from the actual data is 7.15 msecs. Due to the form of sound speed profile, the geometrical structure of the underwater channel and the depths of the transmitter and receiver, the signal comes in two separate clusters. The first energy cluster has a

duration of 0.45 msecs, while the second cluster has a delay of 5.5 msecs and a duration of 1.3 msecs. The above results agree for both the theoretical and experimental methods.

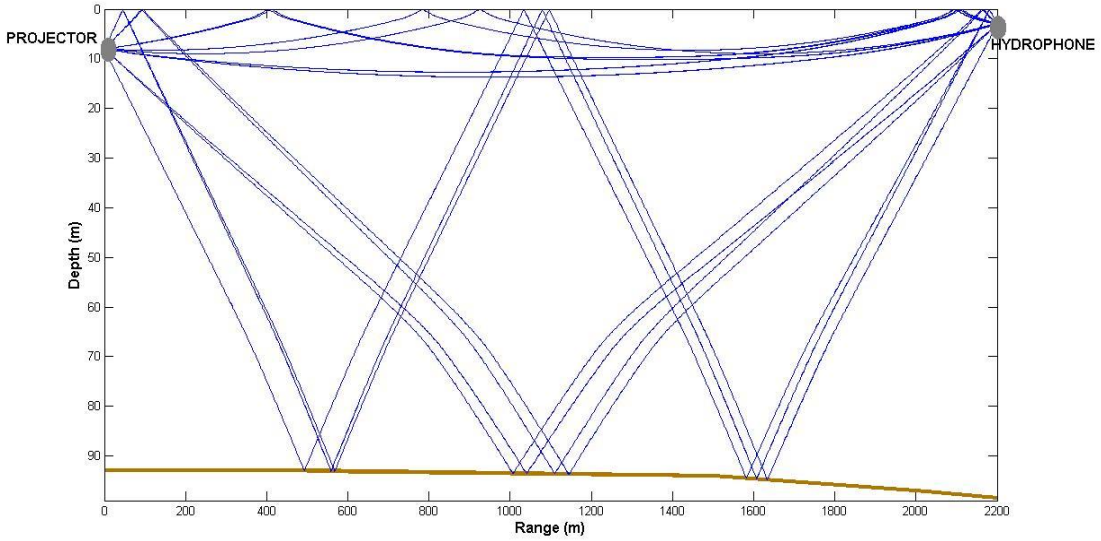

Figure 19. Eigenrays plot for receiver located in 3 meters depth

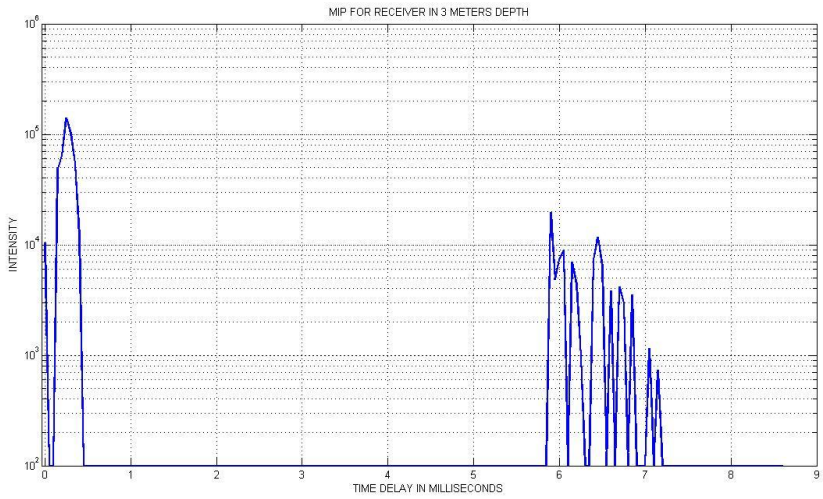

Figure 20. MIP for receiver in 3 meters depth SNR=2 dB – experimental result

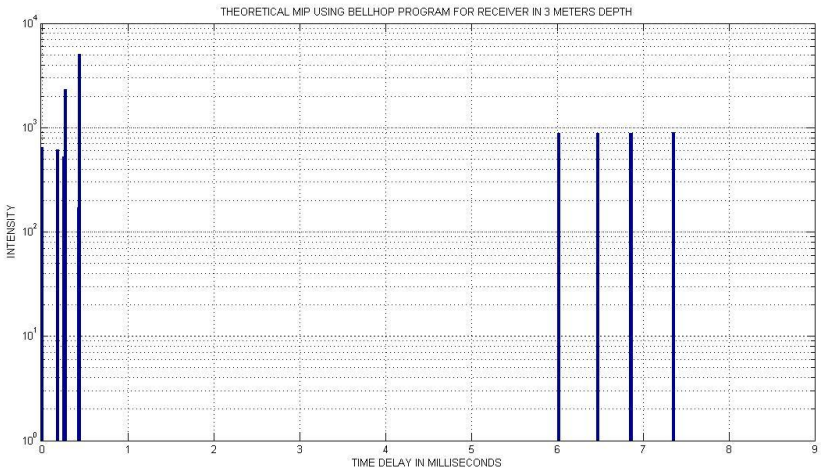

Figure 21. MIP for receiver in 3 meters depth, SNR=2 dB – theoretical estimate

Following the method developed earlier and using the DSSS signal in baseband, the scattering function of the underwater channel (shown in Figure 22) is determined. From this function, Doppler spread and Doppler shift of the dominant paths are estimated, as pointed out earlier. Inspection of the plot shows a small positive Doppler shift and a Doppler spread different for each path.

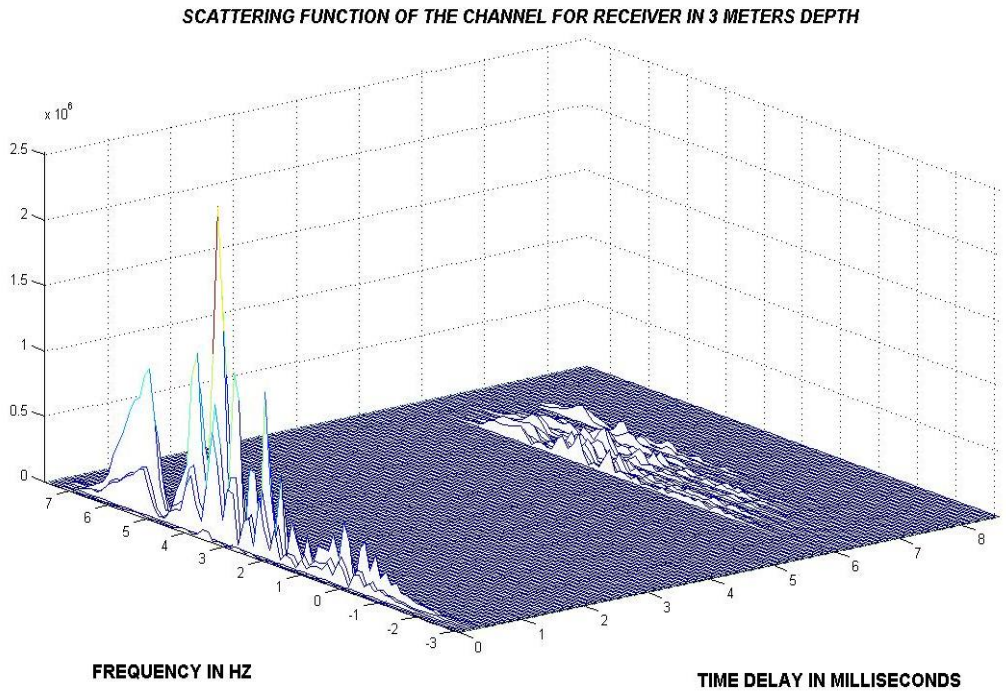

Figure 22. Estimated scattering function, receiver in 3 meters depth, SNR=2 dB

The estimated values of Doppler shift and Doppler spread for the eight strongest paths of this underwater channel are presented in Table 3. An interesting feature that was also apparent in the New England shelf experimental results, is that the Doppler spreads of the stronger paths are smaller than those of the weaker paths. In general there are small values of Doppler shifts for all paths. Those values are positive and vary from 2.7 Hz to 3.8 Hz, corresponding to reasonable drift rates from 0.23 to 0.33 knots. Comparing these values with the whole setup of the experiment reveals a slow drift of both transmitter and receiver, leading to a very slow positive relative motion. Independently of the short values of Doppler shifts, the variability between the paths is high.

PATH WITH TIME DELAY (in msec):	DOPPLER SHIFT (HZ)	DOPPLER SPREAD (HZ)
0.1500	3.2590	2.4645
0.2500	3.3715	2.1326
0.3500	3.3063	2.6067
5.9000	3.1258	3.0987
6.2000	3.1013	3.5745
6.4500	2.6852	4.1648
6.8500	2.7219	5.1129
7.0500	3.8329	4.2672

Table 3. Doppler spreads and shifts of stronger paths for receiver in 3 m

b. Channel Identification for Receiving Hydrophone in 5 Meters Depth

The second example concerns a situation where the transmitting projector is situated in 8 meters depth and the receiving hydrophone is situated in 5 meters depth, 2200 meters from each other. The SNR at the input of the receiver is about 2.5 dB. (Direct sequence processing gain is not included in the value of SNR.) Like the previous example, a signal with code length 511 chips will be used.

The plot in Figure 23 shows the eigenrays characterizing the propagation channel, traced using the Bellhop numerical model. The estimated MIP $P_h\ \tau$ of the channel as a function of the time delay τ is illustrated in Figure 24, while the Bellhop theoretical estimate of the MIP is presented in Figure 25. Comparing Figures 24 and 25 shows a consistency between the theoretically estimated MIP and the one estimated from the actual data. The multipath spread resulted from the theoretical model is 7.3 msecs while the multipath spread from the actual data is 6.7 msecs. The reason for this difference seems to be that either the last path from the theoretical model is not present or or most probably it is very attenuated by the channel. Except for this detail, mostly, the channel's MIP is quite similar to the one estimated in Example a. The signal comes again in two separate clusters. The first energy cluster has a duration of about 0.4 msecs,

while the second cluster shows up 5.4 msecs later and has a duration of 1 msec. (The theoretical duration of cluster is 1.4 msec due to the absence of the fourth arrival in the cluster.)

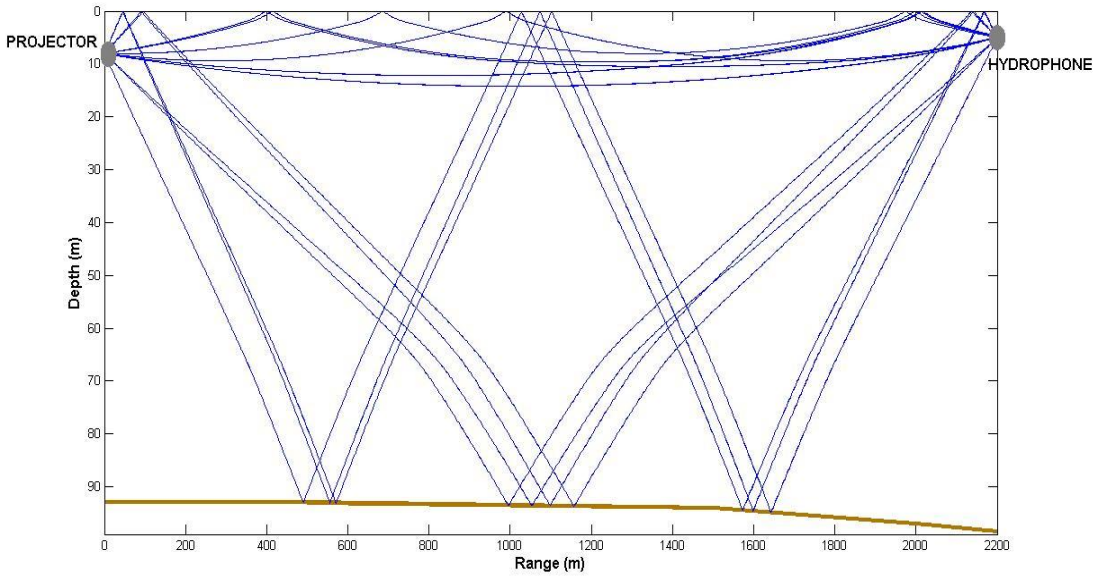

Figure 23. Eigenrays plot for receiver located in 5 meters depth

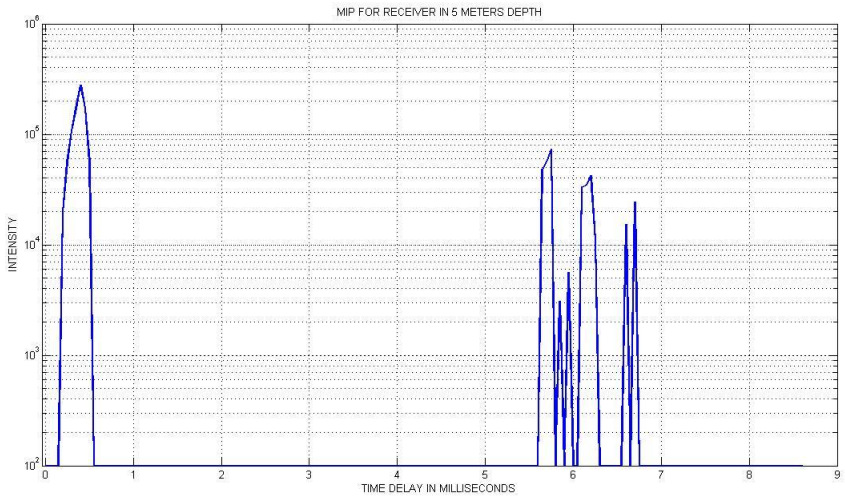

Figure 24. MIP for receiver in 5 meters depth SNR=2.5 dB – experimental result

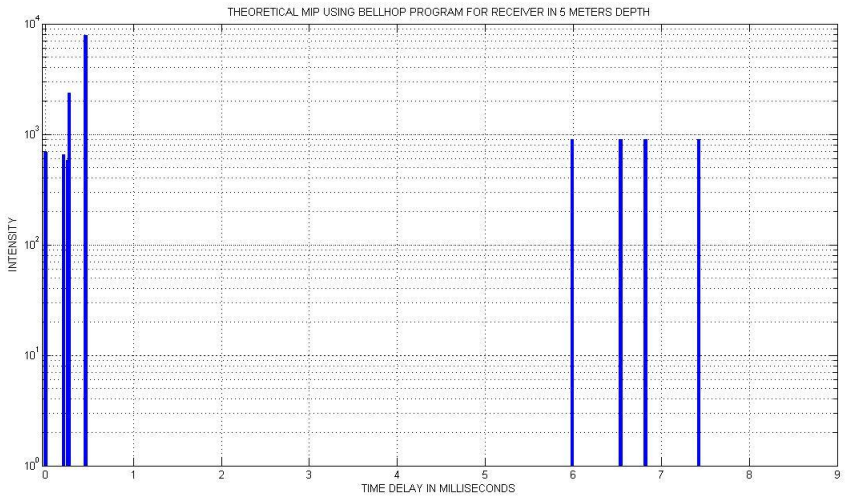

Figure 25. MIP for receiver in 5 meters depth, SNR=2.5 dB – theoretical estimate

Following the method developed earlier and using the DSSS signal in baseband, the scattering function of the underwater channel (shown in Figure 26) is determined. Inspection of the plot reveals that the Doppler shift for this case is still positive, but much smaller than in the first example. It seems that the free drift of the receiving array produces, for the period of the experiment, a larger relative speed (between transmitter and receiver) in the higher hydrophone than in the lower hydrophone. Taking into account the low depth at which the receiving array was situated, it can be deduced that its behavior is probably the result of swaying due to a passing wave or sea surface current.

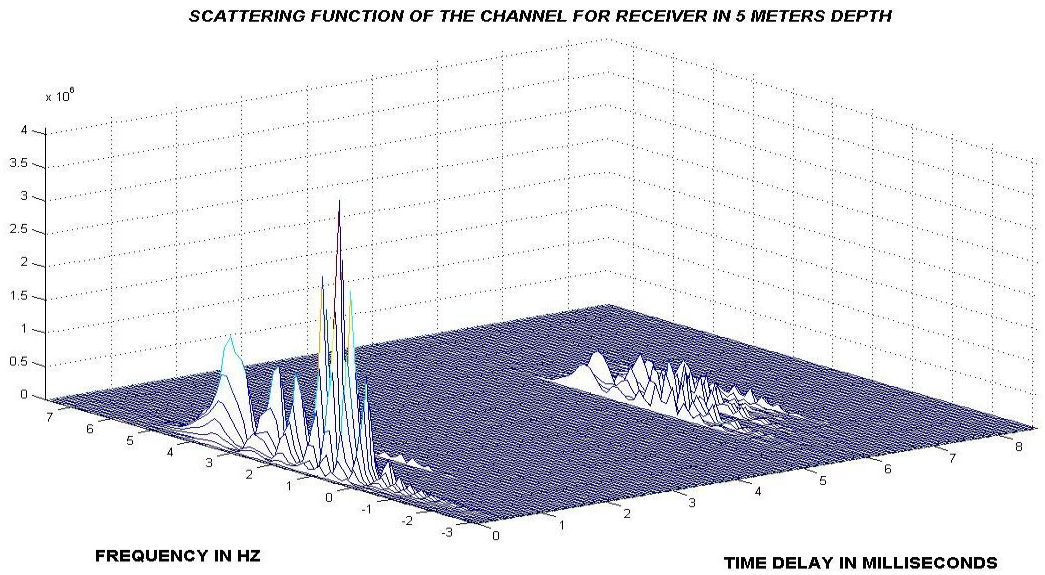

Figure 26. Estimated scattering function, receiver in 5 meters depth, SNR=2.5 dB

The estimated values of Doppler shift and Doppler spread for the eight strongest paths of this underwater channel are presented in Table 4. Even though the two underwater acoustic channels presented are quite similar, the Doppler Effect has a totally different influence in each case. The values of Doppler shifts for all paths are very small. Those values are positive and vary from 1.4 Hz to 2 Hz, corresponding to reasonable drift rates from 0.12 to 0.17 knots.

PATH WITH TIME DELAY (in msec):	DOPPLER SHIFT (HZ)	DOPPLER SPREAD (HZ)
0.3000	1.8436	2.0887
0.4000	1.8721	1.7937
0.5000	1.7970	2.4471
5.6500	1.7729	2.2224
5.7500	1.4036	2.4697
6.1000	1.7959	1.9974
6.2000	1.6711	2.3913
6.6000	2.0451	3.0180

Table 4. Doppler spreads and shifts of stronger paths for receiver in 5 m

IV. SIGNAL SYNCHRONIZATION

This chapter addresses the problem of initial synchronization to determine the starting time of the data packet in a multiuser environment using code-division multiple-access. A robust synchronization method will be presented, compared with other methods and tested using simulations and experimental results.

A. COMMUNICATION IN A MULTIUSER ENVIRONMENT

The goal of this research is to develop a robust acoustic communication scheme for a multiuser environment. Possible users in this environment can be the nodes of an underwater network or a number of autonomous underwater vehicles (AUVs). A multiple access communication method is needed, therefore, to enable many users to communicate without interference.

Among all types of multiple access, CDMA was chosen because it is particularly suitable to time-varying frequency-selective channels, as encountered in the research [83]. Furthermore, in the proposed scheme, direct-sequence CDMA signaling will be used both for channel identification and communication purposes. DS/CDMA systems can also be used for hiding a low-power signal below the noise floor. Another advantage of CDMA systems is covertness, particularly important in military applications.

All multiple access methods require that signals corresponding to different users be separated, so that they do not interfere with each other. Especially for DS/CDMA, in order to satisfy this condition, orthogonal or nearly orthogonal codes are assigned to different users. The orthogonality of the code is exploited at the receiver to despread the appropriate signal to the intended user. Since the receiver's performance depends on the orthogonality between the codes, these codes need to have good autocorrelation and cross-correlation properties. During the experimental work of this research, Gold codes have been used in DS/CDMA.

In DS/CDMA systems, two types of receivers exist: single-user and multiuser receivers. In the first case, the receiver has knowledge of only its spreading code, whereas in the second case it detects any number of signals by having the knowledge of all codes. The performance of multiuser receivers is superior to that of single-users, but their complexity is considerably higher [55]. In this research, the proposed scheme is a single-user receiver with improved performance due to the insertion of an interference cancellation mechanism.

The choice of the code's spreading factor is based on the desired application of the receiver. Since the available bandwidth in underwater acoustic communications is limited, the chip rate of the system will be determined by this bandwidth, while the bit rate is determined by the spreading factor. Therefore, the higher the spreading factor, the lower the bit rate. At the same time, the desired number of supported users is proportional to the spreading factor. For example, in order to support N users to communicate without interference with each other, a spreading factor at least N should be chosen. In general, a higher spreading factor is justified in situations where a high bit rate is sacrificed to either achieve a low probability of detection or to support multiple users [84].

B. INTRODUCTION TO DSSS SIGNAL SYNCHRONIZATION

1. Theoretical Background

A DSSS receiver uses the spreading code to detect the received signal that is hidden in noise and possible interference from other users. In order for the signal to be properly demodulated, the received signal has to be acquired and synchronized.

During the acquisition phase, the received signal is detected and coarsely aligned in time with the locally generated spreading signal. Usually this is accomplished by a preamble, with information known at the receiver [85]. Once the data is acquired, synchronization has to be maintained for the whole demodulation process [85, 86].

2. Single Correlator Performance in a Fading Environment

The simplest method of acquisition is based on the use of a single correlator. This arrangement is suitable for channels where the multipath effect is minimal, since that effect would yield ambiguous results. The situation worsens for time-varying channels with considerable Doppler shift.

The effects of a fading environment on the performance of the single correlator have been studied by computer simulation.

In the simulation, a preamble signal was used which contains three DSSS waveforms generated by Gold sequences. Each waveform consists of 250 chips, with different spreading codes employed for both in-phase and quadrature components. Their duration is 62.5 milliseconds, with a silence period of 100 milliseconds between them. The process of acquisition can be accomplished by a sliding correlator, which cross-correlates the received signal with the known replica of the preamble over successive time intervals.

In the next section, three different channel cases will be examined and the acquisition results obtained during the simulation will be presented and discussed.

a. Signal Acquisition in Ideal AWGN Channel

In the ideal AWGN channel without fading, if a preamble signal is present, the correlator output will be clearly defined by an impulse showing where the preamble starts. Detection is achieved by a simple threshold. A non-fading AWGN example with signal to noise and interference ratio of 10 dB is illustrated in Figure 27. In this case, the maximum of the correlator output, when the preamble is present, is proportional to the duration of the preamble. This means that, by extending the preamble's duration, and thereby suppressing the noise, there are only advantages; later it will be proven that this is not the case for the actual underwater channel.

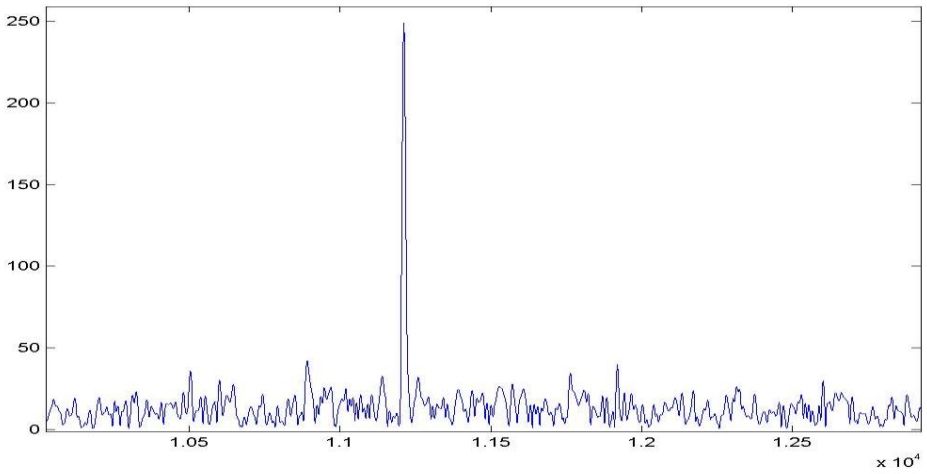

Figure 27. Correlator output for AWGN non-fading case (SNRI=10 dB)

b. Signal Acquisition in Fading Channel—No Doppler Distortion

In a typical underwater channel, multipath fading effects have to be considered. In an ideal case, in the absence of appreciable Doppler shift, the output of the single correlator is bound to have multiple pulses, each one caused by a distinct corresponding propagation path. In any event, by choosing the first peak, not necessarily the strongest in the correlator output, the signal can be acquired by determining the beginning of the preamble. Figure 28 shows an example of a multipath fading channel with AWGN, no Doppler spread, and signal to noise and interference ratio of 10 dB.

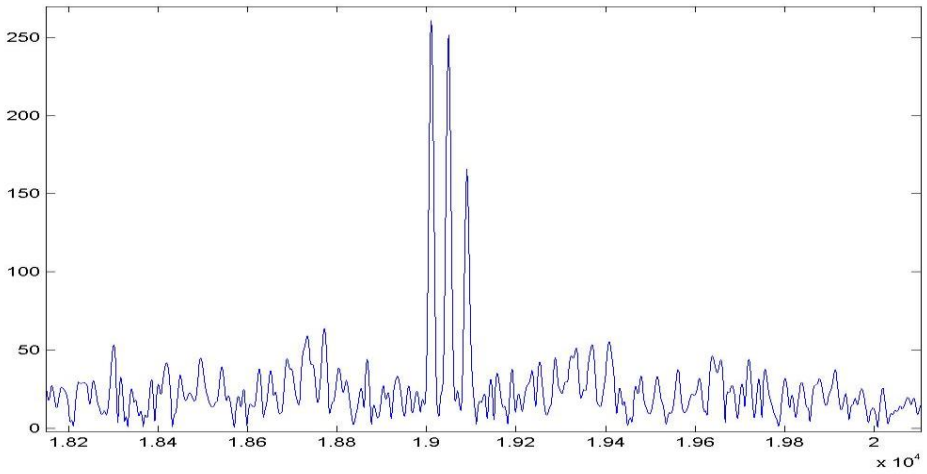

Figure 28. Correlator output for multipath fading case no Doppler distortion (SNRI=10 dB)

c. Signal Acquisition in Fading Channel With Doppler Distortion

In the more realistic case of a time-varying channel with multipath fading, Chapter III notes that the Doppler shift has a different value for each multipath component. Nevertheless, these Doppler shift values are close to each other. Usually the largest Doppler shift value corresponds to the first reception and decreases for the latter receptions. For this type of channel, the signal cannot be acquired by a single correlator, which calls for the development of a different technique.

In the case where the Doppler effect is small (in a sense to be defined later in this section), the acquisition capability will still be satisfactory. But as the Doppler effect gets more severe, acquisition eventually becomes impossible. Figure 29 shows the influence of the Doppler effect on the correlator's output as the Doppler shift increases two and four times from the initial value.

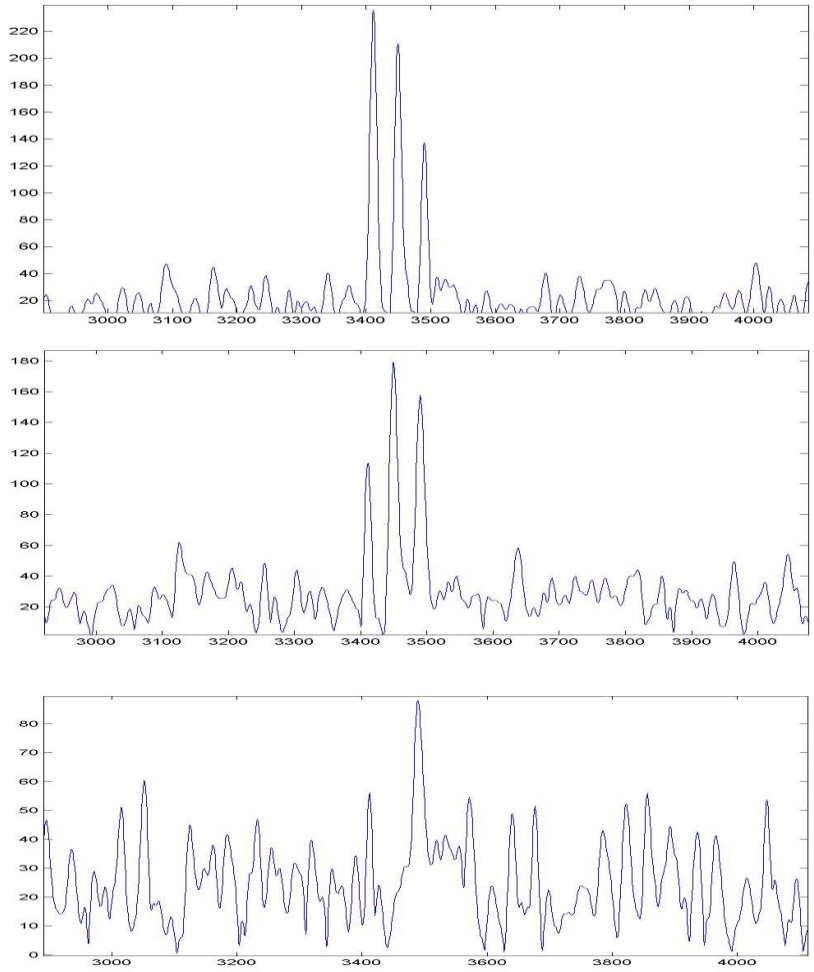

Figure 29. Correlator output for multipath propagation (norm. Doppler=0.0001, 0.0002, 0.0004)

Signal acquisition in the presence of an appreciable Doppler shift is affected by the frequency offset. In this case, the correlation between the received signal and the known preamble is no longer at its maximum. This affects the probability of detection so that it becomes unacceptable for larger values of the Doppler shift.

In order to quantify the effect of the Doppler shift on the preamble, consider that the phase change over the preamble of duration T in the presence of a Doppler shift f_d has to be smaller than some small value θ_o. This condition leads to the following inequality:

$$2\pi f_d T < \theta_o \tag{4.1}$$

From Equation 4.1, it is deduced that in the actual underwater channel there is a trade-off concerning the preamble duration: a short duration will ensure minor phase changes due to Doppler effect, but will result in poor noise suppression, while a longer duration will provide sufficient noise suppression, but result in a greater phase change as well.

Another effect of the induced Doppler effect is its influence on the received signals' bandwidth. As discussed by Stojanovic in [87], a relative motion between transmitter and receiver causes not only a Doppler shift in the received signal, but also a rescaling shift in bandwidth in the baseband signal. This can be seen by expressing the path delay in terms of distance $\ell(t)$ and sound propagation speed c. In this case, the transmitted and received signals $r(t)$ and $s(t)$ are related as

$$r(t) = s\left(t - \frac{\ell(t)}{c}\right) \tag{4.2}$$

Assuming relative motion at constant velocity v, the distance term becomes $\ell(t) = \ell(0) - vt$, and this expression can be written as

$$r(t) = s\left(\left(1 + \frac{v}{c}\right)t - \tau_0\right) \tag{4.3}$$

Although this effect is negligible in wireless radio communications, it cannot be neglected in an underwater environment. Since $s(t)$ is a modulated signal, as

$$s(t) = \mathrm{Re}\ u(t)e^{j2\pi f_c t} \tag{4.4}$$

This causes a shift in the carrier frequency and in the timing of the signal. Thus, a baseband signal of bandwidth B, centered around 0 Hz, is

observed at the receiver as a signal centered around f_d Hz (Doppler shift effect), having a bandwidth of $(1+\alpha)B$ (Doppler spread effect), where the factor α is a small real number depending on the relative motion between the transmitter and receiver. In order to compensate for the distorted bandwidth, the signal at the receiver must be sampled using the following sampling frequency [87]:

$$f_{s,dist} = \frac{f_s}{(1+\frac{f_d}{f_c})} \tag{4.5}$$

where f_c is the carrier frequency and f_s is the sampling frequency used in the transmitter. When f_d is within a few orders of magnitude from f_c, it is evident that the Doppler effect has to be compensated for.

C. DEVELOPMENT OF SYNCHRONIZATION METHODS

When the Doppler distortion is significant, a number of methods can be used to synchronize the data. In this section, several synchronization methods will be presented. The evaluation of the methods over experimental data will follow in the next section.

According to the previous analysis, when the channel has appreciable Doppler distortion, in order to synchronize the data, the duration of the preamble has to be short. The drawback, however, of a short preamble is a low signal to noise ratio. For that reason, in [87], Stojanovic introduces a method where initially a fraction of the whole preamble is used for the sliding correlator in order to have a coarse detection of the beginning of the signal. The time length of the preamble is determined by the maximum expected value of Doppler shift in the acoustic communication channel that will lead to an acceptable phase shift as shown in Equation 4.1. The estimate of the signal delay is then derived from the following Equation:

$$\hat{\tau} = \arg\max_{\tau} \left| \int_0^T v(t+\tau)u^*(t)dt \right| \tag{4.6}$$

where $v(t)$ is the received signal preamble, $\hat{\tau}$ is the estimated beginning of the received preamble, optimized over all time delays τ between the received signal and its replica, T is the duration of the fraction of the preamble and $u(t)$ is its known replica. After the coarse synchronization, the received waveform with the fraction of the known preamble can be used to compute a rough estimate of the Doppler shift by the following expression:

$$\hat{f}_d = \arg\max_{f_d} \left| \int_0^T v(t-\hat{\tau}) u^*(t) e^{-j2\pi f_d t} dt \right| \tag{4.7}$$

After the estimation of the Doppler shift $\hat{f}_d$, the received signal is corrected and resampled by a factor $\frac{1}{(1+\frac{\hat{f}_d}{f_c})}$, where f_c is the carrier frequency. Then the correlation is repeated, this time using the full length of the preamble, in order to get precise acquisition.

Following this method, and using Expression 4.7 to obtain an estimate of f_d, it is clear the received preamble with its replica needs to be aligned in time in order to get a satisfactory result. Using experimental results and simulations, the accuracy of the synchronization method in the case of coarse alignment was examined. It was found that a good estimate $\hat{\tau}$ is crucial for satisfactory synchronization. Concerning the value of the Doppler shift, from the experimental results of Chapter III, we know that every path on the underwater acoustic channel has a different Doppler distortion. From experimental evaluation, it became clear that this method provides an estimate of the average Doppler shifts of all multipath components.

As a different approach, the advantages of a specific signal design, in which three identical preambles are sent, will be explored. Note, that in this phase, the scope is not to eliminate totally the Doppler shift, since every

multipath component has a different Doppler distortion, as proved in Chapter III. The task is to reduce the value of Doppler shift, so that it won't affect the synchronization process.

As previously mentioned, the sampling frequency of the received signal in a Doppler distorted channel is distorted as well. If the distorted sampling frequency could be determined, a rough estimate of the Doppler shift could be obtained by taking advantage of the repetition of the preamble. Consider the output of a correlator for the three identical signal preambles. If the phase change in the duration of the pulses due to the Doppler shift is not large, from every one of the three pulses the output resembles the second plot of Figure 29.

By examining the correlator output, it emerges that the number of samples N_{dist} between the consecutive first principal peaks of every pulse on the received signal has to be equal to the number of samples N separating the preambles on the transmitted signal. Because of the Doppler shift, however, the values N_{dist} and N will be slightly different. Using Equation 4.5, the sampling frequencies at the receiver and the transmitter, $f_{s,dist}$ and f_s can be replaced with the number of samples, N_{dist} and N, obtaining

$$N_{dist} = \frac{N}{(1+\frac{f_d}{f_c})} \tag{4.8}$$

Therefore, by putting N_{dist} and N in Equation 4.8, a rough estimate of the Doppler shift can be found.

There are two important remarks on this point. First, using this method, the resulting value of Doppler shift corresponds to the first reception, which is probably the largest among the Doppler shift values of the other multipath components. The second remark concerns the accuracy of the estimate. The accuracy of the estimation depends on the number of samples between the preambles, so the more samples separating the preambles, the higher the accuracy.

Following is another method to take advantage of the repetition of the preamble in order to determine the Doppler shift. After taking the correlator output for the three preambles, the cross-correlation at zero time lag between the successive received preambles is taken, getting two values, one from the first two preambles and one from the second and third.

In order to make the result of the method clearer, a simplified case of a Doppler distorted channel where there is no multipath effect present will be considered. Let $x(n)$ be the waveform sent in the baseband. Then the first received waveform—in baseband—neglecting the noise, will be as follows:

$$x_1(n) = x(n)e^{j\omega_d n} \tag{4.9}$$

where ω_d is the normalized radial Doppler shift of the channel. Respectively, the second waveform will be:

$$x_2(n) = x(n)e^{j\omega_d (n+N)} \tag{4.10}$$

Estimating their cross-correlation at time lag zero gets:

$$x_1^*(n)x_2(n) = e^{j\omega_d N} \,||\, x(n) \,||^2 \tag{4.11}$$

The information of the Doppler shift is contained in the phase of the estimate of the cross-correlation between the successive preambles in such a way that it can be extracted. Another key point is that two estimates for the phase are obtained, one resulting from the first and second preamble and one from the second and third. In the case of no Doppler shift in the channel, the phase of those values will be close to zero for both of them; in case there is a Doppler shift, the two values will have approximately the same non-zero phase. An indication of the accuracy of the estimate is the similarity of those two values.

In this last method, there is ambiguity in the estimate, since the phase will be always in the range $[-\pi, \pi)$. This problem can be solved by tryinh to find the solution that is closer to the rough estimate of the method which uses the sample counting. Using experimental results and simulations, it was found that this method has accurate results and that the value of the Doppler shift obtained is an average over the Doppler shifts of all multipath components, just as in the

previous method. An important advantage of the method is that it is not sensitive to time misalignment, and therefore more precise estimates in all experimental cases were obtained.

Another method examined for the estimation of the Doppler shifts is the MUSIC algorithm [88]. In simulations, this method did not give all the Doppler frequencies, as expected, but only one, close to the actual ones. In general, the results were poor; however, since the Doppler shift is very small compared to the sampling frequency, it should be expected that this algorithm would fail to correctly determine the value of the Doppler shift. In order for the algorithm to provide an accurate estimate, the noise subspace must have a sufficient size, but due to the limited number of preamble samples, this is not always feasible. According to the simulations, there is a minimum value of the Doppler shift that can be detected. Even in the case where the correct values were received, the spurious roots that are close to the unit circle in the automated algorithm can lead to totally wrong estimation. Finally, the complexity of such a method is higher than the previously described methods.

As mentioned before, the synchronization process is accomplished in two phases. The first, acquisition phase, can be completed with the methods discussed in this section. The second phase is called tracking and is also crucial since, in the highly dynamic underwater acoustic channel, the initially estimated and corrected Doppler shift will not remain constant for the duration of the data detection phase; most probably, it will be heavily time-varying during this phase. This situation brings up the necessity for a mechanism to track the phase shift due to the Doppler shift. The tracking process in the proposed design is combined with the receiving process, in the frame of multiple input signals processing. The exact tracking mechanism is described in the next chapter along with the proposed receiver scheme.

The performance of each acquisition method was tested over experimental data and the findings will be presented in the next section.

D. METHOD PERFORMANCE BASED ON EXPERIMENTAL RESULTS

In this section, acquisition methods in parallel with Doppler shift estimation and correction of experimental data are applied. Acquisition testing was based on the two experiments described in Chapter III. The received data used for channel identification and the corresponding results have been presented in the same chapter.

1. Signal Acquisition on the New England Shelf Experiment

The New England Shelf experiment is described in detail in Chapter III. The signal format of this experiment was suitable for the accurate estimation of the Doppler shift prior to channel estimation. Moreover, based on the experimental data, the scattering function of the channel was determined and presented in Chapter III. The knowledge of this function also provides an accurate estimate for the channel's Doppler shift. Furthermore, the above acquisition methods were applied to the DSSS experimental data.

Successful acquisition was achieved by the use of a sliding correlator with the threshold adaptively adjusted based on the received signal. The methods described in the previous paragraph were then used to estimate the Doppler effect and correct for it. Table 5 illustrates the values of the Doppler shifts received from the various methods, for different signal to noise ratios.

SNR	Multipath effect characterization	Actual fd for larger and smaller multipath component	Stojanovic method	Samples counting	Three preambles processing
37 dB	Heavy	-1.9 Hz – -1.2 Hz	-1.5 Hz	-1.6 Hz	-1.3 Hz
35 dB	Medium	-2.2 Hz – -1.6 Hz	-1.8 Hz	-1.8 Hz	-2.1 Hz
31 dB	Mild	-3.4 Hz – -2 Hz	-3.7 Hz	-3.8 Hz	-3.8 Hz
30 dB	Medium	-3.2 Hz – -2.4 Hz	-1.9 Hz	-2.6 Hz	-2.6 Hz
29 dB	Mild	-3.5 Hz – -3.2 Hz	-3.6 Hz	-3.6 Hz	-3.4 Hz
26 dB	Medium	-3.5 Hz – -2.8 Hz	-3.7 Hz	-3.8 Hz	-3.5 Hz
25 dB	Mild	-3.2 Hz – -3 Hz	-3.3 Hz	-3.6 Hz	-3.6 Hz
16 dB	Heavy	-3.1 Hz – -2.8 Hz	-1.8 Hz	-3.3 Hz	-3.1 Hz
13 dB	Medium	-3.3 Hz – -2.3 Hz	-3.3 Hz	-4.6 Hz	-4.6 Hz
7 dB	Medium	-4.1 Hz – -4 Hz	-5.4 Hz	-5.1 Hz	-4.6 Hz
0 dB	Very Heavy	No data	-1.3 Hz	-3 Hz	-4.6 Hz

Table 5. Doppler shift estimates using different estimation methods

The first column of the table illustrates the signal to noise ratio, which varied during the experiment from a maximum of 37 dB to a minimum of 0 dB. The second column characterizes the multipath fading effect at this distance, for different multipath effects, characterized from mild to very heavy. The third column presents the accurate limit values of Doppler shift for two different arrivals, as determined from the scattering function of the channel. Note that the Doppler shift estimates from the scattering function correspond to the true values of Doppler shift and will be used for comparison purposes. The fourth column illustrates the Doppler shift as estimated from the Stojanovic method, using Equations 4.6 and 4.7. Note that the results are close to the actual ones. The fifth

column illustrates the rough result estimated with the method of samples, counting between successive DSSS pulses. These results are also close to the actual ones. Finally, the sixth column shows the Doppler shift as estimated with the three preambles processing method using Equations 4.9–4.11. The results for this method are the most accurate.

2. Signal Acquisition on MAKAI 2005 Experiment

The MAKAI 2005 experiment is described in detail in Chapter III. The received experimental data were used for the extraction of the scattering function of the channel, while in Chapter III, they are used as input in several types of receivers. Acquisition issues will be presented in this section.

As in the New England shelf experiment, successful acquisition was achieved by the use of a sliding correlator. Its function is similar to the previously described mechanism, which is based on the statistical properties of the received signal. The main difference in the previous case is that the algorithm not only searches for high peaks, but also for signal areas with high energy. When working with experimental data, in many cases, despread signal waveforms are dealt with, where the first high peak is not clearly noticeable. This can happen due to destructive interference among multipath arrivals or/and Doppler distortion. Taking into account that the waveform's time region corresponding to the beginning of the bit is an area of high energy compared to its neighboring regions, a method was designed and implemented where statistical peaks detection is combined with high energy detection in the area of the high peaks (over two or three chips duration). This method leads to more accurate acquisition and tracking.

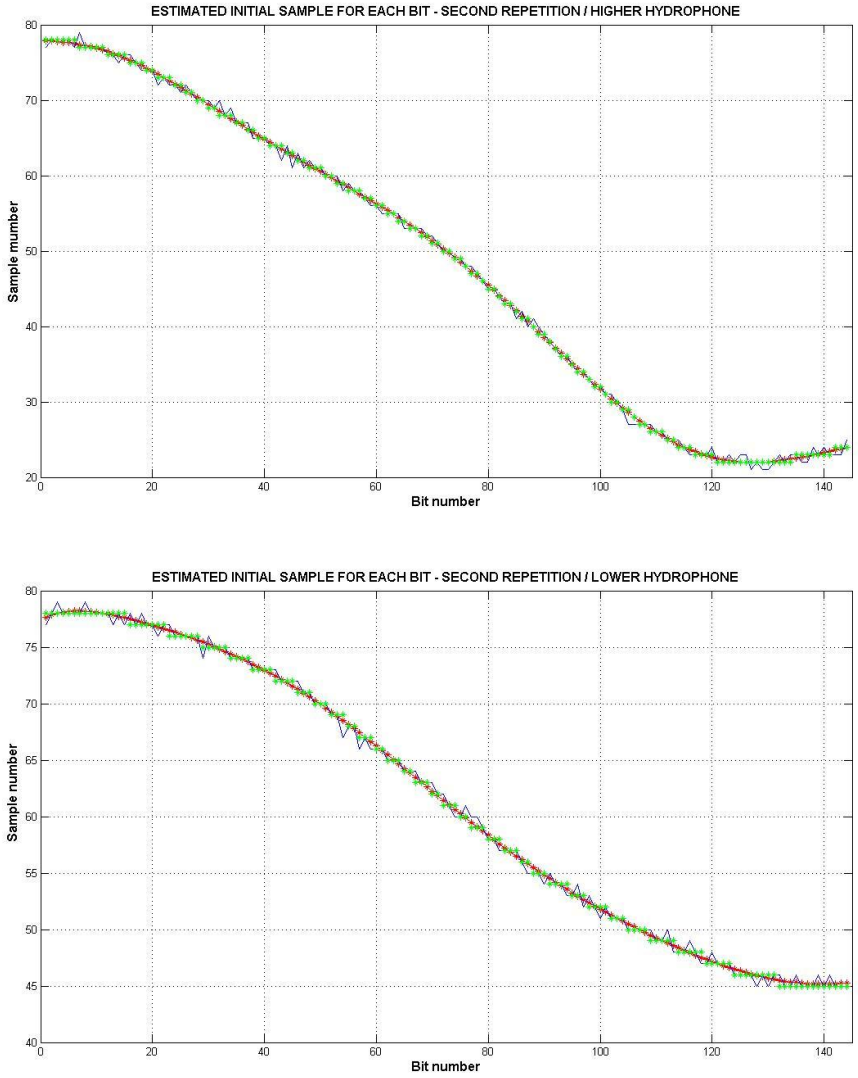

Figure 30. Estimated initial sample for higher and lower hydrophone

Applying this acquisition/tracking method in the experimental data set, successful acquisition and tracking is obtained. An example of the tracking result is shown in Figure 30. The illustrated result corresponds to the estimated initial sample number for each bit of the received data sequence. There are two plots, the first for the higher hydrophone and the second for the lower hydrophone. Using the estimated samples, a smoothing curve was drawn to clearly illustrate the trend for each case.

Inspection of both curves reveals that the starting sample number for each bit is generally falling. As discussed before, this demonstrates a positive Doppler effect in the acoustic communication link. More specifically, the slopes of the illustrated curves are directly proportional to the hydrophones' Doppler shifts. The exact Doppler shift for each case can be evaluated by applying the sampling counting method. For example, in the highest hydrophone plot, a region of high slope can be identified for the period between the 70th and the 100th bit, which corresponds to a positive Doppler shift of 5.5 Hz. On the other side, for the period after the 130th bit, the slope for the higher hydrophone changes, indicating a negative Doppler shift of about 0.7 Hz. Inspection of both plots indicates a high variability in the acoustic communication link.

Furthermore, close inspection of the results also shows that in the higher hydrophone, Doppler distortion is larger than in the lower one. This result is important, since the difference in the Doppler shift values between adjacent hydrophones can lead a multiple input equalizer to fail. As a consequence, correction needs to be made for the Doppler shift, as will be done in a later section.

For the second repetition experimental results and for the same hydrophones, the Doppler shift estimation method was applied using Equations 4.9, 4.10, and 4.11. The results are illustrated in Figure 31.

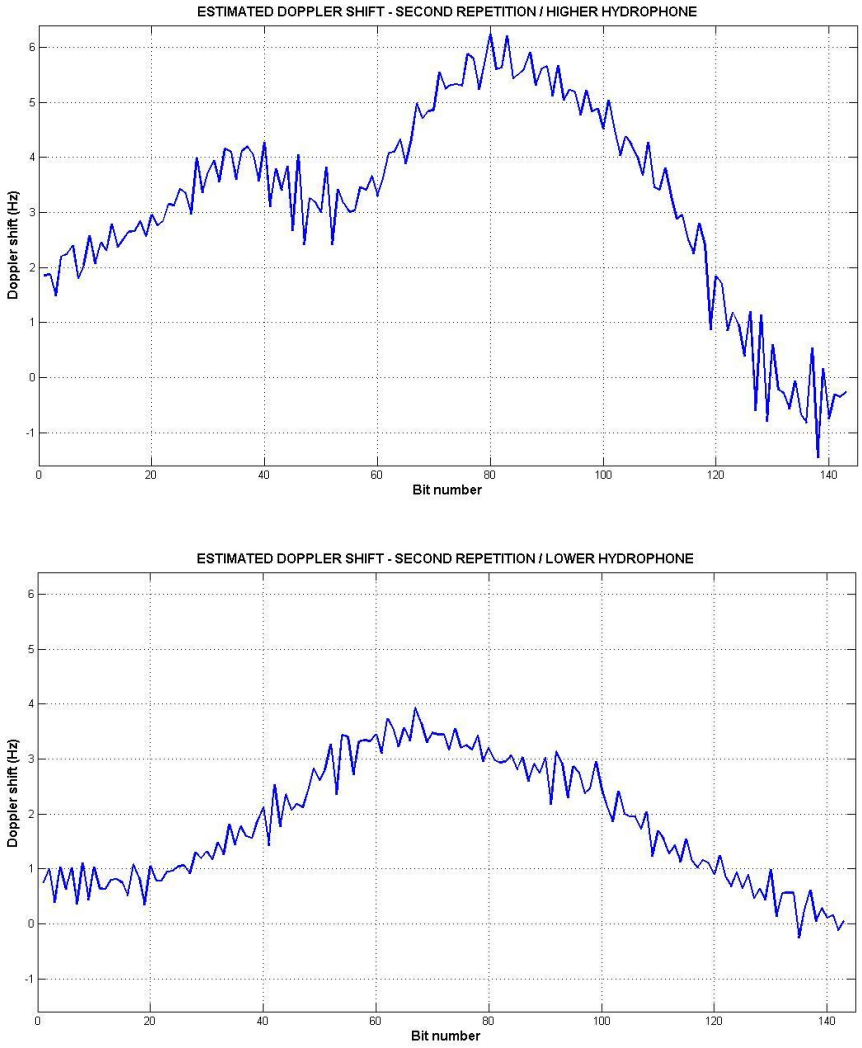

Figure 31. Estimated instant Doppler shift for higher and lower hydrophone

The plot of Figure 31 shows the instant Doppler shift estimates for the higher and lower hydrophones. In the results shown, data acquisition is performed by a preamble consisting of DSSS signal data streams. Comparing the result with Figure 30 shows that the two results are in agreement. For example, if we examine the plot for the higher hydrophone in Figure 30, then, for the period from bit 70 to bit 100, the curve's slope is high, indicating a significant Doppler shift. This fact is verified also in Figure 31. Furthermore, if we examine in Figure 30 the lower hydrophone, then, for the period from bit 130 to bit 144, the

curve's slope is close to zero, indicating a negligible Doppler effect as well. This is again verified from Figure 31, since Doppler shift in that time period is close to zero.

Another finding of Figure 31 is the considerable variation of the Doppler effect. In particular, two types of variation are distinguished: time and spatial (depth) variation. The time variation consists of the varying nature of the Doppler shift with time. The experimental results show that the channel propagation has considerable time variation to the point that the Doppler shift even changes sign (roughly after bit 130) in the higher hydrophone during the transmission of 144 bits. Depth variation in the Doppler effect is also observable from Figure 31, where the Doppler shift is larger in the higher hydrophone.

In order to have a better feeling on how depth variation affects Doppler effect variation in the experiment, the mean Doppler shift during the second repetition for all eight hydrophones was estimated. The estimation method used was preamble processing (Equations 4.9 to 4.11) and the results are shown in Figure 32. During the second repetition time period, there is a trend for Doppler shift values to decrease as hydrophone position gets deeper. This result is explained by considering that the vertical array of hydrophones is anchored on the ocean floor and it is free to sway with currents. In a time period of about 3.6 seconds, wave motion affects the higher hydrophones, by moving them faster than the lower ones (for that period of time), resulting in higher Doppler shift for the higher hydrophones.

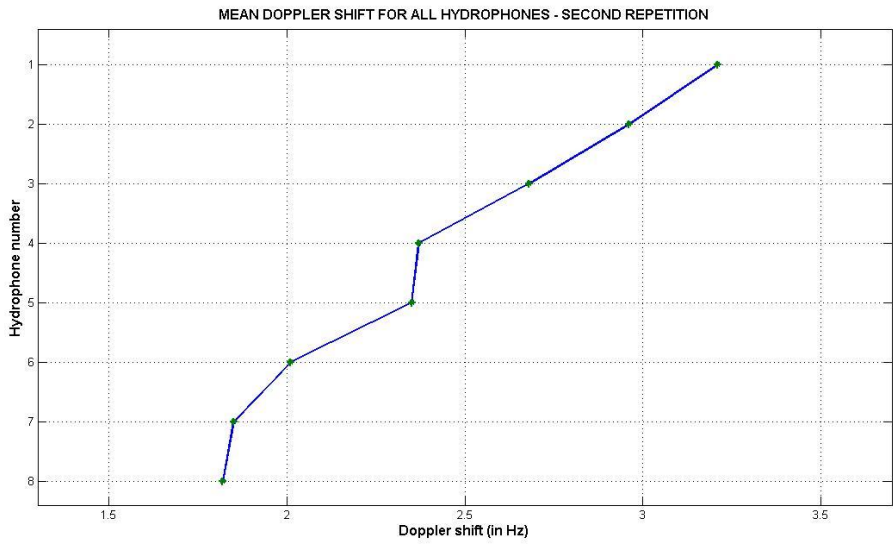

Figure 32. Estimated mean Doppler shift for all hydrophones

Table 6 illustrates the values of the Doppler shifts received from various methods for the different hydrophones. For each hydrophone labeled, the second column illustrates the signal to noise ratio, which varied for different hydrophones from a maximum of 2.6 dB to a minimum of 0.8 dB. The third column indicates the characterization of the multipath fading effect on each hydrophone, from mild to heavy. The fourth column presents the accurate limit values of Doppler shift for two different arrivals, as determined from the scattering function of the channel. The fifth column illustrates the rough mean Doppler shift estimated with the method of samples counting between successive DSSS pulses; the results are close to the actual ones. Finally, the sixth column shows the mean Doppler shift as estimated from the instant Doppler shift using the three preambles processing method (Equations 4.9 to 4.11); the results for this method are the most accurate. Table 6 reveals that for the time period of the experiment, the shallower the location of hydrophone, the higher the Doppler shift.

Hydrophone number	SNR (dB)	Multipath effect characterization	Actual fd for larger and smaller multipath component	Samples counting	Three preambles processing
1	2.1	Medium	2.9 Hz – 3.8 Hz	3.2 Hz	3.2 Hz
2	0.8	Heavy	2.8 Hz – 3.4 Hz	2.9 Hz	2.95 Hz
3	1.1	Heavy	2.4 Hz – 3.0 Hz	2.9 Hz	2.65 Hz
4	1.8	Medium	2.1 Hz – 2.8 Hz	2.65 Hz	2.4 Hz
5	2.1	Mild	2.1 Hz – 2.4 Hz	2.4 Hz	2.3 Hz
6	2.3	Medium	1.6 Hz – 2.4 Hz	2.1 Hz	2.0 Hz
7	2.6	Heavy	1.4 Hz – 2.3 Hz	2.0 Hz	1.85 Hz
8	2.6	Medium	1.4 Hz – 2.0 Hz	1.9 Hz	1.8 Hz

Table 6. Doppler shift estimates using different estimation methods

E. PROPOSED ACQUISITION METHOD

The acquisition stage is an important part of the communication process. An acquisition scheme that provides coarse synchronization, as well as Doppler effect reduction, will improve the performance of the receiver. Therefore, the acquisition mechanism should be able to estimate the coarse Doppler effect beforehand, so that the vast part of the Doppler shift can be corrected prior to the reception process. A reliable acquisition mechanism should be designed based on the environment that will be used. As was analyzed in the previous sections, it is possible that high Doppler shift will prohibit successful acquisition. Therefore, the length of the preamble should be chosen to suppress noise and simultaneously keep the Doppler phase shift low, during its duration.

The proposed acquisition scheme is based on the theoretical and experimental analysis of the current chapter. Three DSSS preambles are sent, either prior to the communication packet, or as part of the communication packet. The length of the preambles is designed based on Equation 4.1, where f_d is the largest expected value of Doppler shift in the actual operational underwater acoustic channel.

Acquisition is performed with a sliding correlator whose function is based on the statistical properties of the received signal. In addition, the algorithm not only seeks high peaks, but also signal areas with high energy. Therefore, statistical peaks detection is combined with high energy detection over two or three chips duration in the neighborhood of the higher peaks, leading to accurate acquisition.

Simultaneously with the acquisition procedure, the algorithm estimates the Doppler shift. The estimation is performed via processing of the three preambles, applying Equations 4.9 to 4.11. This method will lead to the most accurate Doppler shift estimation as indicated through experimental results. A possible phase ambiguity of that method can be resolved with the comparison of the result to the outcome of the samples counting method. Hence, first we apply samples counting and get a rough estimate of the Doppler shift; then, we apply three preambles processing and resolve the phase ambiguity of the result, using the rough Doppler shift estimate.

Using the calculated Doppler frequency shift, the center frequency and the sampling frequency can be corrected for each hydrophone (in case of an array) and the reception performance will be improved. The tracking process, which follows acquisition, will be examined in a later chapter. Tracking is treated as a part of the reception process.

V. RECEIVER AND EQUALIZER DESIGN

This chapter presents several receiver-equalizer designs for the accurate demodulation of the DSSS acoustic signal. In the first parts of the chapter, some well known methods will be mentioned and analyzed while in the latter parts, a new receiver will be presented.

A. PRESENTATION AND THEORETICAL DEVELOPMENT OF RECEIVERS AND EQUALIZERS

1. RAKE Receiver and Its Variants

A type of receiver that is used over fading channels is the RAKE receiver. The ordinary RAKE receiver is based on the knowledge of the communication channel. The channel in this case is modeled as a tapped delay line with time spacing smaller or equal to the chip duration T_c and time-varying channel coefficients. If the multipath arrivals are separated by time intervals greater than T_c, then those arrivals are resolvable and a RAKE receiver can be used. This receiver is made of a number of correlators placed on the taps. On each tap, in case of a DSSS signal, the despreaded received signal is correlated with the estimated channel coefficients and the outputs of the taps are summed. This type of receiver, in practice, takes advantage of time diversity due to the multiple arrivals of the signal.

To better illustrate the principles of the receiver, illustrated in Figure 5.1, the received signal in baseband is first multiplied at each tap by the spreading sequence and then integrated. The result of the operation is that in each tap the amplitude and phase for each time delay is obtained. Assuming there is no noise, that the channel is invariant, and that the paths are resolvable, then the output for the data bit at time n and at the mth tap will be:

$$c_m\ n\ = d\ n\ h_m \tag{5.1}$$

where $d(n)$ is the data bit at time n, and h_m is the channel coefficient for the mth tap (Equation 3.1). The RAKE receiver's operation in this case can be described as

$$y\ n\ = \sum_{m=0}^{M-1} \tilde{h}_m^{\ *}\ c_m(n) \tag{5.2}$$

where M is the number of taps and $\tilde{h}_m$ is the estimated channel's coefficient for the mth tap. From Equation 5.2, using Equation 5.1, the transmitted data can be recovered as follows

$$y\ n\ = d(n) \sum_{m=0}^{M-1} \left| h_m \right|^2 \tag{5.3}$$

provided $\tilde{h}_m \approx h_m$.

In the above analysis, the noise was neglected. If noise is added, the performance of the RAKE receiver is degraded because in each tap an amount of noise will always be present, even if a signal reception is not present. Establishing a threshold is a way to overcome this issue. A signal at a tap will be used in the summation of Equation 5.2 only if its value is above the threshold, that is, if the signal has sufficient energy. Even if a threshold is set, however, RAKE receivers are very susceptible to noise.

The actual performance of this type of RAKE receiver relies heavily on the estimated channel dynamics, thus making it unsuitable to applications with rapidly varying channel propagation characteristics. Also, the relative movement between transmitter and receiver implies Doppler distortion in the communication signal, another drawback in the reliability of this type of receiver.

A way around to these problems is to use differential encoding. In this way the information is carried not by the absolute phase of the transmitted waveform, but by the phase difference between two successive symbols. For example, assuming that the symbol duration is considerably smaller than the time

coherence of the channel, the magnitude and phase shift of the channel have no influence on the decoded symbols. The price paid, however, is a decrease in the SNR [22].

The output signal at time n of the RAKE receiver variant described above, neglecting the noise but not the Doppler effect, will be as follows:

$$y\ n\ = \sum_{m=0}^{M-1} c_m\ \ n-1\ ^{*} c_m\ \ n \tag{5.4}$$

Using Equation 5.1 in 5.4, we get

$$y\ n\ = \sum_{m=0}^{M-1} d\ \ n-1\ ^{*} h_m^{*} d\ \ n\ \ e^{j\theta_d} h_m \tag{5.5}$$

which implies

$$y\ n\ = d\ \ n-1\ ^{*} d\ \ n\ \ e^{j\theta_d} \sum_{m=0}^{M-1} \left|h_m\right|^2 \tag{5.6}$$

where θ_d is the Doppler phase shift. Obviously, data information can be recovered with the use of a differential decoder.

A practical issue in the application of this method is the necessity for alignment of the impulse responses which are sliding, due to the change in the sampling frequency (Doppler effect). Another issue is that the data bit duration should be shorter than the multipath spread of the channel. If this is not the case, then the degradation in the performance will be severe due to intersymbol interference. Finally, even if the data bit duration is shorter than channel's multipath spread, the method has great sensitivity to high levels of noise.

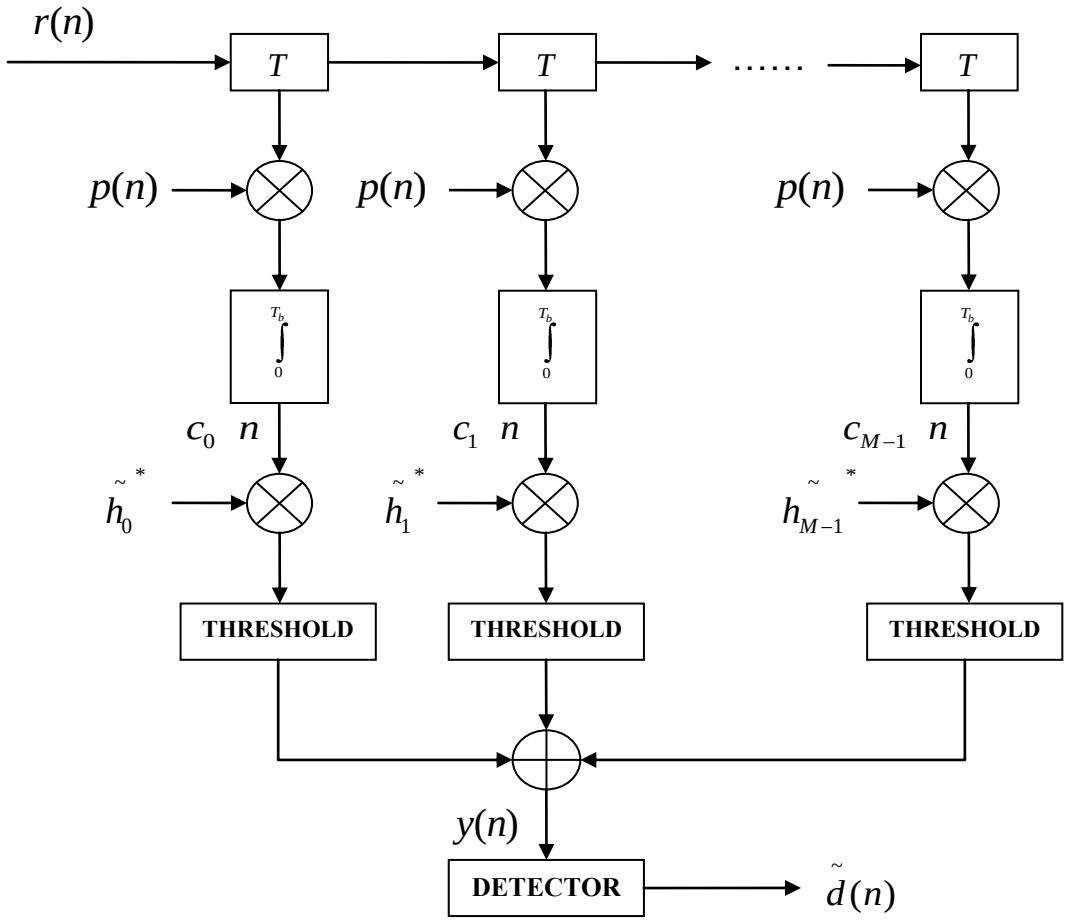

Figure 33. Ordinary RAKE receiver block diagram

2. Principal Component Analysis

Another possible receiver type is based on the processing of the autocorrelation matrix of the despreaded DSSS signal. The scope of this method is to determine the vector that better describes the underwater channel. By using this vector, the phase of the symbols is determined. It was shown in [89] that the vector that better describes the channel is the eigenvector corresponding to the maximum eigenvalue of the autocorrelation matrix. Let the despreaded DSSS signal vector at the chip rate be $\underline{c}(n)$, and the symbols sent be $d(n)$. Then the autocorrelation matrix can be evaluated using Equation 5.7:

$$R_{cc} = E\{\underline{c}(n)\underline{c}^{*T}(n)\} \tag{5.7}$$

By determining that the eigenvector $\underline{f}$ that corresponds to the maximum eigenvalue $\lambda_{\max}$, then the estimated symbol sent can be derived by the formula:

$$\tilde{d}(n) = \underline{f}^{*T}\,\underline{y}(n) \tag{5.8}$$

In this method, the use of a sufficient number of received data samples is necessary in order to form the autocorrelation matrix R_{cc}. Therefore, the method can be reliable only if the channel is slowly varying. The performance of the method was evaluated using simulations and the results will be presented in the next sections. An improvement in the performance and convergence speed can be obtained if only the peaks of the impulse response are used, thus eliminating part of the noise energy.

An important issue of the method is the need to have synchronization between transmitter and receiver. This calls for a reliable algorithm in the acquisition/synchronization part of the receiver. Also, various simulations showed that, as the Doppler shift increases, the performance of the receiver greatly degrades as in most of the receivers; consequently, it is a necessity to reduce the Doppler shift in the initial phase of signal acquisition/synchronization. Another result shown through the simulations is that, in order for the receiver to be robust, even for low SNR and high Doppler shift, the bit duration has to be longer (at least three times) than the multipath spread of the channel.

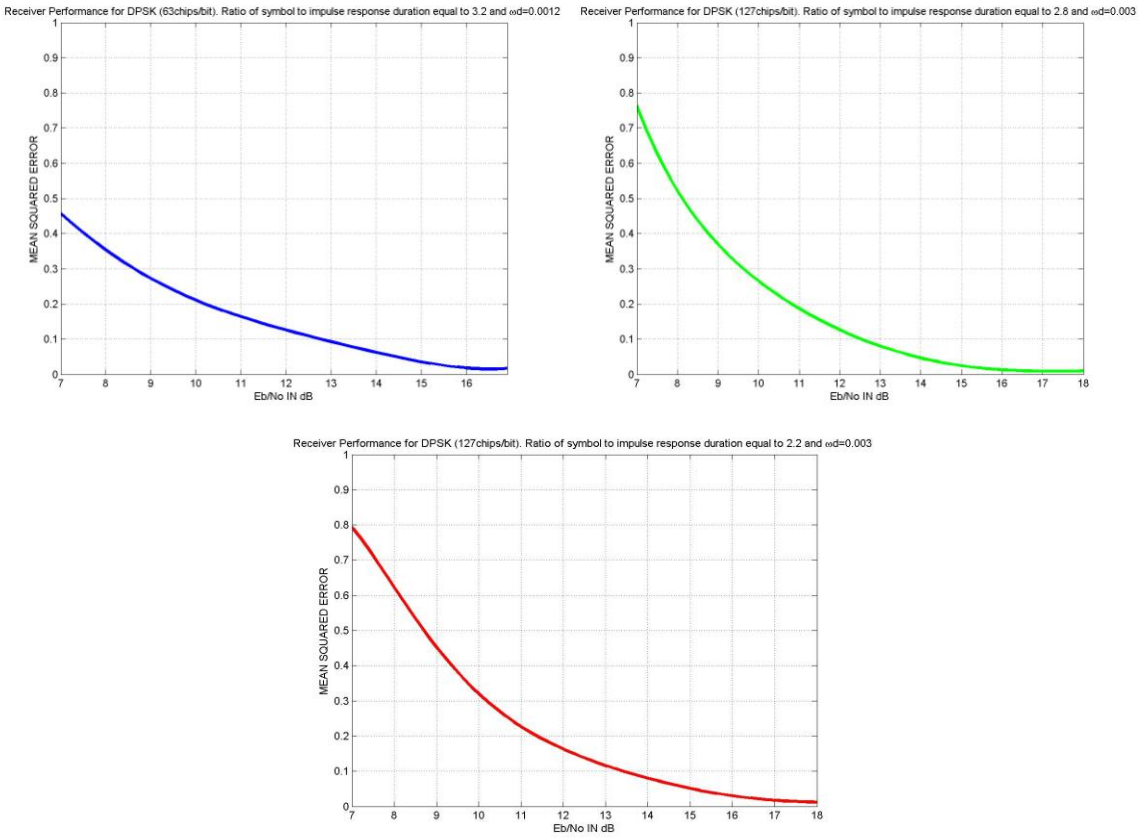

Figure 34. Performance of a Simulated Principal Component Receiver

In Figure 34, the performance of this method for three characteristic examples of underwater channels is examined. All channels are modeled as slowly varying Rayleigh fading channels. The plots show the mean square error in the output of the receiver as a function of $\frac{Eb}{No}$ (energy per bit to noise power spectral density ratio) for DPSK modulation. The plot on the upper left concerns a channel with normalized Doppler radial frequency shift 0.0012 (relative to the carrier frequency) and where the length of the impulse response is 3.2 times the length of the symbol duration. The plot on the upper right concerns a channel with normalized Doppler radial frequency shift 0.003 and where the length of the impulse response is 2.8 times the length of the symbol duration. The lower plot

concerns the most challenging case, where the normalized Doppler radial frequency shift is equal to 0.003 and the length of the impulse response is 2.2 times the length of the symbol duration.

Summarizing the findings of the research regarding principal component analysis, it is evident that this method is not robust for the underwater acoustic environment due to high channel variability and severe Doppler effect.

3. Decision Feedback Equalizer

An alternative way of compensating for the time-varying nature of the channel is to use an Adaptive Decision Feedback Equalizer based on either the RLS or LMS algorithm. Although this has been proved suitable for use in wireless applications, DFE is particularly challenging when implemented in acoustic channels [31, 90].

In the case of an acoustic channel with high Doppler distortion, a DFE with differentially encoded M-ary PSK data yields a simple way of achieving carrier synchronization. In the presence of frequency offset due to the Doppler shift caused by relative motion between transmitter and receiver, a phase correction needs to be computed recursively to prevent phase rotation from symbol to symbol. An assumption important for the receiver to perform efficiently is that the parameters of the equalizer do not change significantly from symbol to symbol. Figure 35 illustrates the receiver [91].

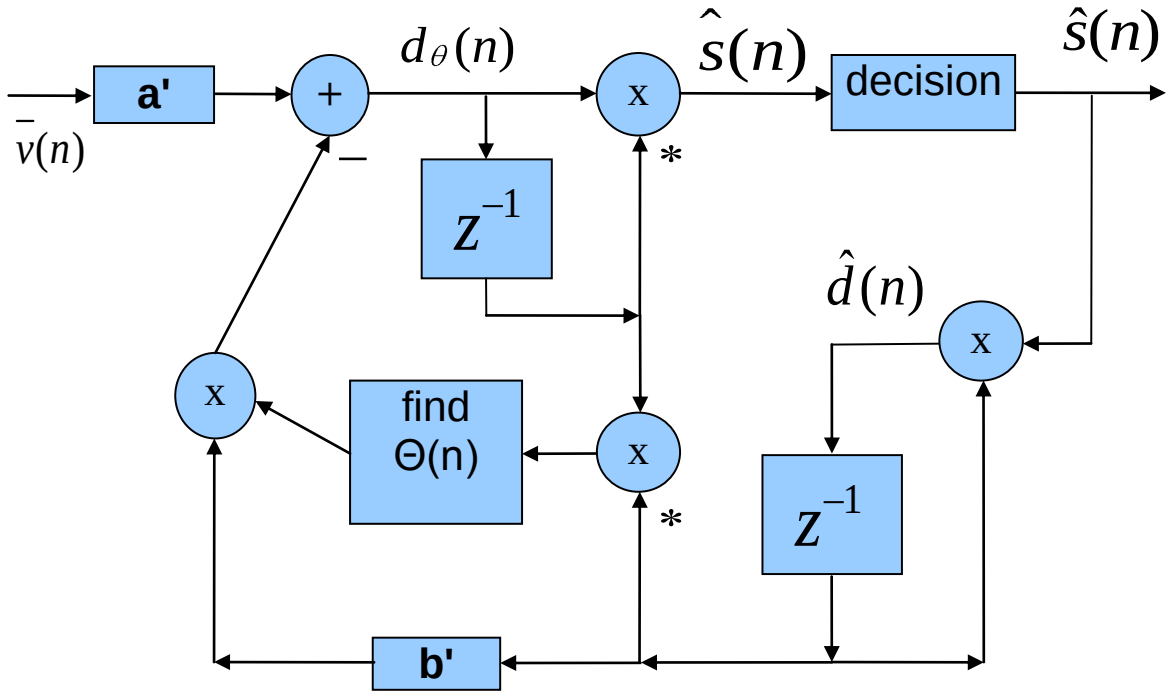

Figure 35. DFE receiver for differentially coherent detection

In particular, assume the M-ary symbols $s(n)$ defined as:

$$s(n) \in \left\{1, e^{\frac{i2\pi}{M}}, ..., e^{\frac{i2\pi(M-1)}{M}}\right\} e^{-i\frac{\pi}{M}} \tag{5.9}$$

and the data transmitted for differentially encoded signals will be:

$$d(n) = s(n)d(n-1) \tag{5.10}$$

The baseband signal in the receiver will have the form:

$$v(t) = \sum_n d(n)h(t-nT)e^{i\theta(t)} + z(t) \tag{5.11}$$

where $h(t)$ is the overall impulse response, including transmit filtering, channel distortion and receive filter:

$$h(t) = g_T(t) * h(t) * g_R(t) \tag{5.12}$$

Also, $z(t)$ is the filtered noise and $\theta(t)$ is the unknown carrier phase.

Define the composite equalizer vector as:

$$\bar{c}' = \left[\bar{a}' \quad -\bar{b}' \right] \tag{5.13}$$

where the vectors $\bar{a}$ and $\bar{b}$ are the equalizer's feedforward and feedback filter coefficient vectors, respectively. Define the previously estimated data decisions vector and the received signals vectors as follows:

$$\bar{d}(n-1) = \begin{bmatrix} \hat{d}(n-1) \\ \cdot \\ \cdot \\ \hat{d}(n-N) \end{bmatrix}, \quad \bar{v}(n) = \begin{bmatrix} v(n) \\ \cdot \\ \cdot \\ v(n-K+1) \end{bmatrix} \tag{5.14}$$

Then the phase estimate, which is the output of the receiver, will be:

$$\hat{s}(n) = \hat{d}_\theta(n)\hat{d}_\theta^*(n-1) \tag{5.15}$$

where:

$$d_\theta(n) = \bar{a}^{*T}\bar{v}(n) - \bar{b}^{*T}\bar{d}(n-1)e^{i\theta(n)} \tag{5.16}$$

If $\Theta(n)$, $\bar{y}(n)$ is defined as:

$$\Theta(n) = e^{i\theta(n)} \tag{5.17}$$

$$\bar{y}(n) = \begin{bmatrix} \bar{v}(n) \\ \bar{d}(n-1)\Theta(n) \end{bmatrix} \tag{5.18}$$

then the decision feedback equalizer receiver performs the following operation:

$$d_\theta(n) = \bar{c}^{*T}\bar{y}(n) \tag{5.19}$$

Both feedback and feedforward terms in Equation (5.16) have to be aligned in time. The adaptive equalizer is capable of tracking slow phase variations but not a large frequency offset; therefore, a separate residual phase correction is included [91]. In order to determine the residual phase, the following recursion can be employed:

$$\Phi(n) = \frac{d_\theta(n)d^*(n)}{\left| d_\theta(n)d^*(n) \right|} \tag{5.20}$$

$$\Delta\phi(n) = \mathrm{Im}\ \ \Phi(n)\Phi^{*}(n-1) \tag{5.21}$$

This calls for a recursive estimator of the form

$$\Delta\theta(n+1) = \lambda\Delta\theta(n) + (1-\lambda)\Delta\phi(n),\ \ \lambda \in [0,1) \tag{5.22}$$

$$\theta(n+1) = \theta(n) + \Delta\theta(n+1) \tag{5.23}$$

The initial condition for the recursive estimator can be set to zero as

$$\theta(0) = \Delta\theta(0) = 0 \tag{5.24}$$

The adaptation of equalizer's feedforward and feedback filters is based on a single error [91]:

$$e(n) = b(n) - \hat{b}(n) = b(n) - \bar{c}^{*T}\bar{Y}(n)\bar{c} \tag{5.25}$$

where $\bar{Y}(n) = \bar{y}(n)\bar{y}^{*T}(n-1)$

This error is to be used to determine the equalizer vector based on the Minimum Mean Square Error (MMSE) criterion in the sense of trying to minimize the MSE:

$$\eta = E\ \ |e(n)|^2 \tag{5.26}$$

For example, if the stochastic gradient approach is used for the minimization of the MSE, the following algorithm [91] results:

$$d_\theta(n) = \bar{c}'(n)\bar{y}(n) \tag{5.27}$$

$$\hat{b}(n) = d_\theta(n)d_\theta^{*}(n-1) \tag{5.28}$$

$$e(n) = \tilde{b}(n) - \hat{b}(n) \tag{5.29}$$

$$\bar{c}(n+1) = \bar{c}(n) + \mu\left[e^{*}(n)\bar{y}(n)d_\theta^{*}(n-1) + e(n)\bar{y}(n-1)d_\theta^{*}(n)\right] \tag{5.30}$$

The choice of the updating algorithm greatly influences the speed of convergence. The DFE is an adaptive method that tracks the changes in the underwater channel using previously identified symbols. The choice of the tap structure in the feedforward and feedback filters and of the forgetting factor principally influences the DFE's performance [91].

There is not a method to determine in advance a set of parameters to ensure good convergence in all different underwater channels, so heuristic methods are usually employed. As discussed in Chapter III, each of the different paths in the multipath propagation has a different value of Doppler shift and Doppler spread. Also, the results from the experiments showed that the weaker components of the impulse response usually have higher Doppler spreads than the stronger ones, since they have a larger variability. Since the weaker components change more rapidly, this high variability of the weaker paths can cause this type of equalizer to fail. As a result, the DFE performance shows variability analogous to the variability of the channel itself, so the desired reliability is not achieved. Taking also into account the algorithm's high computational load compared to other methods, the conclusion is that this method does not meet the necessary requirements [51, 67, 92].

B. DUAL INPUT KALMAN ESTIMATOR

1. Theoretical Background

This section presents the novel approach of combining a number of received signals using a technique based on Kalman Filtering. In particular, it turns out that, in the presence of receiver diversity, the transmitted sequence can be viewed as part of the "state" of a dynamic system whose inputs and outputs are the received signals. This "state" (therefore the transmitted sequence) can be estimated by a Kalman-filter-like structure, whereas the recursive nature of the Kalman filter allows the inclusion of a decision feedback. The channel in this case can be estimated blindly, by the reconstructed symbols, or by a combination of the two.

Let $x(n)$ be the transmitted sequence. It can be the row DSSS signal at the chip rate, or data symbols at the symbol rate. There are a number of receptions of the signal through *L* different channels with impulse responses $h_1(n),...,h_L(n)$. Define the *L* received signals $y_1[n],...,y_L[n]$ as:

$$
\begin{aligned}
y_1[n] &= h_1(n) * x(n) + w_1[n] \\
&\ldots \\
y_L[n] &= h_L(n) * x(n) + w_L[n]
\end{aligned}
\tag{5.31}
$$

This is shown in Figure 36 where for simplicity $L = 2$ is assumed.

Following Figure 36, the resulting signals $y_1[n]$ and $y_2[n]$ might represent a number of situations, such as the reception of row chipped data at the chip rate or despreaded sequences at the data rate. The channels $h_1(n)$ and $h_2(n)$ represent delayed receptions at different receivers due to multipath propagation. Using a sliding correlator at the receiver, which cross-correlates the received signals with the known replica of the preamble over successive time intervals, the received signals are despreaded and downsampled (by *N*), determining the impulse response vectors $h_1(n)$ and $h_2(n)$ of length *N*. Due to the nature of the underwater channels from those *N* fingers (taps) of the receiver output, only a few will correspond to the principal path receptions and as so only M_1, M_2 fingers will be used in the demodulator, for the two channels, $h_1(n)$ and $h_2(n)$, respectively. The initial values of the two channel vectors can then be assumed known, but always corrupted by noise. For the sake of simplicity, in the following analysis the case with $M_1 = 3, M_2 = 3$ is addressed, but the analysis presented can easily be generalized.

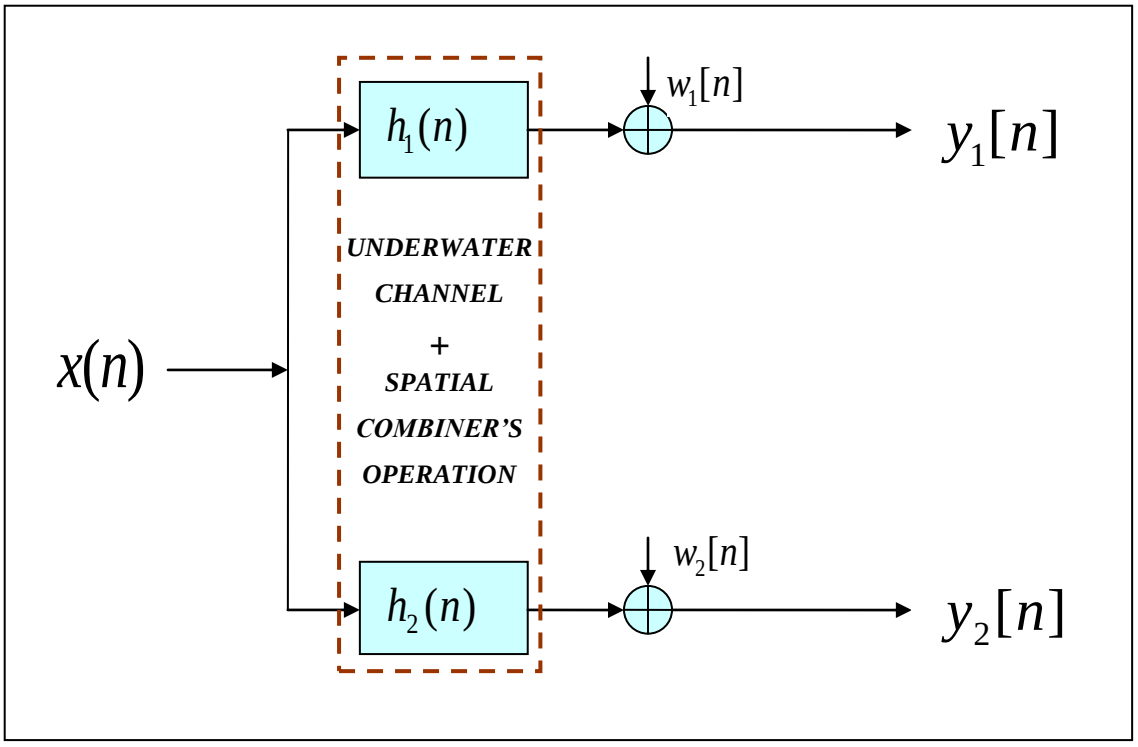

Figure 36. Illustration of transmitted signal, received signals and channels

Following Figure 36, in the time domain the relations between the transmitted sequence and the received signals are given by the following Equations (for simplicity the method will be described for a channel length of *3)*:

$$\begin{aligned} y_1[n] &= x[n] + h_{1,2}[n]x[n-1] + h_{1,3}[n]x[n-2] + w_1[n] \\ y_2[n] &= h_{2,2}[n]x[n-1] + h_{2,3}[n]x[n-2] + w_2[n] \end{aligned} \tag{5.32}$$

where the impulse responses $h_1(n)$ and $h_2(n)$, are assumed to be known at the receiver and they are defined as follows, for $n = 1,2,3,...$

$$\begin{aligned} h_1(n) &= \begin{bmatrix} 1 & h_{1,2}[n] & h_{1,3}[n] \end{bmatrix} \\ h_2(n) &= \begin{bmatrix} 0 & h_{2,2}[n] & h_{2,3}[n] \end{bmatrix} \end{aligned} \tag{5.33}$$

In Equations 5.32 and 5.33, without loss of generality, to make the analysis simpler, a time delay of one is forced in the first signal and the first component is normalized to one.

Define the signal vector as:

$$\underline{x}(n) = \begin{bmatrix} x[n-1] \\ x[n-2] \end{bmatrix} \tag{5.34}$$

The Equation 5.32 can be written in the following form:

$$\begin{aligned} x[n] &= y_1[n] - h_{1,2}[n]x[n-1] - h_{1,3}[n]x[n-2] - w_1[n] \\ y_2[n] &= \quad h_{2,2}[n]x[n-1] + h_{2,3}[n]x[n-2] + w_2[n] \end{aligned} \tag{5.35}$$

and, from this last set of equations, the final form of the equation is:

$$\left\{ \begin{aligned} \underline{x}(n+1) &= \begin{bmatrix} -h_{1,2}[n] & -h_{1,3}[n] \\ 1 & 0 \end{bmatrix} \underline{x}(n) + \begin{bmatrix} 1 \\ 0 \end{bmatrix} y_1[n] + \begin{bmatrix} -1 \\ 0 \end{bmatrix} w_1[n] \\ y_2[n] &= \begin{bmatrix} h_{2,2}[n] & h_{2,3}[n] \end{bmatrix} \underline{x}(n) + [0] y_1[n] + [1] w_2[n] \end{aligned} \right\} \tag{5.36}$$

Equation 5.36 shows a state space model relating the received signals y_1, y_2 and the transmitted signal x. As a consequence, the standard Kalman filter can be applied to estimate the state and the transmitted sequence. Using the Kalman filter, the state of the following general model will be determined, which has the form of Equation 5.37:

$$\left\{ \begin{aligned} \underline{x}(n+1) &= A\underline{x}(n) + By_1[n] + Gv[n] \\ y_2[n] &= C\underline{x}(n) + w[n] \end{aligned} \right\} \tag{5.37}$$

where $v[n]$, $w[n]$ are uncorrelated zero mean white noise sequences with covariances Q, R, respectively.

Comparing Equations 5.36 and 5.37, the following equalities appear:

$$A = \begin{bmatrix} -h_{1,2}[n] & -h_{1,3}[n] \\ 1 & 0 \end{bmatrix},\ B = \begin{bmatrix} 1 \\ 0 \end{bmatrix},\ G = \begin{bmatrix} -1 \\ 0 \end{bmatrix},\ C = \begin{bmatrix} h_{2,2}[n] & h_{2,3}[n] \end{bmatrix} \tag{5.38}$$

A recursive estimate of the transmitter data vector $x(n)$ can be computed by the time-varying Kalman filter based on the model of Equation 5.37:

$$\left\{\begin{array}{l}\underline{\hat{x}}(n+1)=A\underline{\hat{x}}(n)+By_1[n]+K(n)\ \ y_2[n]-C\underline{\hat{x}}(n)\\ K(n)=AP(n)C^T\ \ CP(n)C^T+R\\ P(n+1)=AP(n)A^T+Q-K(n)\ \ CP(n)C^T+R\ \ K^T(n)\end{array}\right\} \tag{5.39}$$

where $P(n)$ is the state error covariance matrix whereas $K(n)$ is the filter gain matrix.

The initial conditions used in iterating Equation (5.39) are $\hat{x}[0]=x_0$, the best a priori estimate of $x[0]$. $P(n)$ is the error covariance matrix, with initial condition $P(0)=\sigma_0{}^2 I$. Since $x[0]$ is not assumed to be known a priori, $\hat{x}[0]$ is chosen arbitrarily (say *0*) and σ_0 large with respect to the range of values of $x[n]$.

In steady state, if $h_1(n),\ h_2(n)$ represent the impulse responses of different channels, and there is no common roots between the two z-Transforms, then the system of Equation 5.37 is observable, and $P(n)$ is going to converge to a solution $P(\infty)$ for any initial conditions $P(0)$. At convergence, $P(\infty)$ is the solution to the Algebraic Riccati Equation.

This estimator can be formulated also as the combination of two digital filters, directly derived from the state space estimator. Starting from the first Equation of 5.39, it can be written:

$$\underline{\hat{x}}(n+1)=\ \ A-K(n)C\ \ \underline{\hat{x}}(n)+By_1[n]+K(n)y_2[n] \tag{5.40}$$

also the transmitted data estimate for discrete time $[n-1]$ is given by the relation:

$$\hat{x}[n-1]=[1\quad 0]\,\underline{\hat{x}}(n) \tag{5.41}$$

By inspection of Equation 5.40, two input signals $y_1[n]$, $y_2[n]$, and one output vector $\underline{\hat{x}}(n)$ can be identified. Following this observation, the conclusion is that there are two transfer functions $G_1(z),\ G_2(z)$ (in the z-domain), that, if they are applied to the received data $y_1[\mathrm{n}]$, $y_2[n]$, will produce the transmitted data estimate at discrete time $[n-1]$. The following operation is illustrated in Figure

37. From Equations 5.40, and 5.41, the estimates of $G_1(z)$, $G_2(z)$ in the z-domain, where the Kalman gain *K* in steady state is a constant is derived:

$$\left\{\begin{array}{l} G_1(z) = [1 \quad 0]\ zI - (A - KC)^{-1} B \\ G_2(z) = [1 \quad 0]\ zI - (A - KC)^{-1} K \end{array}\right\} \tag{5.42}$$

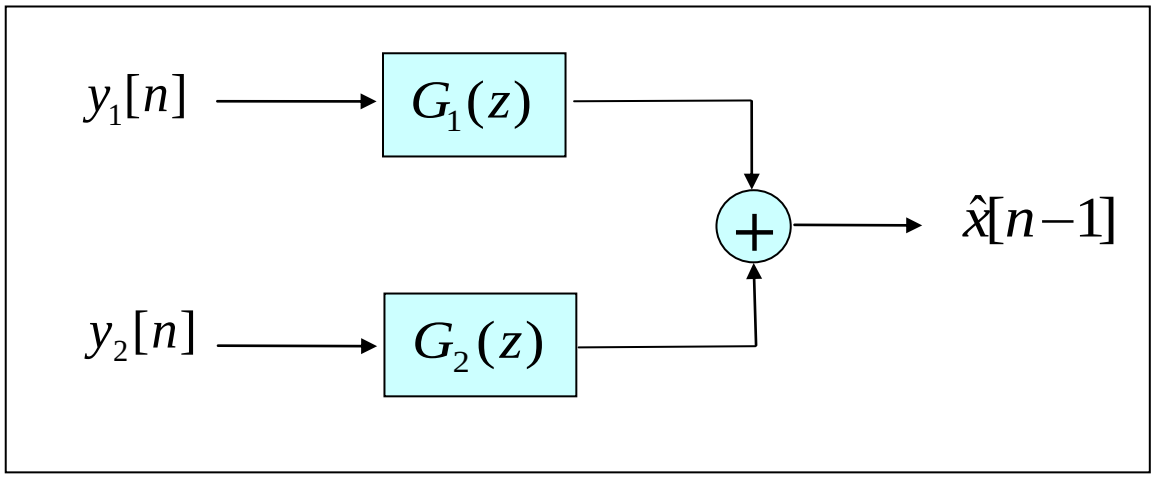

Figure 37. Graphic illustration of transfer function representation approach

Both transfer functions $G_1(z)$, $G_2(z)$ have the form:

$$G_1(z) = \frac{J_1(z)}{V(z)},\ G_2(z) = \frac{J_2(z)}{V(z)} \tag{5.43}$$

that yields the estimator for $\hat{x}[n-1]$ in Figure 37 as follows:

$$z^{-1}\hat{X}[z] = \frac{J_1(z)}{V(z)} Y_1(z) + \frac{J_2(z)}{V(z)} Y_2(z) \tag{5.44}$$

which also implies that

$$z^{-1}\hat{X}[z]V(z) = J_1(z)Y_1(z) + J_2(z)Y_2(z) \tag{5.45}$$

The relation of Equation 5.45 can be written in the discrete time domain (in the general case) as follows:

$$\hat{x}[n-1] = \underbrace{J_1[1] \quad J_1[2] \quad . \quad .}_{J1(n)} \begin{bmatrix} y_1[n] \\ y_1[n-1] \\ . \\ . \end{bmatrix} +$$

$$+ \underbrace{J_2[1] \quad J_2[2] \quad . \quad .}_{J2(n)} \begin{bmatrix} y_2[n] \\ y_2[n-1] \\ . \\ . \end{bmatrix} - \qquad (5.46)$$

$$- \underbrace{V[1] \quad V[2] \quad . \quad .}_{V(n)} \begin{bmatrix} \hat{x}[n-2] \\ \hat{x}[n-3] \\ . \\ . \end{bmatrix}$$

Equation 5.46 is the final relation that will be used in the equalizer to recover the transmitted data. In the next section, it will be demonstrated how theoretical analysis is going to be used in the actual problem, while some other issues of the actual estimation are going to be addressed.

2. Development of the Estimator for the Underwater Channel

In the previous sections, a robust theoretical method was developed for recovering the transmitted data from a number of received signals in the presence of multipath effect and additive noise. In this section, the theoretical method to underwater acoustic communication will be applied, dealing with issues characteristic of the underwater acoustic environment.

As mentioned before, the initial values of the overall channel vectors $h_1(n)$ and $h_2(n)$ can be assumed to be known. If they are not known, they can be estimated from the received data with the possible addition of a training sequence at the beginning of the reception. The estimation of the transfer functions $G_1(z)$, $G_2(z)$ of Equation 5.43, which are the foundation of the solution of the data estimation problem, is then based on those initial values of the overall channel vectors.

There are a number of issues to be considered. The first is the necessity of a robust method for estimating the initial values of $h_1(n)$ and $h_2(n)$. Another aspect is that $h_1(n)$ and $h_2(n)$ can be time-varying and, as a result, the transfer functions $G_1(z)$, $G_2(z)$ of the problem solution will be time-varying as well. In this case, the Kalman Filter must be made adaptive to track the time varying channel characteristics. Finally, a method needs to be developed to estimate the Doppler shift and compensate for its effect. The solution to both problems (channel and Doppler shift estimations) is at the basis of a reliable implementation.

Although the transfer functions $G_1(z)$, $G_2(z)$ are computed from the estimated channels $h_1(n)$ and $h_2(n)$, they need to be updated online in order to track channel variations. In order to prevent the Kalman filter from becoming unstable, the denominator of the transfer functions are kept constant and only the coefficients of the numerators are updated. Using the LMS algorithm, the data symbol estimation error is defined:

$$e[n] = \tilde{x}[n] - \hat{x}[n] \tag{5.47}$$

with $\tilde{x}[n]$ the estimated data symbol sent after the decision and $\hat{x}[n]$ is the estimated value of the data symbol.

The LMS algorithm updates the values of the vectors J_1, J_2, which are the numerator polynomials of the filters in Equations 5.43 and 5.44, on each iteration, according to Equation 5.48:

$$\begin{aligned} J_1(n+1) &= J_1(n) + \mu e^*[n]\underline{y}_{f1}(n) \\ J_2(n+1) &= J_2(n) + \mu e^*[n]\underline{y}_{f2}(n) \end{aligned} \tag{5.48}$$

where the vectors $\underline{y}_{f1}(n)$, $\underline{y}_{f2}(n)$ are, respectively, the vectors $\underline{y}_1(n)$, $\underline{y}_2(n)$, filtered by $\frac{1}{V(z)}$ as in Equation 5.44, and μ is the step size of the LMS algorithm.

In cases of high SNR and with modulation schemes with constant modulus—such as BPSK and Quadrature Phase Shift Keying (QPSK)—the effect of the Doppler shift on the phase can be estimated by taking the power (square for BPSK and fourth for QPSK) of the estimated symbol. The phase difference between the symbol estimated and the symbol decoded yields an estimate of the Doppler phase shift. By proper averaging, the effect of noise and fluctuations can be attenuated. For QPSK, this can be done as follows: let the instant phase difference be φ_{inst}. It can be estimated as follows:

$$\varphi_{inst} = \frac{\angle \quad \hat{x}(n)^{4}}{4} \tag{5.49}$$

Then, the phase correction can be iteratively estimated using Equation 5.50:

$$\vartheta(n+1) = (1-\lambda)\vartheta(n) + \lambda\varphi_{inst} \tag{5.50}$$

where λ is a forgetting factor between zero and one, usually small (e.g., $\lambda = 0.01$) and the initial value of $\vartheta(n)$ is:

$$\vartheta(0) = 0 \tag{5.51}$$

In the next section, the development of a simulation for the dual input equalizer will be described and the results of the simulation will be illustrated.

3. Simulation of Dual Input Kalman Estimator

After the completion of the theoretical development of the dual input Kalman estimator, a validation of the performance of the algorithm is presented. Toward this goal, an artificial time-varying environment is created. In this environment—following Figures 38 and 39—the assumption is that there are two input signals y_1, y_2 at the receiver. The input signal y_1 has passed through an artificial channel whose impulse response has four coefficients, whereas y_2 has passed through an artificial channel whose impulse response has three coefficients. It is also assumed that the transmitter and the receiver are stationary, which implies that there is no Doppler shift due to relative motion.

Nevertheless, the channel is assumed to be time-varying, due to the changes of the transmission medium (the water column). The artificial channel is developed so that each path has a different time-varying nature.

In this simulation, the performance of the previously developed algorithm with QPSK signaling is evaluated in the presence of noise and time-varying channels.

The initial values of the channel coefficients $h_1(n)$, $h_2(n)$ are assumed to be known at the receiver and the two transfer functions $G_1(z)$, $G_2(z)$ of the problem estimator (see Equation 5.43) are recursively updated to track channel variations. The adaptation is done using the LMS algorithm as described in the previous section (Equations 5.47, 5.48) with a small step size μ ($\mu = 0.3$) to ensure convergence of the algorithm.

In the first simulation, the channel coefficients remain almost constant for the duration of 16000 symbols transmission. The channel coefficients $h_1(n)$, $h_2(n)$ are designed to have four and three taps, respectively. Concerning the power distribution on the channel coefficients, the first arrival for both channels holds around 50 percent of the signal power, the second arrival holds around 30 percent of the power and the other arrivals hold the remainder. The algorithm seems to be effective for this case, and the resulting curves of bit error probability and mean squared error are shown in Figures 38 and 39, respectively.

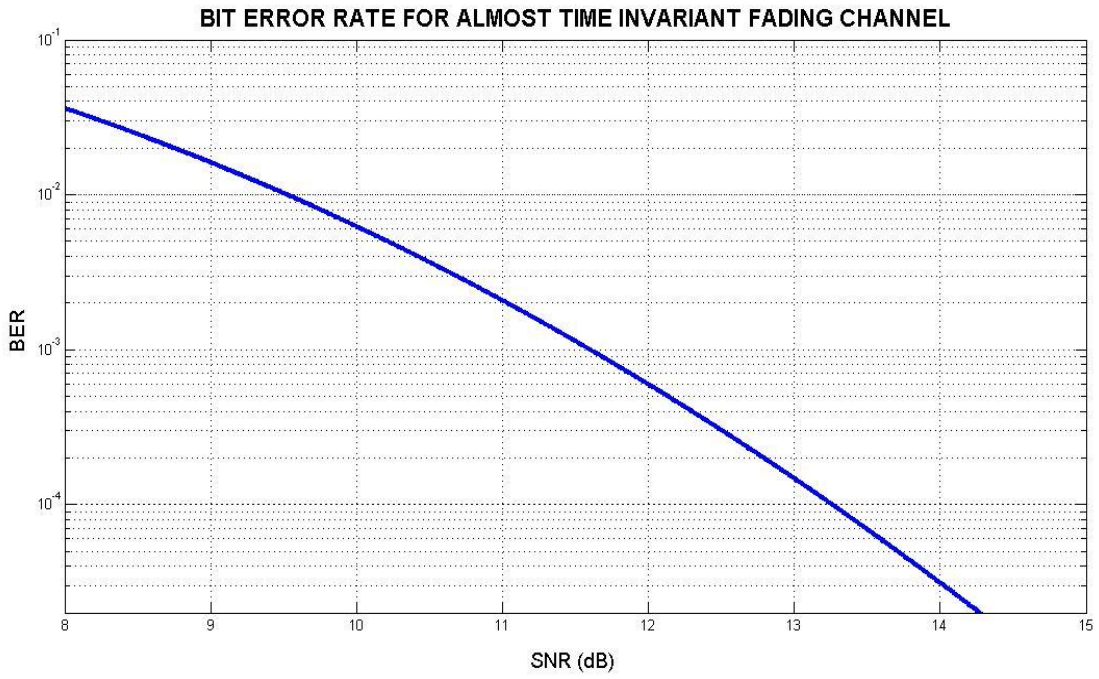

Figure 38. Bit error rate for dual input Kalman estimator with time invariance

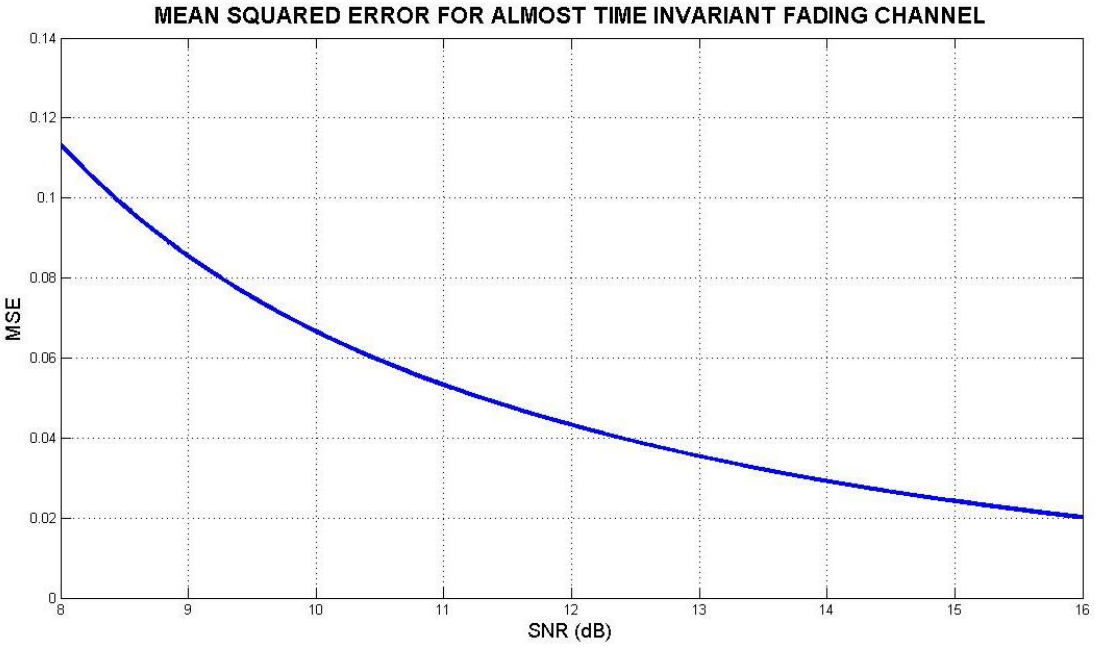

Figure 39. MSE for dual input Kalman estimator with time invariance

During the second simulation, a slowly varying communication channel is reproduced. In this case, the slow time variation produces a value of Doppler spread with a value less than 0.5 Hz. The algorithm seems to be effective again, but the resulting curves of bit error probability and mean squared error, shown in Figures 40 and 41 indicate a very slight degradation in the performance of the estimator compared to the case of no variation at all.

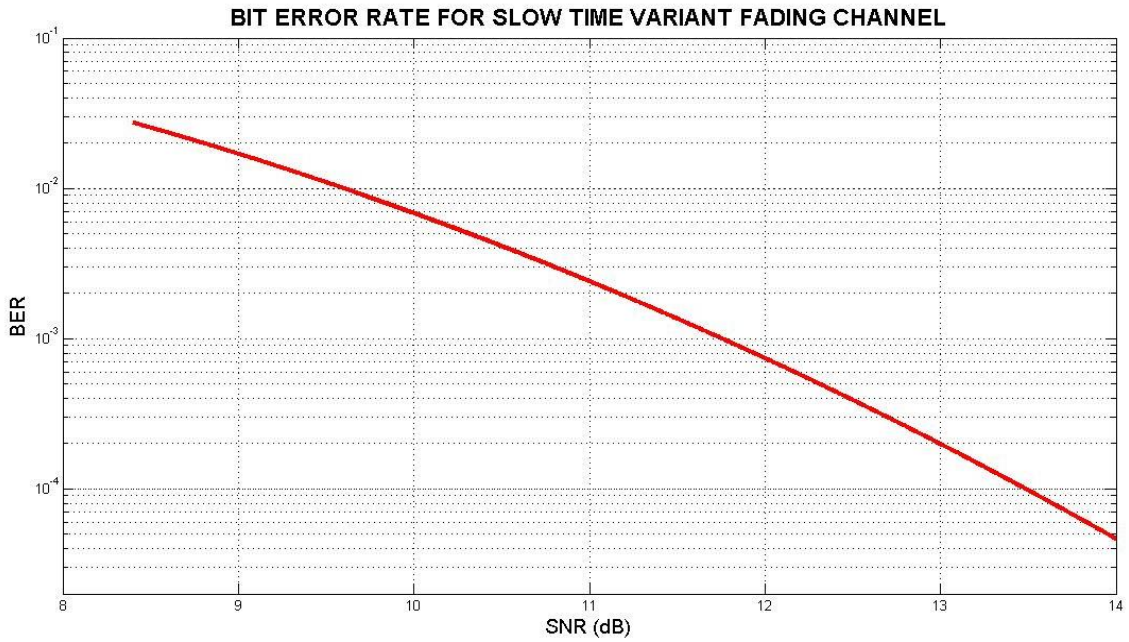

Figure 40. Bit error rate for dual input Kalman estimator – slow time-varying channel

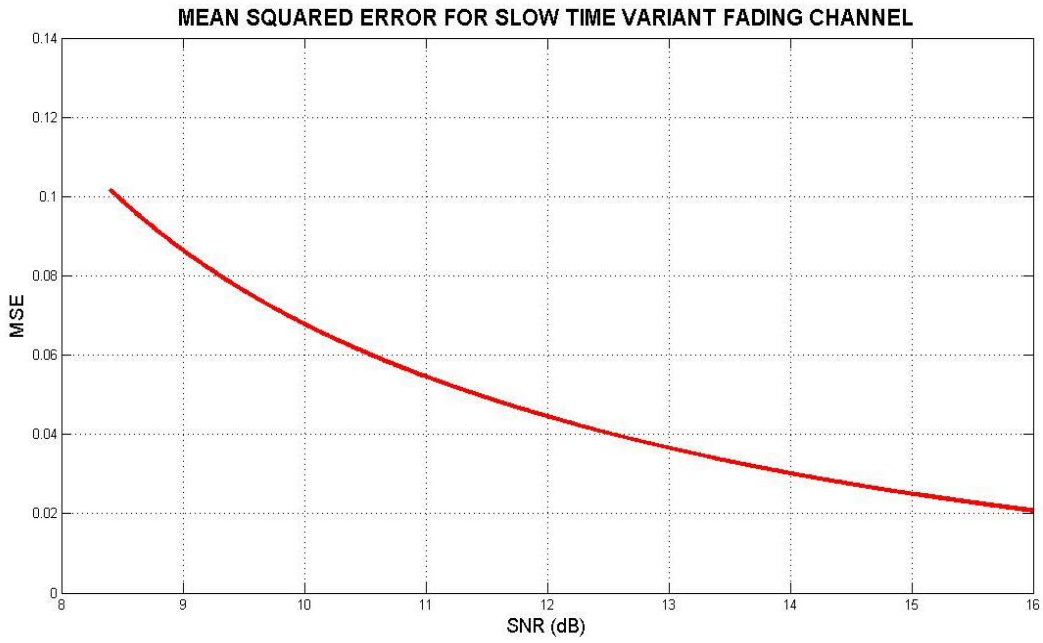

Figure 41. MSE for dual input Kalman estimator – slow time varying channel

The third case involves a fast-varying communication channel, where the high time variation produces a value of Doppler spread on the order of few Hz. In that case the channel can be considered constant only for a time period of about a few tens of symbols. The results, which are shown in Figures 42 and 43, indicate that the degradation in the performance is severe, due to the fast variation. It seems that the algorithm can barely track the channel changes.

Figure 42. Bit error rate for dual input Kalman estimator – fast time-varying channel

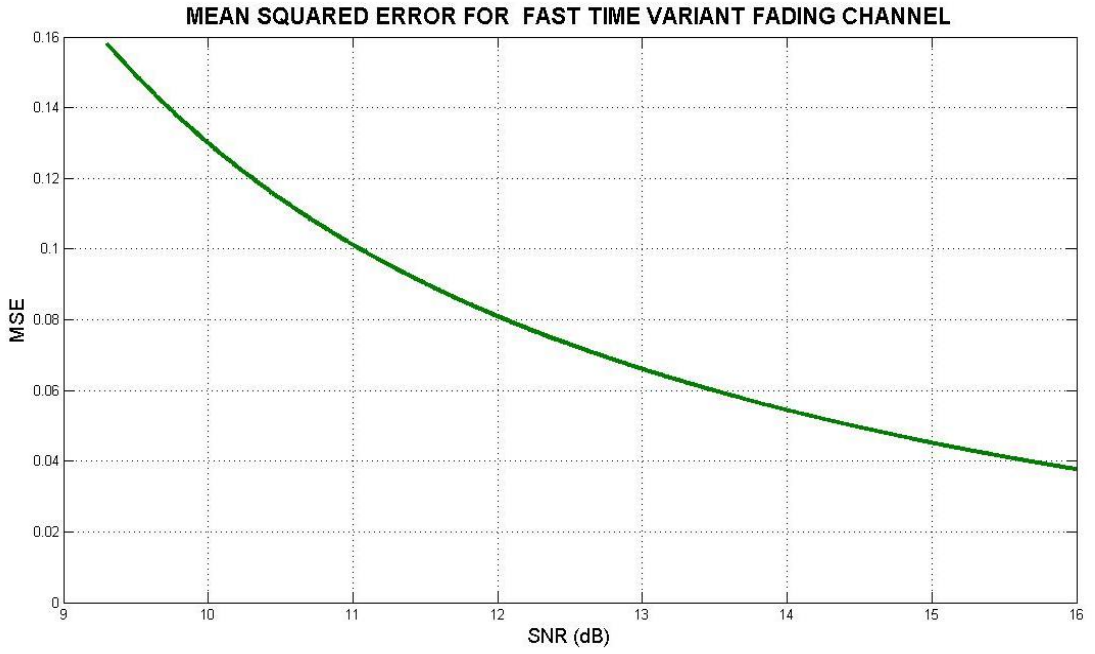

Figure 43. MSE for dual input Kalman estimator – fast time-varying channel

The comparison plots of all three cases are illustrated in Figures 44 and 45. From those figures, it is evident that the fast variation of the channel heavily degrades the performance of the receiver, and therefore a solution to this issue needs to be developed. In Chapter VI, this issue is addressed.

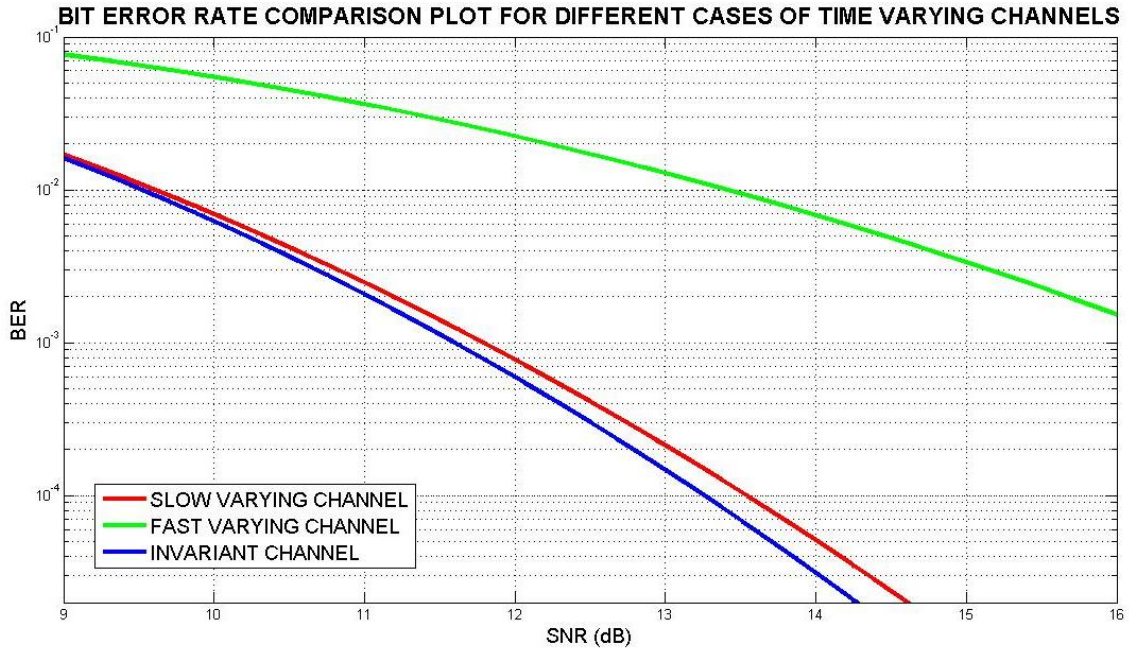

Figure 44. Comparison plot of BERs for different time variant channels

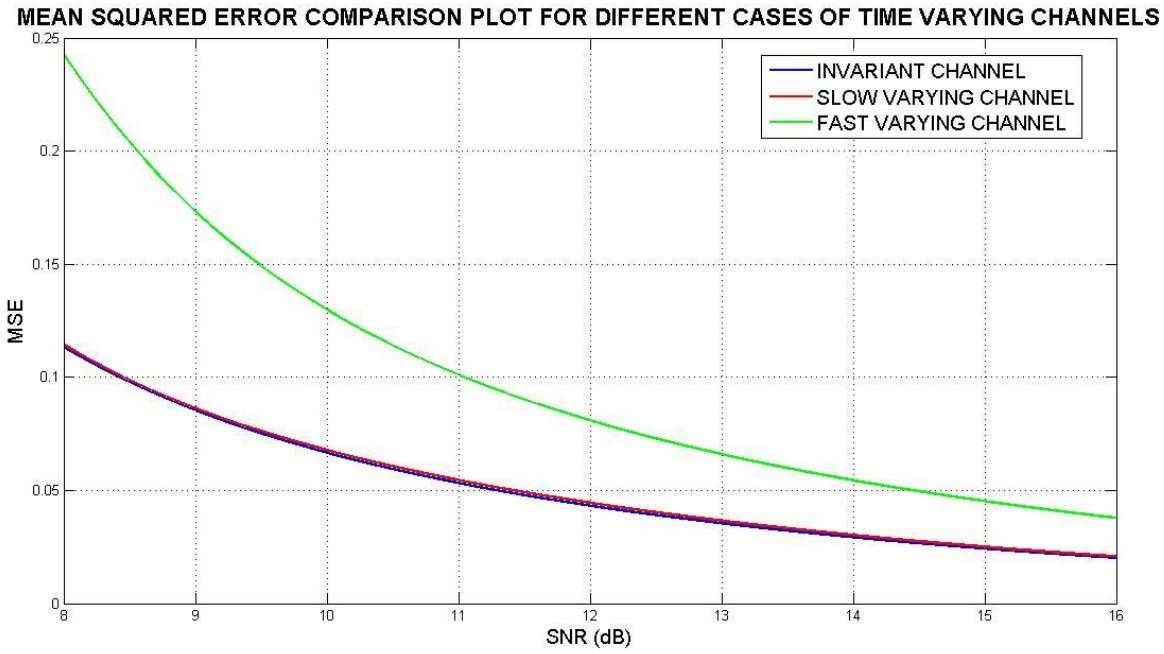

Figure 45. Comparison plot of MSEs for different time-varying channels

C. SPATIAL PROCESSING OF ACOUSTIC COMMUNICATION SIGNALS

1. Theoretical Background - Development of the Estimator

An important feature of underwater communication is the benefit received if spatial diversity is brought into the communication channel. By using an array of several hydrophones in the receiver, instead of a single hydrophone, spatial diversity is introduced into the communication link. Then, by employing appropriate signal processing algorithms, environmental noise can be attenuated and signal multipath propagation can be exploited to maximum advantage. This section develops the approach for spatially combining the signals from hydrophones to enhance the power of the received signal. The result can then be further equalized to compute estimates of the transmitted symbols.

Consider an underwater communication channel where the transmitter is a single projector in the water column transmitting an acoustic BPSK signal. Call $d[n]$ the transmitted signal data symbol in baseband. Also consider a vertical array of hydrophones situated close to the bottom of the water column. This array

is constituted by M hydrophones. A single hydrophone will receive multiple replicas of the signal sent, distorted in time and frequency due to multipath effect and Doppler shift. The mth hydrophone receives the acoustic signal $y_m[n]$:

$$\begin{aligned} y_m[n] &= h_{m,1}[n]d[n-N_{m,1}]+...+h_{m,l}[n]d[n-N_{m,l}]+... \\ &+h_{m,L}[n]d[n-N_{m,L}]+w_m[n] \end{aligned} \tag{5.52}$$

where $h_{m,l}[n]$ is the impulse response associated with the lth path and the mth hydrophone, $N_{m,l}$ is the number of time samples delay associated with the lth path and the mth hydrophone, and $w_m(n)$ is the environmental noise received by the mth hydrophone. The $Mx1$ vector $\underline{y}[n]$ containing the array's received signals is defined as follows:

$$\underline{y}[n] = \begin{bmatrix} y_1[n] \\ y_2[n] \\ . \\ y_M[n] \end{bmatrix} \tag{5.53}$$

Then, Equation 5.52 can be written in matrix form:

$$\underline{y}[n] = \underline{H}[n]\underline{d}[n] + \underline{w}[n] \tag{5.54}$$

where $\underline{H}[n]$ is the MxK impulse response matrix, where K is the time sample delay corresponding to the longer channels' impulse response

$$H[n] = \begin{bmatrix} h_{1,1}[n] & h_{1,2}[n] & . & . & h_{1,K}[n] \\ h_{2,1}[n] & . & . & . & . \\ . & . & h_{m,l}[n] & . & . \\ . & . & . & . & h_{M-1,K}[n] \\ h_{M,1}[n] & . & . & h_{M,K-1}[n] & h_{M,K}[n] \end{bmatrix} \tag{5.55}$$

Also, $\underline{d}[n]$ is the $Kx1$ transmitted signal vector

$$\underline{d}[n] = \begin{bmatrix} d[n] \\ d[n-1] \\ . \\ d[n-K+1] \end{bmatrix} \tag{5.56}$$

and $\underline{w}[n]$ is the $MX1$ environmental noise vector:

$$\underline{w}[n] = \begin{bmatrix} w_1[n] \\ w_2[n] \\ . \\ w_M[n] \end{bmatrix} \tag{5.57}$$

The function of the spatial combiner is to enhance the signal reception by constructively combining all received signals. Based on the underwater acoustic experiments that took place all around the world [9, 12, 43, 92-103], in the vast majority of the cases there is a strongest reception among all multipath receptions. Sometimes, but not always, this is the direct propagation path reception. Taking advantage from this fact, a spatial combiner was designed that detects the angle of arrival of the strongest reception and steers the array to this specific angle. In that way, the strongest reception is amplified while the remaining multipath receptions and the environmental noise are suppressed. For the accurate focusing of the array, not only the phase shift created by the angle of arrival in the different hydrophones must be taken into account, but also the time delays that exist due to the angle of arrival.

The algorithm used for the spatial combiner is similar to the eigenvalue method analyzed in [104]. The method described in that paper enhances the bearing-resolving capabilities of an array. In order to understand the development of the algorithm, an understanding of the array processing methods is required. Therefore, before describing the actual spatial processing algorithm, a simplified ideal case of array processing is presented next.

Consider the case illustrated in Figure 46. A single acoustic pressure plane wave propagates through the water and is received by an array of equally spaced hydrophones. The incoming plane wave forms an angle θ_0 with respect to the array axis. Assuming there is no noise and following Figure 46, in this simplified case, using Equation 5.52 with $L=1$ the received signal $y_m[n]$ by the mth hydrophone will have the following form:

$$y_m[n] = A[n]\exp\left(i\omega_o(n - m\frac{r\cos\theta_0}{c}) + i\varphi \right), \qquad m \in \{0,1,...,M-1\} \tag{5.58}$$

where c is the wave's speed in the medium, $A[n]$ is its amplitude, and r is the distance between adjacent hydrophones. The signal in a beam pointed at angle θ with respect to the array axis is given by the following relation:

$$Y1(n,\theta) = \sum_{m=0}^{M-1} a_m y_m[n] \tag{5.59}$$

The coefficients a_m in Equation 5.56 have the following form:

$$a_m = |a_m| \exp(jm\omega_o \frac{r\cos\theta}{c}) \tag{5.60}$$

Following Equation 5.60, the magnitude of coefficients a_m adjusts the shaping of the beam, minimizing, for example, the side lobes. For the purposes of the communication scheme, $|a_m| = 1$ is chosen. The other term in Equation 5.60 is responsible for the tilt of the beam at an angle θ. By using Equation 5.60 and by setting $|a_m| = 1$, Equation 5.59 becomes:

$$Y1(n,\theta) = \sum_{m=0}^{M-1} y_m[n] \exp(jm\omega_o \frac{r\cos\theta}{c}) \tag{5.61}$$

The wavenumber component on the beam axis is given by the relation $k = \omega_o \frac{\cos\theta}{c}$. Then from Equation 5.61 the following relation results:

$$Y1(n,\theta) = \sum_{m=0}^{M-1} y_m[n] \exp\ ikmr \tag{5.62}$$

From Equation 5.62 the conclusion is that beamforming is the same as computing the spatial Fourier transform of the *M* signals from the array. The spatial frequency *k* corresponds to the look angle θ.

For the task of the sound wave direction finding in frequency analysis, each of the *M* channels is filtered, and the spatial Fourier transform is estimated. In the case of Figure 46, the square of the magnitude of this transform will have a peak when $k = k_0$ [105].

Therefore, in this simplified case, in order to achieve the goals and combine the arriving signals, the beam can be steered to the direction of arrival of the sound waves θ_0, thus combining spatially the incoming signals in an optimum manner. The hydrophones' received signals can then be spatially combined using Equation 5.62, with $k = k_0$.

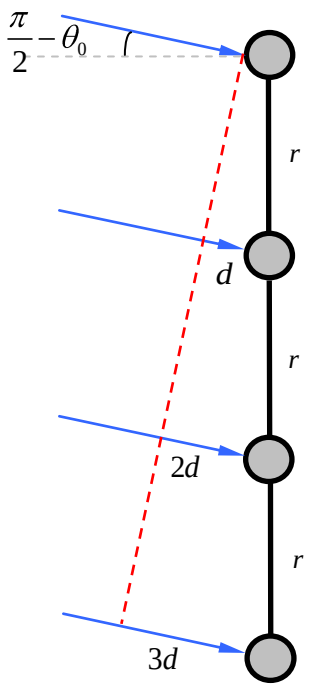

Figure 46. Acoustic pressure plane wave approaching a four hydrophones array

In the general problem, a number of rays arrive at the hydrophone array and the received signals in the array are distorted by noise. The task will be to

obtain a set of weights—steering vector for the hydrophones' inputs that will steer the receiving beam with the highest possible accuracy to the direction of the strongest reception. Equations 5.59, 5.61 and 5.62 present a simple method to calculate the direction of arrival of a single sound wave where noise level is very low. In the actual case though, with multiple arrivals where noise levels are high, this method cannot be successful. Therefore, this section will describe and apply an improved algorithm, an adaptive method based on the particular signal and noise field received by the array, which is similar to the eigenvalue method presented in [104]. The task in this method will be, as previously stated, to determine the constant value of phase shift between adjacent hydrophones. As a result, the spatial combination of the hydrophone input signals will be optimum, taking advantage of spatial diversity. This constant phase shift will correspond to the strongest reception among all arrivals on the array.

Let the overall received signal on the hydrophone array be the $Mx1$ vector $\underline{y}[n]$, where M is the number of hydrophones in the array. The algorithm operates as follows. Using the M hydrophone output signals, the MxM autocorrelation matrix R_{yy} of the array hydrophone receptions is formed. The spatial correlation matrix is defined as:

$$R_{yy} = E\ \underline{y}[n]\underline{y}^{*T}[n]\ \simeq \frac{1}{N}\sum_{n=0}^{N-1}\ \underline{y}[n]\underline{y}^{*T}[n] \tag{5.63}$$

where *N* is the number of signal samples used in the empirical computation of the spatial correlation matrix. The assumption is that *N* is very large.

Examining the simplified case where $L=1$, it will be shown next that the largest eigenvector corresponds to the direction vector of a single plane wave arriving on the array.

From Equation 5.53 and 5.54, using Equation 5.58, the following relation results:

$$\underline{y}[n] = d[n]\underline{v_0} + \underline{w}[n] \tag{5.64}$$

where $\underline{v_0}$ is a plane-wave direction-of-look $M \times 1$ vector. Each element of $\underline{v_0}$ is given by $v_{oi} = \exp(-im\frac{r\cos\theta_0}{c})$ with $m \in \{0,1,...,M-1\}$, while $d[n] = A[n]\exp\ i\omega_o n + i\varphi$.

From Equation 5.63, using Equation 5.64, for R_{yy} the following results are achieved:

$$R_{yy} = \frac{1}{N}\sum_{n=0}^{N-1} \underline{v_0}\,\underline{v_0}^{*T} A(n)^2 \ + \frac{1}{N}\sum_{n=0}^{N-1} \underline{w}[n]\underline{w}[n]^{*T} \tag{5.65}$$

which implies

$$R_{yy} = \underline{v_0}\,\underline{v_0}^{*T}\left\{\frac{1}{N}\sum_{n=0}^{N-1} A(n)^2 \right\} + \left\{\frac{1}{N}\sum_{n=0}^{N-1} \underline{w}[n]\underline{w}[n]^{*T} \right\} \tag{5.66}$$

where in this result the cross terms involving signal and noise are assumed to be negligible. From Equation 5.66, it is evident that R_{yy} contains two matrixes, one corresponding to signal and the other to noise. Then:

$$R_{yy} = \underline{v_0}\sigma_d{}^2\underline{v_0}^{*T} + \sigma_w{}^2 Q \tag{5.67}$$

where Q is the noise correlation matrix. By inspection of Equation 5.67 and assuming that signal is much stronger than noise in the receiving hydrophones, so that $\sigma_d{}^2 >> \sigma_w{}^2$, the conclusion is that the eigenvector corresponding to the maximum eigenvalue of R_{yy} will be the signal direction vector $\underline{v_0}$.

In the general case, where a number of rays arrive on the hydrophone array, the method will operate as follows. First, apply singular value decomposition on the spatial correlation matrix:

$$R_{yy}\underline{v_i} = \lambda_i \underline{v_i} \tag{5.68}$$

where λ_i are the eigenvalues associated with the eigenvectors $\underline{v_i}$. The autocorrelation matrix R_{yy} can be expressed as:

$$R_{yy} = V\Sigma V^{*T} \tag{5.69}$$

where $\underline{\Sigma}$ is a diagonal MxM matrix containing the eigenvalues λ, V is an MxM matrix containing the eigenvectors $\underline{v_i}$ and ^{*T} stands for complex conjugate transpose.

In the general case where there are L paths and M hydrophones in the array with $M > L$, the form of the array Σ will be as follows:

$$\Sigma = \begin{bmatrix} \sigma_1 + \sigma_{w1} & 0 & 0 & 0 & 0 & 0 \\ 0 & . & 0 & 0 & 0 & 0 \\ 0 & 0 & \sigma_L + \sigma_{wL} & 0 & 0 & 0 \\ 0 & 0 & 0 & . & 0 & 0 \\ 0 & 0 & 0 & 0 & \sigma_{w(M-1)} & 0 \\ 0 & 0 & 0 & 0 & 0 & \sigma_{wM} \end{bmatrix} \tag{5.70}$$

where in general $\sigma_i >> \sigma_{wi}, \quad i = 1, 2, ..., M$.

Inspection of Equation 5.70, reveals that the L eigenvectors corresponding to the largest eigenvalues are related to signal receptions from different paths. Additionally, they are much larger than the $M - L$ other eigenvectors, which do not correspond to the signal but to environmental noise. In this general case, the *L* eigenvectors corresponding to the largest eigenvalues comprise an orthonormal basis for the vector space containing the signal vectors. Consider the eigenvector $\underline{v_{prin}}$ corresponding to the largest eigenvalue $\lambda_{\max}$. Its principal component is the strongest received signal—strongest arrival—while the other weaker arrivals consist of a small—noise-like—contribution.

As explained before, since a plane sound wave incidence is assumed, there will be a constant phase shift θ_p between adjacent hydrophones. Using the above described method, an estimate of the strongest arrival direction vector $\underline{v_o}$ is obtained. The use of $\underline{v_o}$ can lead to the optimum spatial combination of the received signals, giving the signal $y_{sc}[n]$ through Equation 5.71:

$$y_{sc}[n] = \underline{v_o}^{*T}\,\underline{y}[n] \tag{5.71}$$

Instead of using the vector v_{prin} (which is the estimate of the direction vector $\underline{v_o}$) in Equation 5.71, the direction vector can be reconstructed by evaluating the phase shift between adjacent hydrophones θ_p. To do that, first the Fourier transform of the principal eigenvector is estimated:

$$\underline{v_f} = FFT\ \ \underline{v_{prin}} \tag{5.72}$$

and normalized to the maximum value of the vector $\underline{v_f}$

$$\underline{v_{f,norm}} = \frac{\underline{v_f}}{\max\ \ abs\ \ \underline{v_f}} \tag{5.73}$$

The best estimate of the phase shift between adjacent hydrophones for the strongest reception angle, θ_p, will be that value in the spectrum of values of θ_p, which corresponds to the maximum of the magnitude of $\underline{v_{f,norm}}$, which has a value of 1.

Finally, by using the computed phase shift θ_p, the associated time delay τ_p between adjacent hydrophones receptions can be estimated using the following relation:

$$\tau_p = \frac{\theta_p}{\omega_o} \tag{5.74}$$

Figure 47 illustrates an example of the result of this algorithm. In this example, the strongest reception has a phase shift -0.11 radians between adjacent hydrophones in the array.

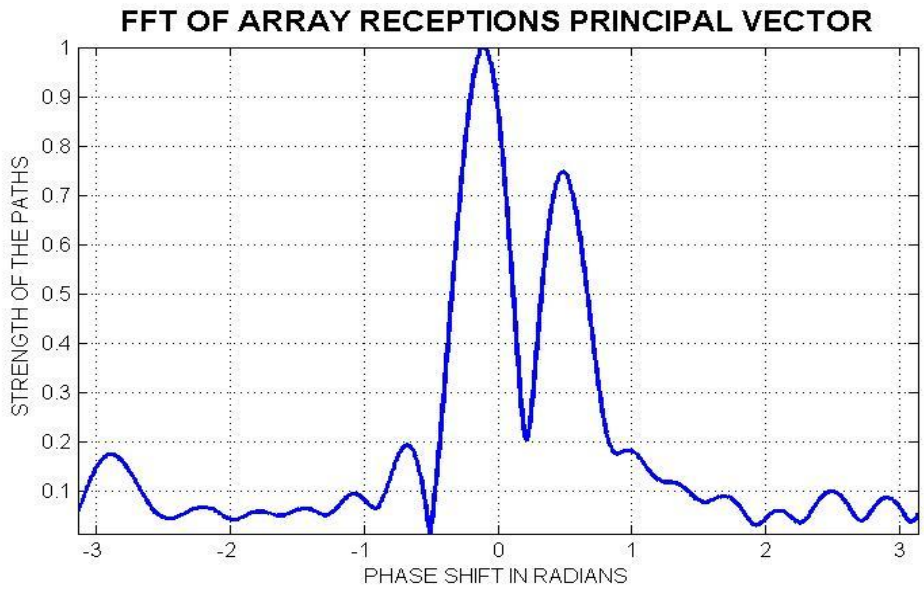

Figure 47. Example of result of the spatial combiner's algorithm

The obvious limitations in the accuracy of the method described above are, first, the number of receiving elements and, second, the phase ambiguity. Other parameters that limit the performance of the method in a real environment are the geometry of the channel, the length of data used to form the autocorrelation matrix, and the approximations (e.g., plane wave incidence). For reasons that will become clearer in the next section, only the phase shift information concerning the strongest reception is used in the spatial combiner operation. The spatial combiner can then operate as follows: Correct the phase in each branch—in each hydrophone—by using the known phase shift, then align in time the signal pulses for each branch by using the known time delay between adjacent hydrophones, and finally, sum up all the waveforms. The output waveform is a surprisingly clear waveform that can be used as input to a possible next stage of the receiver (some form of equalizer). Noise, reverberation and multipath effect are suppressed.

2. Simulation Results

In order to verify the effectiveness and robustness of the spatial combiner's algorithm to determine the main receptions, a simulation was developed. In this simulation, only three straight line (ray–like) propagation paths are considered—direct, bottom bounce and surface bounce—having relative strengths 1, 0.7 and 0.8, respectively. The signal is also distorted by AWGN with the signal to noise ratio in the receiver on the order of 7 dB. A BPSK signal with radial frequency of 50000 rads/sec and sampling frequency of 200000 samples/sec is sent through this type of underwater channel. In each simulation, 60 bits at a data rate of 1333 bits/sec are transmitted. The communication acoustic signal is received from an array of hydrophones and processed, in order to extract the phase shifts and path strengths of the different paths.

During the simulations, values for depth of the sea from 70 to 300 meters, for receiver-transmitter, distances from 3000 to 8000 meters were used. The receiving hydrophone array lies close to the bottom of the sea, while the transmitting projector lies in the middle of the water column or lower. The array has 12 to 16 hydrophones with spatial separation of 0.8 to 1.5 meters among them.

The results of the simulation are extremely accurate for the phase shift of the strongest path for all simulations. Therefore, attention was concentrated to the strongest path, which gives the highest reliability for its phase shift value's accuracy. The resulting phase shift corresponds to a value of time difference between the arrival times of two wave pulses in two adjacent hydrophones. From now on this value is called, “time delay between adjacent hydrophones” τ_p and it is related to the estimated phase shift θ_p from Equation 5.74.The spatial combiner will then correct the phase in each branch by using the estimated phase shift θ_p, while also aligning in time the waveforms of each branch by using the known time delay between adjacent hydrophones τ_p. Finally, it will sum up all waveforms. This operation is described in the following equation:

$$s(t) = \sum_{m=0}^{M-1} x_m(t - m\mathrm{T} + m\tau_p) e^{-im\theta_p}, \qquad m \in \{0,1,...,M\} \tag{5.75}$$

The results of the simulations are very promising. In order to test the effectiveness of the combiner, the mean squared error for both cases of a single hydrophone and multiple (array) hydrophones detection are computed. As expected, the performance of the array processor is substantially better and yields an improvement, in terms of the MSE, of at least 1 to 2 orders of magnitude.

The plot of Figure 48 illustrates an example of the performance of single hydrophone detection versus an eight-hydrophones' array detection. The simulation concerns a 240 meters water column where three main paths—of straight line sound propagation—are present in the reception. The distance between transmitting and receiving elements is 7000 meters. A single transmitting projector is situated at a depth of 100 meters in both cases. The lower hydrophone of the array is situated in a depth of 230 meters while the distance between successive elements is 0.8 meters. Finally, the single receiving hydrophone lies at a depth of 230 meters. Following Figure 48, it is evident that, for this set of parameters, the array's use gives an improvement in the resulting MSE greater than 9 dB compared to the single hydrophone case.

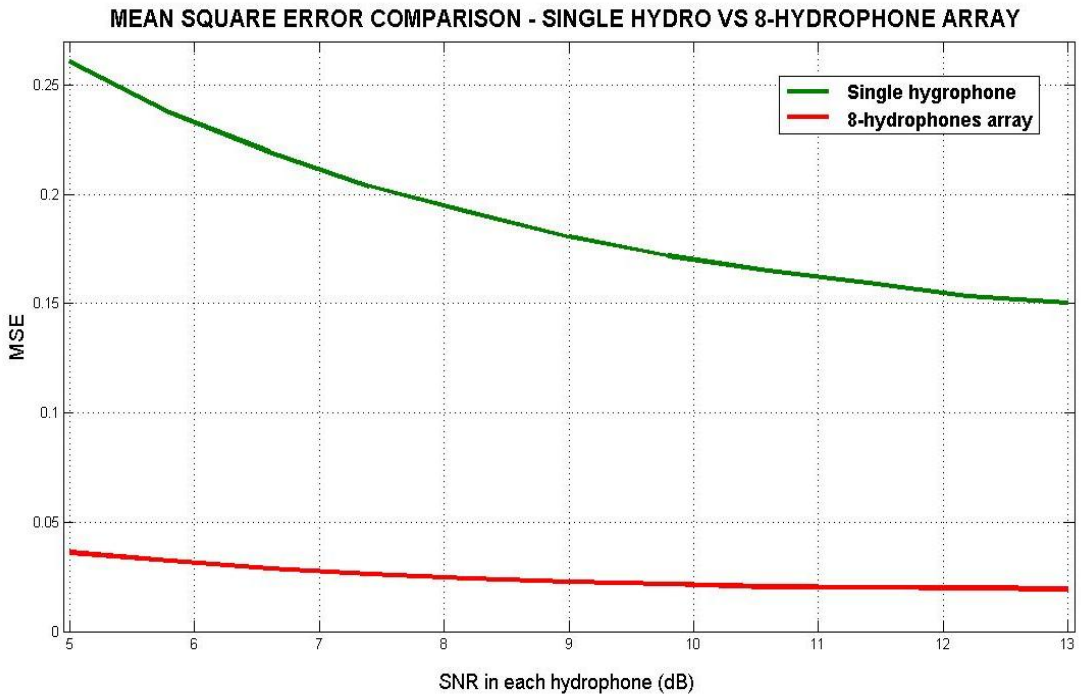

Figure 48. Simulation result of array versus single hydrophone performance

A great number of samples per bit seem to be necessary for the method to be accurate. The number of samples that will be used to form the autocorrelation matrix must be large, (the larger the better). The Doppler effect is not affecting the method's performance at all. The information of the Doppler shift value is not a requirement for the proper function of the method of strongest path's phase shift estimation. As a result, the Doppler shift estimation and correction can be possibly encountered as a separate problem in next stage of the receiver (equalizer). Finally, this first stage of the receiver must be somehow adaptive, since the underwater acoustic environment is quite dynamic. It is crucial that the spatial combiner operates properly in order to make the task of receiver's next stage straightforward.

VI. PROPOSED RECEIVER AND EQUALIZER SCHEME

This chapter introduces an innovative equalizer/receiver for the accurate demodulation of the DSSS acoustic signal. Its performance will be presented and compared with other reception schemes.

A. THEORETICAL DEVELOPMENT OF THE EQUALIZER

Multiple receiver equalizers present a great advantage, as opposed to systems based on single receivers, due to the spatial diversity offered by an array of hydrophones. In the case of a deep faded acoustic environment, not only will the signal to noise ratio be increased, but the probability of deep fading will be considerably reduced, resulting in improved data recovery.

There are two necessary requirements to ensure spatial diversity. First, sufficient spacing must exist between the hydrophones in order to ensure that the different multipath components have different propagation delays, and so the hydrophones' received signals will fade independently. According to [22], several wavelengths' separation between the receivers (hydrophones in this case) is required. The second requirement is the optimum processing of the numerous input signals by the equalizer. The question that then arises is, what computational cost is needed for the design of this robust receiver?

Multiple input equalizers are known to offer optimum performance in digital communications, even with a relatively small number of input channels. A receiver with two or more inputs which provides blind estimation of its parameters is suggested in [47]. This receiver has two running modes: in the beginning a linear equalizer is enabled. When the estimated mean squared error of the processed data falls below a preset value, the receiver turns to a conventional decision feedback equalizer. As the number of input channels increases, however, the computational complexity of such a design gets very high for the underwater applications being examined, even for relatively low data rates and carrier frequencies as in acoustics communications. This high computational

complexity will lead to high computational time that is not suitable for the underwater acoustic communication network. Also, it will shorten the battery life of the nodes in the acoustic network.

In order to take maximum advantage of the spatial diversity while reducing the dimensionality of the DFE, the signals are preprocessed by a spatial combiner to improve the SNR. For example, in [106] and [107], a spatial combiner, in conjunction with a multichannel decision feedback equalizer, is presented. The many-to-few spatial combiner is used to combine the received signals and reduce the dimensionality of the multichannel DFEs. Receiver operations are optimized jointly in this scheme. Finally, a receiver scheme containing a beamformer and a single input equalizer was proposed in [36].

Motivated by the above ideas, this chapter presents a robust communication receiver that will take advantage of the spatial diversity of an array of hydrophones with an acceptable computational complexity.

The general structure at the basis of the proposed design is an array of hydrophones, followed by a spatial combiner and a dual input equalizer based on a Kalman filter estimator, having a relatively low computational complexity. The spatial combiner is designed based on array processing theory, whereas the equalizer will be based on optimal estimation. The effectiveness of the proposed techniques will be assessed on the basis of the MSE of the processed data from experiments performed under various conditions.

Figure 49 illustrates a general design for this idea of two processing stages with a dual input estimator structure. An array of M hydrophones receives M signals, supplying them to the spatial combiner, which processes them and produces two output signals to be processed again by a dual-input Kalman filter estimator. The first input will be the result of the spatial combining of the upper M/2 hydrophones and the other one of the lower M/2 hydrophones. Following the example of Figure 49, the array has four hydrophones in the water column, receiving three main acoustic signals (direct, bottom-bounced and surface-

bounced acoustic signals) plus environmental noise. The outputs of the upper and the lower two hydrophones are combined separately (by combiners A and B) and used as inputs to the next receiver's stage, which is the dual input Kalman filter estimator. The output of the estimator is then the extracted data sequence.

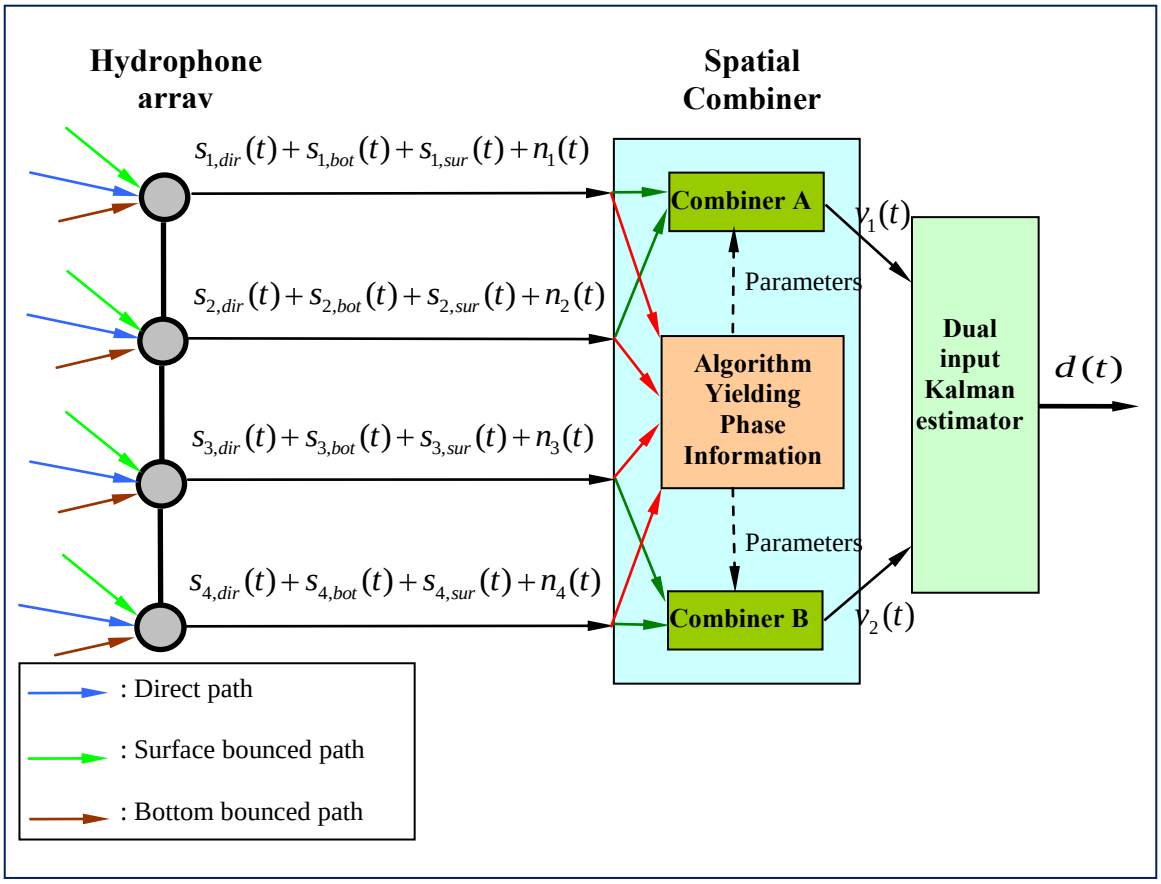

Figure 49. Two processing stages dual input equalizer with array of four hydrophones

A system like the one described above can be designed to achieve the desired performance with acceptable computational complexity. In the next section, based on the general structure of Figure 49, an innovative receiver structure will be developed, starting from a relatively simple configuration, and gradually improving the structure of the receiver toward a more reliable and

robust communication scheme. All receiver configurations are evaluated using the experimental data from MAKAI 2005 experiment, which was briefly described in Chapter III.

B. DEVELOPMENT OF ACTUAL IMPLEMENTATION

The implementation of the two processing stages dual input estimator is based on the theoretical background of the Kalman estimator and spatial processing developed in Chapter V, together with the principal component analysis and the channel identification algorithm developed in Chapter III.

Before starting the development of the receiver, information regarding the experiment MAKAI 2005 will be presented in the following section.

1. The MAKAI 2005 Experiment

The receiver proposed in this dissertation has been tested on data from the MAKAI 2005 experiment, which was briefly described in Chapter III in terms of the estimated underwater channel and its scattering function. The duration of the experiment was approximately 14 minutes. The setup consisted of one transmitting projector situated at 8 meters depth and a receiving array of hydrophones situated at 3 meters depth and below. The receive array consisted of eight hydrophones separated by approximately 25 centimeters. The distance between the transmitting element and the receiving array was about 2200 meters and the signal to noise ratio in the received data was very low, between 0.5 and 2.5 dB, depending on the receiving element in the array.

The transmitting source was deployed over the side of the drifting Kilo Moana vessel, and the 8-element receiving array was drifting as well. Since transmitting and receiving systems were both drifting freely, the distance between them stayed almost constant at about 2200 meters, but at the same time, the Doppler shift was expected to be significant, as was verified in Chapter III.

For channel identification purposes, the DSSS/BPSK signal with code length 511 chips was chosen. For the communication scheme, the most suitable signal to be used was the DSSS/BPSK with code length 63 chips. From channel identification, as described in Chapter IV, the multipath spread of the acoustic channel was 7-8 msecs. Since the bit duration was 3.15 msecs, the multipath effect spanned 3 bits. In each repetition of the transmission during the experiment, 144 bits were sent; roughly every 70 seconds. In total, the signal train was transmitted repetitively 12 times.

2. Description of Signal's Preprocessing

The received sequence from the eight hydrophones is a spread spectrum bandpass signal with center frequency at 35 KHz. In order to have a signal ready to be used in the spatial combiner and/or the Kalman estimator, some preprocessing is necessary as described below.

First, the signal needs to be acquired by the receiver and synchronized. As discussed in Chapter IV, during the acquisition phase the received signal is demodulated to baseband and despreaded by cross-correlating the in-phase and quadrature components with two different Gold sequences. This yields 144 vectors of data. The next step is to align these vectors by tracking the beginning of the bit on each vector, as discussed in Chapter IV.

The aligned vectors can be seen as noisy estimates of the channel, carrying the phase of the 3 last bits (since the multipath spread spans 3 bits) and the phase shift induced by the Doppler effect.

A typical despreaded signal (for the lower hydrophone) is illustrated in Figure 50. As seen in this figure, there are two strong returns with high SNR and other weak returns imbedded in noise. In the preprocessing stage only the strong components are kept and the weaker components are completely eliminated (by thresholding).

The received power in Figure 50 consists of the contribution from two paths.

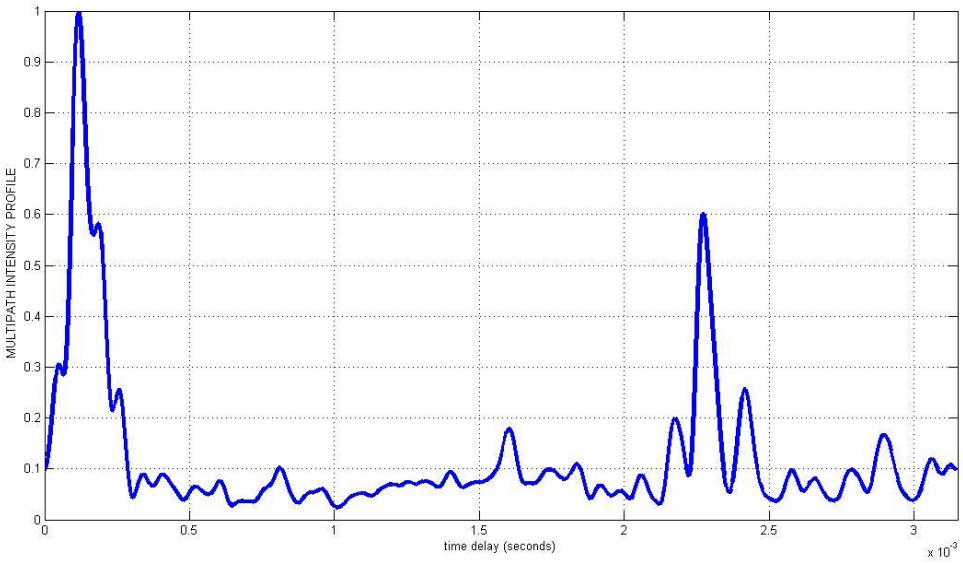

Figure 50. Average power density estimate

In order to attenuate effects due to reverberation and noise, the power density estimate of Figure 50 is used and the positions of the most significant peaks are detected. The choice of the peaks is based on the statistics of the data set. In order to choose which peaks to keep, a threshold was set in advance based on the statistical characteristics of the estimate. The following threshold rule was set for the surviving peaks during the experiment:

$$peaks \;\; P_h(\tau) \;\; > 1.75 std \;\; P_h(\tau) \tag{6.1}$$

where *std* stands for standard deviation and $P_h(\tau)$ is the power density estimate at time τ .

It was ascertained during the experimental processing that by keeping the neighboring data points of the most significant peaks, better performance is achieved. The average power density shown in Figure 50 after processing for noise reduction will have the form of Figure 51.

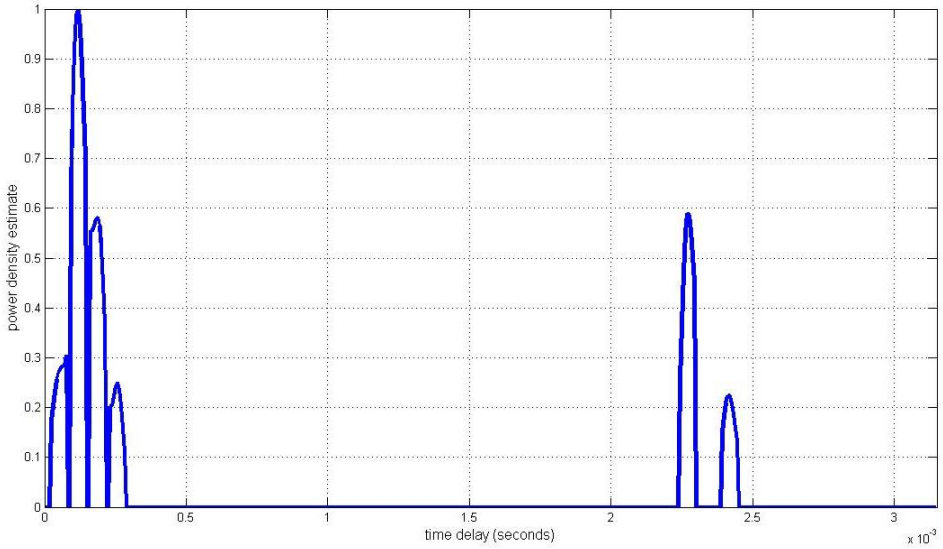

Figure 51. Average power density estimate with only the principal contributions

In summary, after the preprocessing, there are 144 data vectors, which contain only the most significant peaks and their neighboring data points. Those significant peaks correspond to the strongest sound arrivals, whereas the rest of the data points correspond to noise, reverberation and weak arrivals, and they were eliminated. These vectors will be used as input to the equalizer/receiver schemes that will be described next. Each element of the array has a different set of vectors that correspond to the same 144 data bits.

3. Spatial Combiner Configuration

The first structure that will be presented is a spatial combiner that uses array processing methods to detect the information data. This scheme does not include any type of equalization and as such is affected by multipath propagation, so the performance of this type of receiver is based on the structure of the multipath effect. In the case that there is a strong arrival and the rest of the

arrivals are weak, this type of receiver will have a relatively good performance, while, as the relative power contained in the rest of the weaker arrivals increases, the performance will deteriorate.

The proposed receiver spatially combines the vectors from the upper four hydrophones and produces an estimate for the information data, whereas simultaneously the vectors from the lower four are combined in the same way. The two outputs from the upper and lower sub-arrays are combined in the end to give the final result for the received information data. An important aspect is the distance between the centers of the two arrays. This distance is about 1 meter that corresponds to 24 wavelengths, which means that the two sub-array outputs will have significant spatial diversity. An illustration of the configuration is presented in Figure 52.

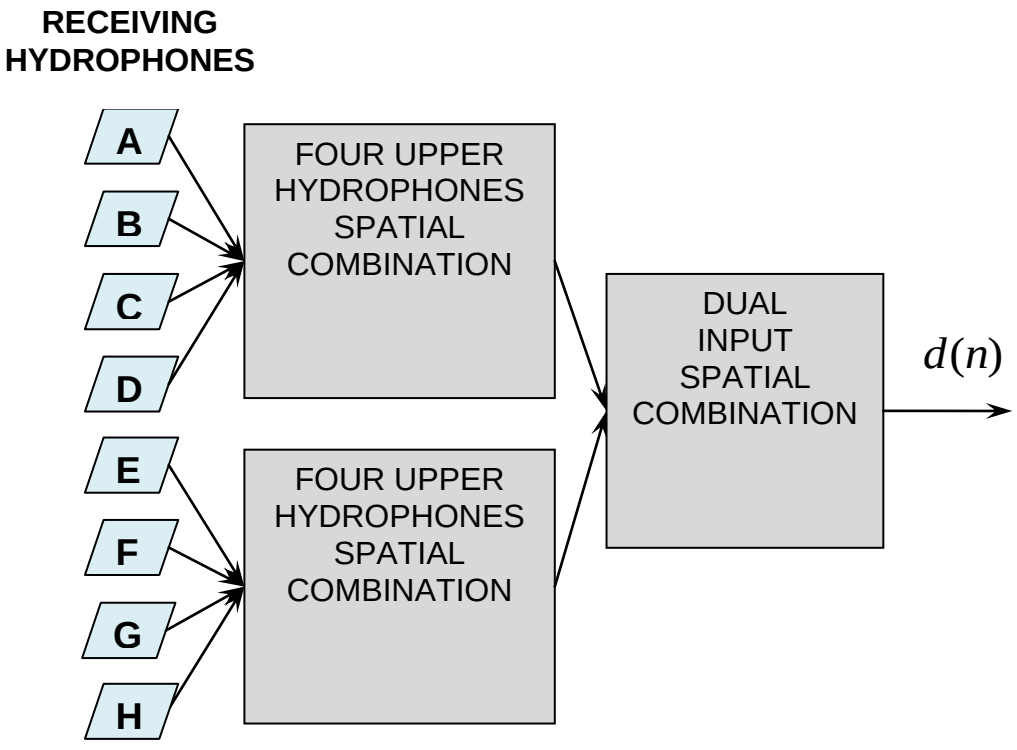

Figure 52. Spatial combiner configuration

As explained in Chapter V, magnitude and phase information of the data is extracted from the strongest direction of arrival, based on the autocorrelation matrix of the received data. This is done separately on the upper half and lower half of the array and then combined together.

Call $\underline{y}_1[n], \underline{y}_2[n]$ the data vectors in the upper and lower half of the array at time *n*, preprocessed so as to keep only the strongest received component. From the two autocorrelation matrices $R_{y_1y_1}, R_{y_2y_2}$ vectors $\underline{v}_1[n],\ \underline{v}_2[n]$ are estimated associated to the strongest directions of arrival for the two sub-arrays, so that

$$\underline{y}_i[n] = d[n]\underline{v}_i[n] + \underline{w}_i[n] \tag{6.2}$$

for $i = 1,2$ with $d[n]$ indicating transmitted data and $\underline{w}_i[n]$ noise. The vectors $\underline{v}_i[n]$ expressing magnitude and phase shift at each hydrophone are estimates of the stronger arrival direction vectors for each sub-array, as analyzed in Chapter V.

The spatial combination on the sub-arrays is performed as described in Chapter V (Equation 5.71):

$$y_{sci}[n] = \underline{v}_i^{*T}[n]\underline{y}_i[n] \tag{6.3}$$

for $i = 1,2$.

In the case of a time-varying channel, as in this experiment, the vectors $v_i[n]$ are time-varying due to Doppler effect. In order to estimate the Doppler shift due to motion between the transmitted and received arrays, successive vectors $\underline{v}_1[n],\ \underline{v}_2[n]$ are cross-correlated and the changes are tracked by a PLL. In particular, let

$$\Delta\theta_i[n] = phase\ \ \underline{v}_i^{*T}[n-1]\underline{v}_i[n] \tag{6.4}$$

be the instant phase shift due to Doppler effect between two successive receptions. Then the phase drift $\varphi_i[n]$ due to the Doppler effect can be computed as;

$$\varphi_i[n] = (1-\kappa)\varphi_i[n-1] + \kappa\Delta\theta_i[n] \tag{6.5}$$

where κ is a forgetting factor between zero and one, usually small (e.g., $\kappa = 0.1$) with initial value

$$\varphi[0] = 0 \tag{6.6}$$

In order to recover the data bits in each sub-array, differential reception is employed using the following equation:

$$d_i[n] = y_{sci}^*[n-1]y_{sci}[n]e^{-i\varphi[n]} \tag{6.7}$$

The result of the data estimation for the upper four elements is illustrated in Figure 53 as a "constellation plot." The experimental data are binary, thus transmitting either +1, or -1. If there was a perfect data reception, in the constellation plot two points would be shown at +1 and -1. In the actual case of imperfect reception, the received data values are complex valued and scattered around the points +1, or -1. The spread of the data points in the constellation plot shows imperfect reception due to environmental noise, multipath spread, and Doppler distortion. The MSE for the case of Figure 53 is 0.034.

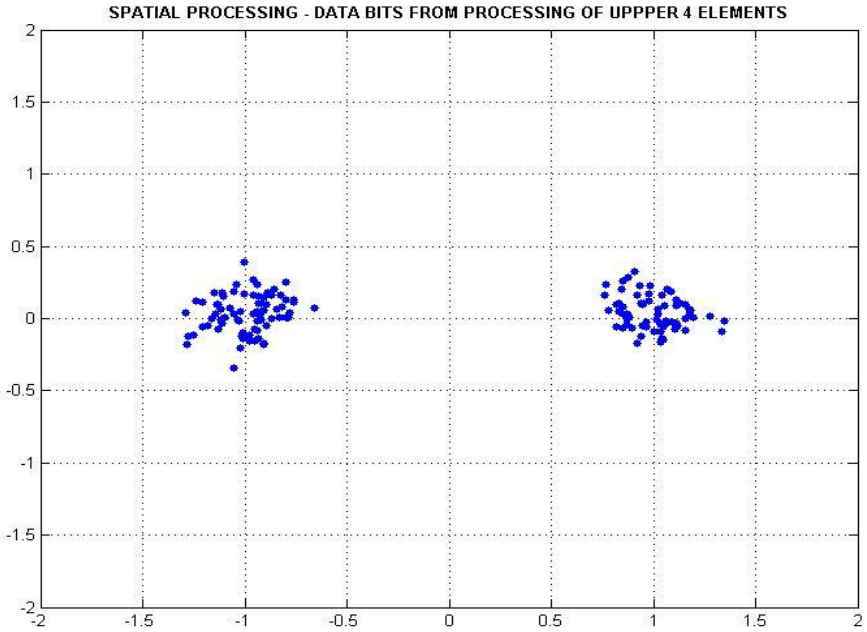

Figure 53. Second repetition. Received data bits. Spatial processing 4 upper elements

The vectors from the lower four hydrophones are processed in the same way. The received data for the lower four elements is illustrated in Figure 54. The MSE for this case is 0.035.

The results from the two sub-arrays can be combined to take advantage of the spatial diversity. This is illustrated in Figure 55. As expected, due to diversity, the combined MSE is lower than the MSE in both estimates. The final MSE for the reception using a spatial combiner scheme is 0.022.

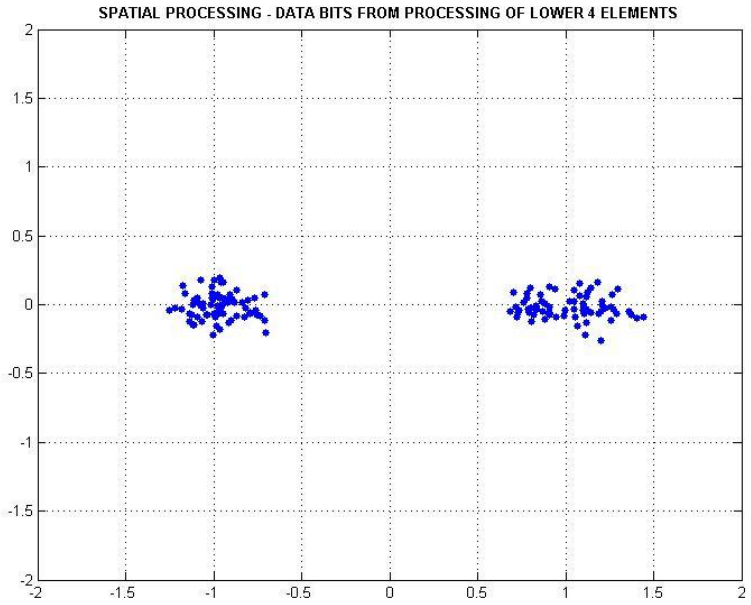

Figure 54. Second repetition. Received data bits. Spatial processing 4 lower elements

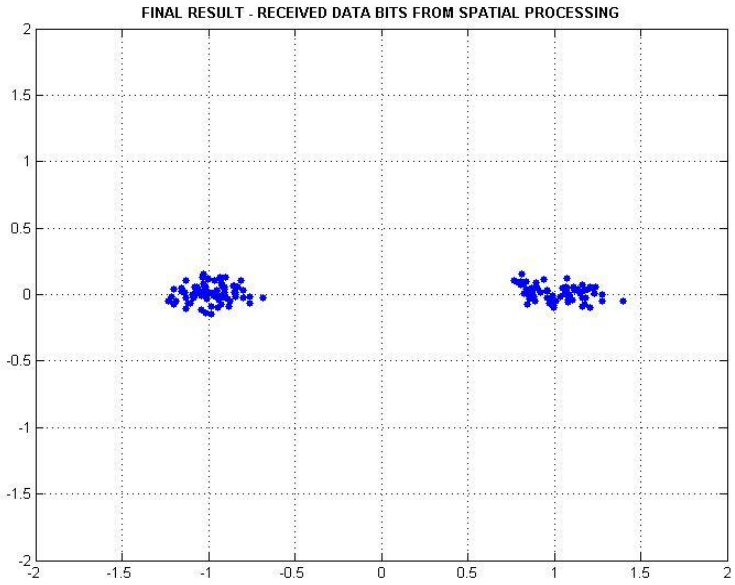

Figure 55. Second repetition. Received data bits. Spatial processing method

There is not strong multipath effect in this experiment, which is why the performance of this type of receiver seems to be robust. Under a severe multipath environment, the performance of this type of receiver would drastically deteriorate unless we properly equalize the received signal.

4. Four Parallel Kalman Estimators Scheme

In this section, an estimation approach based on Kalman filtering operating on pairs of hydrophones and then combined is proposed. Since there are eight hydrophones, this leads to the four Kalman estimators shown in Figure 56.

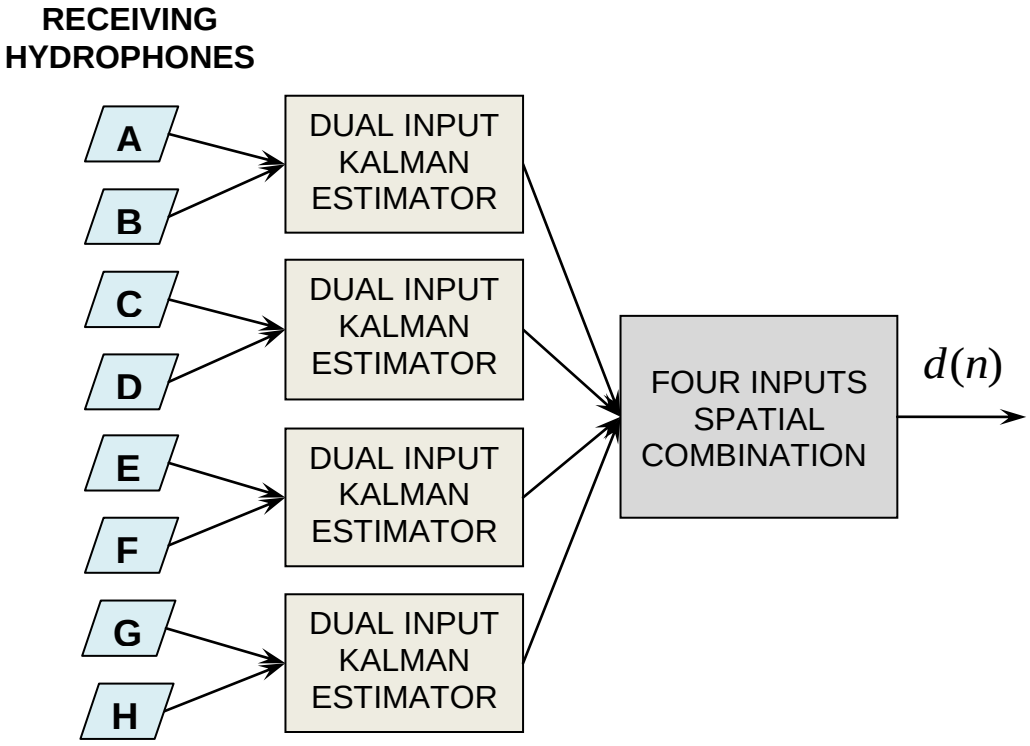

Figure 56. Four parallel Kalman estimators configuration

In order for the equalizer to operate, an initial channel estimate is needed based (say) on the first 16 of the total 144 symbols sent. By examining Figure 57, it can be said that each peak corresponds either to a single arrival, due to a single data bit, or to the combination of multiple arrivals. By knowing the transmitted 16 bits data stream and by examining the received peaks, it can be distinguished which one belongs to each data bit (current bit, previous bit, etc.), and which one is a result of simultaneous arrivals of multiple bits. In the proposed approach, all peaks caused by colliding bit receptions are eliminated and only the peaks related to single bits are kept.

In order to discriminate between these two classes, the variance of each peak over a number of received symbols is examined. Call I the number of peaks, M the number of symbols considered for channel estimation (16 in this case). Let $\upsilon_i[n], i = 1,...I, n = 0,...,M-1$ be the *i*-th peak at the *n*-th symbol.

Then form the data sets $m_{i,k}[n]$:

$$m_{i,k}[n] = \upsilon_i[n]d[n-k] \tag{6.8}$$

for $1 < i < I$, $0 < k < \mathrm{K} - 1$ where K is the is an upper bound on the channel's impulse response, in number of data symbols.

Then for every i,k, the standard deviation of the data set $m_{i,k}[n]$ is estimated by averaging over $n = 0,...,M-1$ the received symbols, as

$$S_{i,k} = std \ \ m_{i,k}(n) \tag{6.9}$$

Next, for the $i_o\mathrm{th}$ signal peak the data bit delay k_{io} is determined, which results in the minimum value of $S_{i_o,k}$,

$$S_{i_o,k_i} = \min \ \ S_{i_o,k} \tag{6.10}$$

The value of k that minimizes the function $S_{i_o,k}$, is taken as the best estimate of the true bit delay for the $i_o\mathrm{th}$ signal peak. The function $S_{i,k}$ cannot be zero, since the peak signals υ_i will always carry data.

In order to eliminate the weak arrivals and those caused by a combination of multiple arrivals, thus improving the performance of the receiver, a threshold was set on the value of S_{i_o,k_i}. This is because in the case of strong dependence on a previous bit, the value of S_{i_o,k_i} will be very small, while in the opposite case—arrivals combination or weak receptions—it will be large. In the MAKAI experiment, the threshold is set to *1* as follows:

$$S_{i_o,k_i} < 1 \tag{6.11}$$

If this threshold is exceeded, the related signal peak is eliminated. At this point, by knowing which data bit delay is responsible for each signal peak, the

estimate is formed of the impulse response of the channel for the first hydrophone. The impulse response estimate is computed by summing the surviving signal peaks for each data bit delay and then averaging out over the M samples.

The above operations are repeated for the rest of the hydrophones.

After forming the impulse responses for all hydrophones the dual input Kalman estimator method is applied to successive hydrophones as shown in Figure 58. The method used is the one described in Chapter V, Section C. The only modification to the described Kalman estimator is that the reception of the data is done in blocks of 32 data bits. In the end of every block of data, except the LMS adaptation (presented in Chapter V), adaptation of the impulse response estimate is also applied using the previously received symbols and the method described in this section. Then the Kalman filter method estimates new filter weights, while the LMS algorithm keeps track of the slight changes of the channel.

Next, the four outputs of the estimators are combined spatially as described in Section 3. For the correction of the possible Doppler shift, a Doppler shift correction mechanism followed by a first order PLL was used. The Doppler shift correction mechanism is presented in Chapter V (Equations 5.49 to 5.51). The final received data plot is illustrated in Figure 57. The performance of the receiver is very good; the final MSE for the second repetition case is reduced to 0.015.

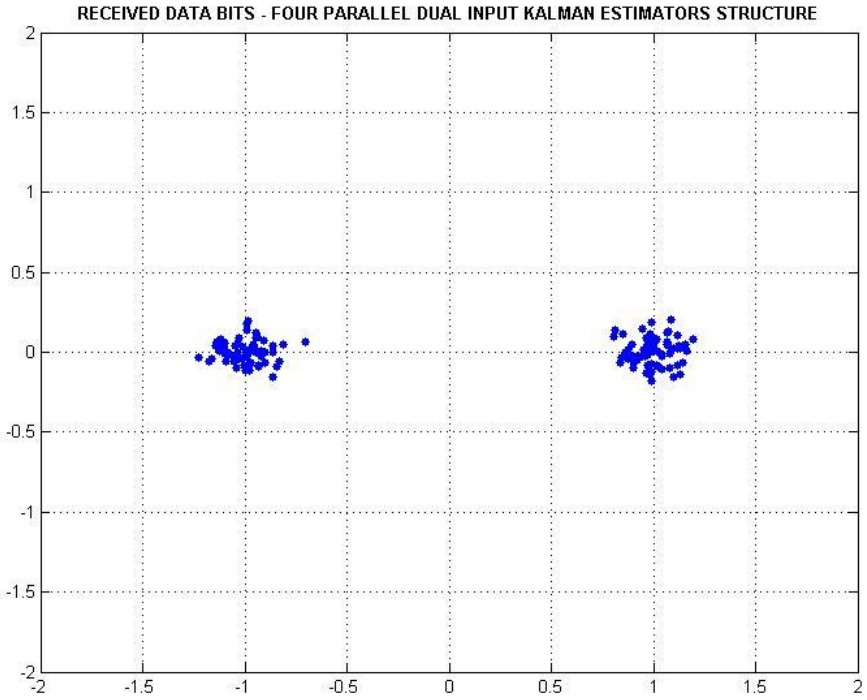

Figure 57. Second repetition. Received data bits. Four parallel Kalman estimators

A comparison of this scheme, based on Kalman Filter, with the spatial combiner shown in Section 3 (without Kalman Filter) shows an improvement of about 1.7 dB in the mean square error. More importantly, the scheme with the Kalman Filter processes multiple returns, and thus is expected to be more robust in the presence of multipath propagation.

An issue to be addressed in the next section is the performance in the presence of a Doppler shift.

5. Dual Processing Level Kalman Estimator Scheme

In this section, an alternative estimation scheme is proposed with the purpose of providing the best estimate for the data together with the Doppler shift, if present. In particular, the data is preprocessed from the hydrophones by

estimating at least two dominant subspaces with the strongest energy and then applying the Kalman Filtering technique already described.

There are two advantages with this approach, fully supported by processing of the data in the Makai experiment. One is the data reduction and the use of data with the highest SNR. The other advantage is that the tracking of the dominant singular vectors yield the information on the Doppler shift by comparing two subsequent estimates in a running window. An illustration of the configuration is presented in Figure 58.

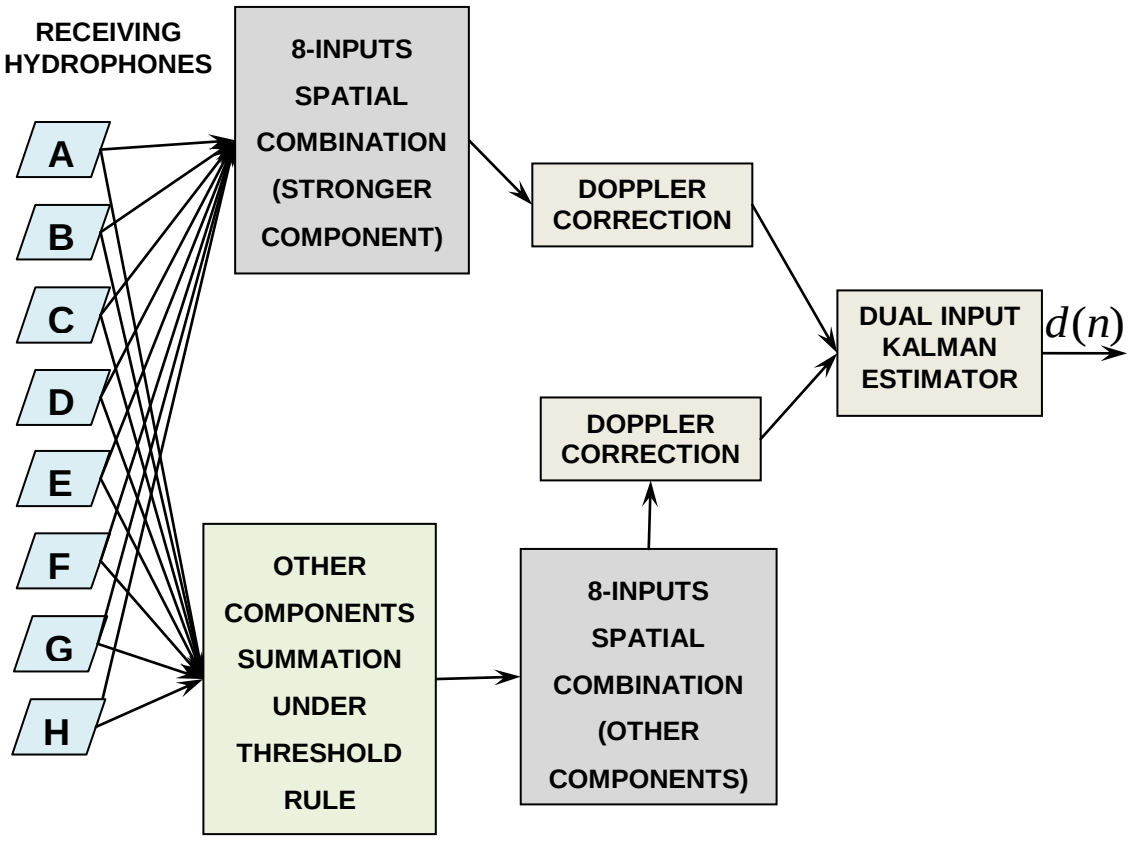

Figure 58. Dual Kalman estimator with Doppler shift correction configuration

The Kalman Filter presented is based on a mathematical model of the channel which reflects the time-varying nature due to Doppler shift. In particular,

let $y[n]$ be the complex vector of data received by the hydrophones (eight in this case), after dispreading. It can be represented in terms of a time-varying linear system as:

$$y[n] = h[n,0]d[n] + ... + h[n,N]d[n-N] + w[n] \tag{6.12}$$

Assuming the Doppler shift constant within the length of a few data bits, in Equation 6.12, the impulse response terms $h[n,k]$ have the form:

$$h[n,k] \cong h[n-1,k]e^{-j\theta_d} \tag{6.13}$$

with θ_d accounting for the Doppler shift.

By taking a running window of the data as

$$Y[n] = \; y[n-L+1], \quad \cdots \quad y[n] \tag{6.14}$$

with *L* sufficiently large within the time coherence of the channel, its singular value decomposition (SVD) can be recursively determined as

$$Y[n] = U[n]S[n]V^{*T}[n] \tag{6.15}$$

with $S[n]$ a diagonal matrix with positive entries $\sigma_1[n] \geq \sigma_2[n] \geq ... \geq 0$ and $U[n] = \left[\underline{u}_1[n], \quad \cdots, \quad \underline{u}_L[n]\right]$.

The dominant vectors can be considered almost constant apart from the Doppler shift. Then, for small *M,* two corresponding singular vectors can be related as

$$\underline{u}_\ell[n] \simeq \underline{u}_\ell[n-M]e^{jM\theta_d} \tag{6.16}$$

In order to design a Kalman estimator robust to Doppler effects, a different structure has been proposed. In this structure (see Figure 60), the strongest reception in all eight hydrophones can be detected and an 8x1 vector created of each of the strongest receptions. Next, in a way similar to Section 3, the autocorrelation matrices are formed for each set of receptions and singular value decomposition is applied to estimate eigenvectors and eigenvalues of the covariance matrix. This is done over a sequence of sliding overlapping windows. In the experimental data there are 144 transmitted data samples and a window length of 30 samples is used, with 24 samples overlapping.

Based on this consideration, two singular values can be compared as

$$C = \underline{u_1}[n]\underline{u_1}^{*T}[n-M] \tag{6.17}$$

This coefficient *C* can be used to assess the accuracy of the modeling assumption and the consistency of the received data. In the case of strong receptions with constant multipath propagation, the only difference between two subsequent receptions is the Doppler shift. In this case (6.16) holds and

$$|C| \cong 1 \tag{6.18}$$

In different cases with less consistent channel and time-varying multipath propagation, coefficient *C* is such that

$$|C| < 1 \tag{6.19}$$

For example, Figure 59 shows the correlation coefficient $|C|$ between the strongest reception and other receptions. The second, third and fourth receptions yield a coefficient $|C| \approx 1$, thus showing consistency, while the fifth reception yields |C|<0.8, less consistent.

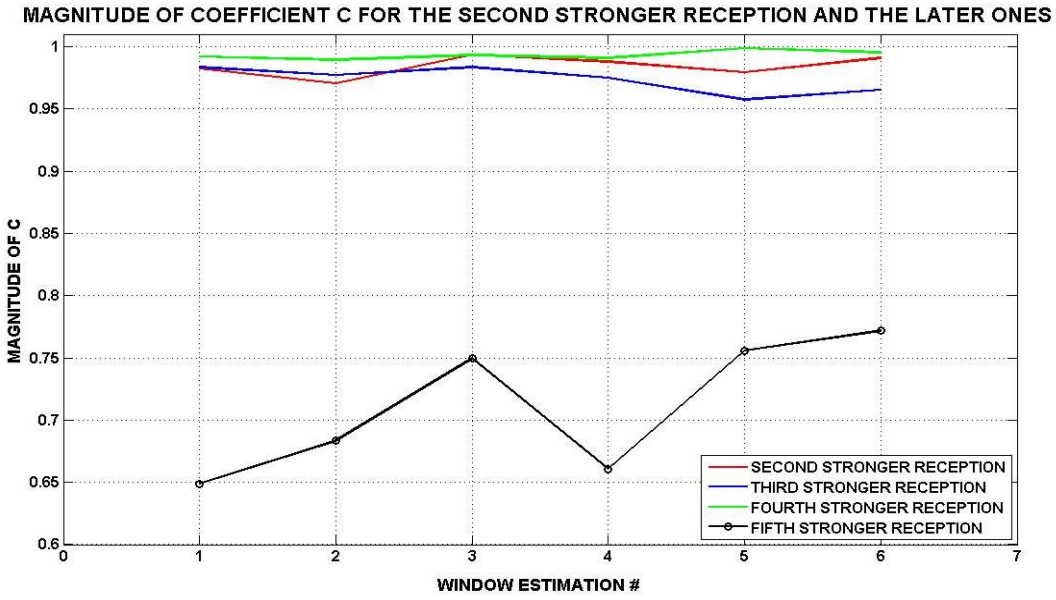

Figure 59. Magnitude of coefficient C for the second, third, fourth and fifth strongest receptions

Based on the above argument, the two inputs of the equalizer are defined on the basis of channel consistency by choosing the components with the largest coefficient *C.* In particular, the dominant component can be chosen as $\underline{y}_1[n]$ and the other component as a combination of other consistent components as

$$\underline{y}_2[n] = \underline{y}_{2nd}[n] + \underline{y}_{3rd}[n] + \ldots, \quad \text{under the rule: } |C| > 0.95 \tag{6.20}$$

Finally, in the case of consistent channel, the Doppler shift can also be estimated on the basis of the coefficient *C* as

$$phase\ C = M\theta_d \tag{6.21}$$

where θ_d is the Doppler phase shift in the channel. Based on this knowledge of θ_d, the Doppler shifts are corrected from the two inputs before being processed by the Kalman estimator.

As in Section 4, the assumption is known the first 16 of the total 144 symbols sent and, based on this knowledge, an initial estimate of the two impulse responses is acquired. The dual input Kalman estimator is capable to compensate for a coarse estimate of the Doppler shift. Therefore, it must be followed by a first order PLL for correcting the remaining Doppler shift and refining the result.

The final received data plot is illustrated in Figure 60. The performance of the receiver is very good; the final MSE for the second repetition case is 0.008. The enhancement in the performance (MSE is ~2.7 dB smaller), compared to the structure of Section 4, is due to the correction of the Doppler shift “before” the signal enters the equalizer scheme. Under more severe conditions of Doppler effect, the enhancement in the performance will be even greater, or even the structure of Section 4 could fail.

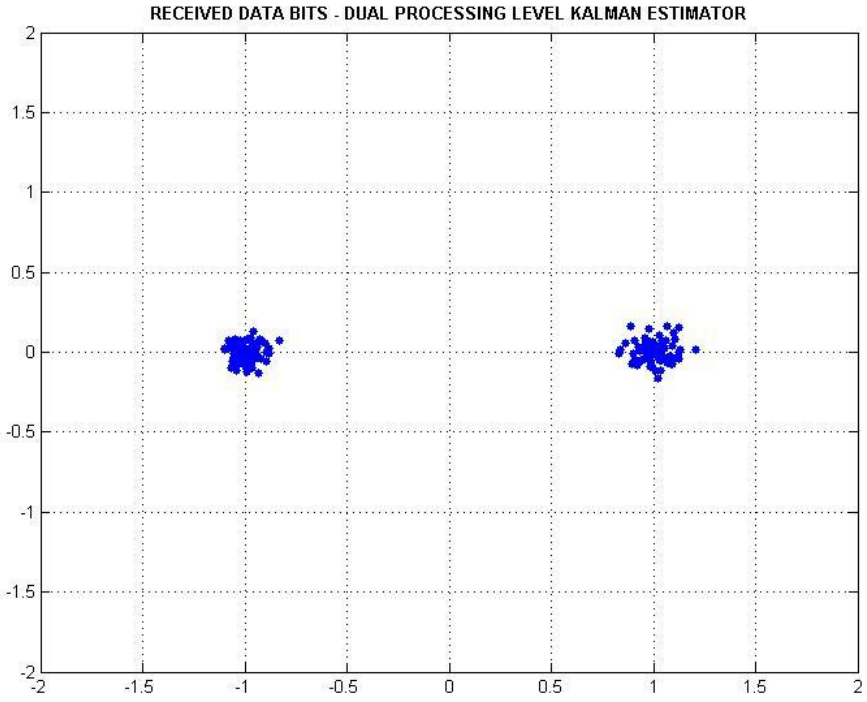

Figure 60. Second repetition. Received data bits. Dual process level Kalman estimator (without interference canceller)

The proposed scheme seems to be robust in the presence of both multipath effect and Doppler shift due to relative motion between the transmitter and receiver.

In what follows, a scheme is proposed to compensate for external interference at the received signal, after the channel has been estimated. It is shown that with a good estimate of the channel model, a signal correlated to the interference can be computed, which can be used in a noise cancelling adaptive scheme.

6. Dual Processing Level Kalman Estimator With Interference Canceller

In order to design a Kalman estimator robust to external interferences, a noise and interference cancellation algorithm was developed suitable to the acoustic channel. The core and the structure of the Section 5 receiver were kept the same, while the cancellation algorithm was introduced to operate in parallel with the adaptive Kalman estimator. The theoretical background of the canceller has not been analyzed in previous chapters and will be developed next.

a. Interference Cancelation Algorithm

Consider a single input multiple output transmitter–receiver scheme, where for simplicity only two received signals are assumed. From Equation 5.32, for $N=2$ the received signals $y_1[n], y_2[n]$ can be written in the standard convolution forms with additive disturbances $w_1[n], w_2[n]$.

$$\begin{aligned} y_1[n] &= h_1[n] * x[n] + w_1[n] \\ y_2[n] &= h_2[n] * x[n] + w_2[n] \end{aligned} \tag{6.22}$$

Assuming that the two channels' impulse responses $h_1[n], h_2[n]$ have been estimated (say by training data) define the sequence $\phi[n]$ as

$$\phi[n] = h_2[n] * y_1[n] - h_1[n] * y_2[n] \tag{6.23}$$

By simple use of linearity, this sequence, under perfect channel estimation, is strongly correlated to the disturbances and uncorrelated to the transmitted signal. In fact, it can be seen that

$$\phi[n] = h_2[n] * w_1[n] - h_1[n] * w_2[n] \tag{6.24}$$

When the disturbance is correlated in time, so that it is predictable, the signal $\phi[n]$ can be used for noise or interference cancellation.

This can be combined within the Kalman Filter estimator with an additional set of gains $Q(z) = q_0 + q_1 z^{-1} + ... + q_M z^{-M}$ as

$$\hat{X}[z] = \underbrace{\left\{ \frac{J_1(z)}{V(z)} Y_1(z) + \frac{J_2(z)}{V(z)} Y_2(z) \right\}}_{\text{MESSAGE AND DISTURBANCE}} + Q(z) \underbrace{\left(\frac{H_2(z)}{V(z)} Y_1(z) - \frac{H_1(z)}{V(z)} Y_2(z) \right)}_{\text{DISTURBANCE ONLY}} \qquad (6.25)$$

where the terms $J_1(z), J_2(z)$ have been introduced in Paragraph B of Chapter V.

The first term of Equation 6.25 is the relation used in the equalizer to recover the transmitted data. It contains the signal, noise and interference from other users. The second term, as proved earlier, contains only disturbance and in the ideal case of zero noise and zero disturbance, it will be zero. The term $Q(z)$ can be determined on the basis of an adaptive LMS to minimize the mean square value of $\hat{x}[n]$. Provided good estimates of the channels $h_1[n], h_2[n]$ are available and the disturbances $w_1[n], w_2[n]$ are uncorrelated with the transmitted data $x[n]$, the term $Q(z)$ can be set, recursively, by minimizing $E\left|\hat{x}[z]\right|^2$.

b. Experimental Results of the Disturbance Cancelling Method

The result of the data estimation for the dual processing level Kalman estimator with interference canceller is illustrated on the plot of Figure 61. The performance of the receiver is very satisfactory; the final MSE for the second repetition case is 0.006. In the experimental setup, there was no external interference. The improvement observed is related to noise cancellation. This improvement in the performance (MSE is ~1.3 dB smaller) compared to the result of the structure of Section 5 is very small, but under a heavy interference environment this improvement can be much greater.

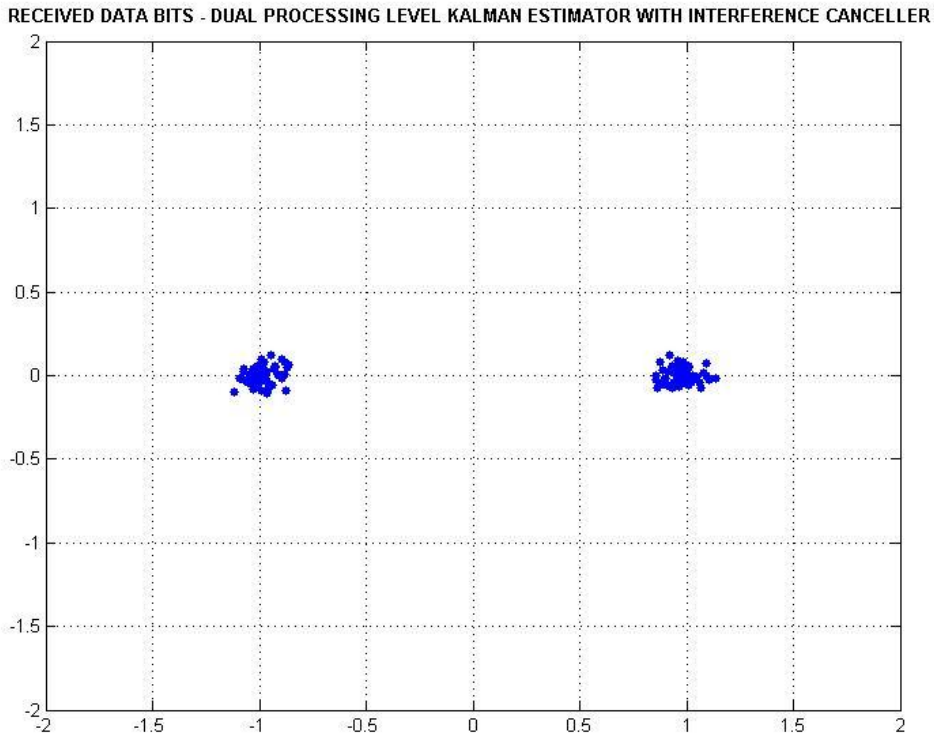

Figure 61. Second repetition. Received data bits. Dual process level Kalman estimator with interference canceller

c. Sinusoidal Interference Simulation

Using the experimental data from the MAKAI 2005 experiment, a simulation was created to evaluate the performance of the interference cancelation algorithm. In order to calculate the effectiveness of the algorithm, artificial sinusoidal interferences were added in the communication channels and the mean squared errors were estimated for the two different cases, with and without interference cancellation, as a function of signal to interference ratio.

The resulting mean squared errors for the two cases are illustrated in Figure 62. There is a large improvement in the performance of the receiver, even in the presence of a higher level of interference.

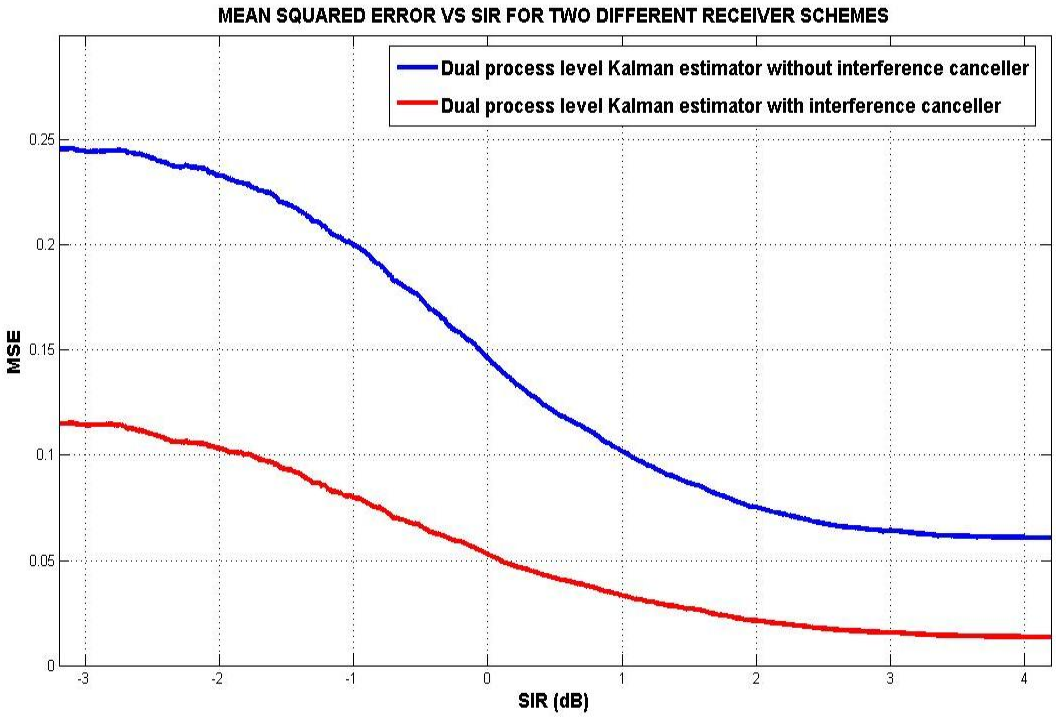

Figure 62. Mean squared error vs. SIR for two different Receiver schemes

THIS PAGE INTENTIONALLY LEFT BLANK

VII. CONCLUSIONS

A. SUMMARY AND CONTRIBUTIONS

In this dissertation, an innovative receiver has been introduced for usage in the underwater environment. The major design goal is the receiver's robustness on a Doppler distorted, fast-varying, multipath-fading channel, for applications in multiuser environments. Another important design goal is the necessity of relatively low complexity in signal processing.

The goal of the proposed receiver is to be able to adapt to acoustic channel variations; therefore, a robust mechanism for channel identification was developed. The proposed candidate receiver structures were developed and tested on simulations and on experimental data.

The final receiver scheme is based on an array of hydrophones and a direct sequence code division multiple access technique in order to support multiuser communications (e.g., control of autonomous underwater vehicles). It uses a robust signal acquisition method, which reduces the effects of the multipath and Doppler phase shifts, together with a spatial combiner and adaptive equalization. Furthermore, an interference cancellation can be added as an adaptive LMS once the channel from the intended receiver has been estimated. The receiver has been tested with a wide range of actual data collected from a number of experiments around the world.

A feature that distinguishes the proposed approach is the state space formulation of the MIMO receiver. In the case of multiple receivers through diverse multipath propagation channels, the transmitted signal can be regarded as the state of a dynamic system. In this system the array of received signals is partitioned into "inputs" and "outputs," not in the usual dynamic system approach of cause and effect, but in the estimation framework of "predictors" and "correctors." In this light, the signal can be estimated by a standard Kalman Filter, which has a well-known degree of optimality.

To summarize, the contributions in this dissertation are as follows:

- We have reformulated the MIMO receiver problem as a state estimation problem. In the presence of receiver diversity, the transmitted sequence can be viewed as part of the "state" of a dynamic system whose inputs and outputs are the received signals. This "state" was estimated by a Kalman filter-like structure, whereas the recursive nature of the Kalman filter allowed the inclusion of a decision feedback.
- We have developed an algorithm for optimal MIMO estimation using Kalman Filtering.
- We have tested the innovative algorithm on real data and gotten satisfactory results.
- We inserted a method to dynamically estimate and correct the Doppler shift, thus reducing bit error probability.
- By use of the proposed algorithm on real experimental data, we have shown improvement in the mean squared error estimate.
- We have extended the algorithm for interference cancellation for use in a multiuser underwater environment. Also, we have tested the effectiveness of the interference cancellation algorithm on simulations and on real data.

B. FURTHER WORK

The state space model approach of the MIMO receiver opens itself to a wide variety of approaches for receiver design. The standard Kalman Filter is well-known to be optimal in the case of Gaussian noise and linear models; however, its performance degrades when some of these assumptions are not valid, as in most real world applications.

A number of extensions of the Kalman Filter have been recently developed to accommodate issues of non-Gaussian noise and nonlinear models. The state space formulation proposed in this dissertation lends itself to any of these formulations, including more general models for noise and channel propagation characteristics. Therefore, an issue to be investigated will be the replacement of the standard Kalman filter approach by an extension more suitable to the underwater acoustic environment.

Finally, issues in the implementation must be addressed. A number of extensive simulations must be performed to investigate what the improvement is in data rates for various realistic acoustic channels. A number of new experiments should then take place in order to validate the findings of the simulations using real data.

THIS PAGE INTENTIONALLY LEFT BLANK

LIST OF REFERENCES

[1] J. Rice, D. Green, “Underwater Acoustic Communications and Networks for the US Navy’s Seaweb Program,” *SENSORCOMM 08*, Vol. 1, pp. 71–-722, August 2008.

[2] M. Stojanovic, J. Preisig, “Underwater acoustic communication channels: Propagation models and statistical characterization,” *IEEE Communications Magazine*, pp. 84–89, January 2009.

[3] J. F. Pieper, J. G. Proakis, R. R. Reed, J. K. Wolf, “Design of Efficient Coding and modulation for a Rayleigh Fading Channel,” *IEEE transactions of Information theory,* Vol. IT-24, No 4, pp. 457–468, July 1978.

[4] A. R. Baggeroer, “Acoustic Telemetry – An Overview,” *IEEE Journal of Oceanic Engineering*, Vol. OE-9, No 4, pp. 229–235, October 1984.

[5] S. D. Morgera, “Multiple Terminal Acoustic Communications System Design,” *IEEE Journal of Oceanic Engineering*, Vol. OE-5, No 3, pp. 199–204, July 1980.

[6] D. J. Garood, “Applications of the MFSK Acoustical Communications System,” *Proceedings Oceans 81*, Vol. 13, pp. 67–71, September 1981.

[7] A. B. Baggeroer, D. E. Koelsch, K. von der Heydt, J. Catipovic, “DATS – A Digital Acoustic Telemetry System for Underwater Communications,” *Proceedings Oceans 81*, Vol. 13, pp. 55–60, September 1981.

[8] J. Catipovic, A. B. Baggeroer, K. von der Heydt, D. Koelsch, “Design and Performance Analysis of a Digital Acoustic Telemetry System for the Short Range Underwater Channel,” *IEEE Journal of Oceanic Engineering*, Vol. OE-9, No 4, pp. 242–252, October 1984.

[9] D. B. Kilfoyle, A. B. Baggeroer, “The State of the Art in Underwater Acoustic Telemetry,” *IEEE Journal of Oceanic Engineering*, Vol. 25, No 1, pp. 4-27, January 2000.

[10] F. C. Jarvis, “Description of a Secure Reliable Acoustic System for Use in Offshore Oil Blowout Preventer (BOP) or Wellhead Control,” *IEEE Journal of Oceanic Engineering*, Vol. OE-9, No 4, pp. 253–258, October 1984.

[11] R. F. W. Coates, “A Deep-Ocean Penetrator Telemetry System,” *IEEE Journal of Oceanic Engineering*, Vol. 13, No 2, pp. 55–63, April 1988.

[12] M. Stojanovic, “Recent Advances in High-Speed Underwater Acoustic Communications,” *IEEE Journal of Oceanic Engineering*, Vol. 21, No 2, pp. 125–136, April 1996.

[13] J. Catipovic, M. Deffenbaugh, L. Freitag, D. Frye, “An Acoustic Telemetry System for Deep Ocean Mooring Data Acquisition and Control,” *Proceedings Oceans 89*, pp.887–892, October 1989.

[14] J. A. Catipovic, “High Data Rate Acoustic Telemetry for Moving ROVS in a Fading Multipath Shallow Water Environment,” *Proceedings of AUV 90*, pp. 296–303, June 1990.

[15] L. E. Freitag, J. Stevens Merriam, D. E. Frye, J. A. Catipovic, “A Long-Term Deep Water Acoustic Telemetry Experiment,” *Proceedings Oceans 91,* Vol. 1, pp. 254–260, October 1991.

[16] G. R. Mackelburg, “Acoustic Data Links for UUVs,” *Proceedings Oceans 91*, Vol. 1, pp. 1400–1406, October 1991.

[17] S. Coatelan, A. Glavieux, “Design and Test of a Multicarrier Transmission System on the Shallow Water Acoustic Channel,” *Proceedings Oceans 94*, Vol. 3, pp. 472–477, September 1994.

[18] K. F. Scussel, J. A. Rice, S. Merriam, “A New MFSK Acoustic Modem for Operation in Adverse Underwater Channels,” *Proceedings Oceans 97*, Vol. 2, pp. 247–254, October 1997.

[19] M. D. Green, J. A. Rice, “Error Correction Coding for Communications in Adverse Underwater Channels,” *Proceedings Oceans 97*, Vol. 2, pp. 854–861, October 1997.

[20] J. G. Proakis, “Coded Modulation for Digital Communications Over Rayleigh Fading Channels,” *IEEE Journal of Oceanic Engineering*, Vol. 16, No 1, pp. 66–73, January 1991.

[21] M. D. Green, J. A. Rice, “Channel-Tolerant FH-MFSK Acoustic Signaling for Undersea Communications and Networks,” *IEEE Journal of Oceanic Engineering*, Vol. 25, No 1, pp. 28–39, January 2000.

[22] J. G. Proakis, *Digital Communications*, fourth edition, McGraw-Hill, New York, 2001.

[23] G. R. Mackelburg, S. J. Watson, A. Gordon, “BENTHIC 4800 Bits/s Acoustic Telemetry,” *Proceedings Oceans 81*, Vol. 13, pp. 72, September 1981.

[24] L. O. Olson, J. L. Backes, J. B. Miller, “Communication, Control, and Data Acquisition Systems on the ISHTE Lander,” *IEEE Journal of Oceanic Engineering*, Vol. OE-10, No 1, pp. 5–16, January 1985.

[25] A. Kaya, S. Yauchi, “An Acoustic Communication System for Subsea Robot,” *Proceedings Oceans 89*, Vol. 3, pp. 765–770, September 1989.

[26] M. Suzuki, T. Sasaki, T. Tsuchiya, “Digital Acoustic Image Transmission System for Deep-Sea Research Submersible,” *Proceedings Oceans 92*, Vol. 2, pp. 567-570, October 1992.

[27] G. Ayela, J. M. Coudeville, “TIVA: A Long Range, High Baud Rate Image/Data Acoustic Transmission System for Underwater Applications,” *presented at Underwater Defense Technology conference*, Paris, France, 1991.

[28] G. S. Howe, O. R. Hinton, A. E. Adams, A. G. J. Holt, “Acoustic Burst Transmission of High Rate Data Through Shallow Underwater Channels,” *IEEE electronic letters*, Vol. 28, No 5, pp. 449–451, February 1992.

[29] J. H. Fisher, K. R. Bennett, S. A. Reible, J. H. Cafarella, I. Yao, “A High Data Rate Underwater Acoustic Data-Communications transceiver,” *Proceedings Oceans 92*, Vol. 2, pp. 571–576, October 1992.

[30] J. G. Proakis, “Adaptive Equalization Techniques for Acoustic Telemetry Channels,” *IEEE Journal of Oceanic Engineering*, Vol. 16, No 1, pp. 21–31, January 1991.

[31] M. Stojanovic, J. Catipovic, J. G. Proakis, “Adaptive Multichannel Combining and Equalization for Underwater Acoustic Communications,” *Journal of Acoustical Society of America*, Vol. 94, issue 3, pp. 1621–1631, September 1993.

[32] M. Stojanovic, J. Catipovic, J. G. Proakis, “Phase-Coherent Digital Communications for Underwater Acoustic Channels,” *IEEE Journal of Oceanic Engineering*, Vol. 19, No 1, pp. 100–111, January 1994.

[33] M. Stojanovic, J. G. Proakis, J. Catipovic, “Performance of High Data Rate Adaptive Equalization on A Shallow Water acoustic Channel,” *Journal of Acoustical Society of America*, Vol. 95, issue 5, pp. 2809–2810, 1994.

[34] A. Goalic, J. Labat, J. Trubuil, S. Saoudi, D. Rioualen, “Toward a Digital Acoustic Underwater Phone,” *Proceedings Oceans 94*, Vol. 3, pp. 489–494, September 1994.

[35] J. Labat, “Real Time Underwater Communications,” *Proceedings Oceans 94*, Vol. 3, pp. 501–506, September 1994.

[36] P. S. D. Tarbit, G.S. Howe, O. R. Hinton, A. E. Adams, B. S. Sharif, “Development of a Real-Time Adaptive equalizer for a High-Rate Underwater Acoustic Data Communications Link,” *Proceedings Oceans 94*, Vol. 1, pp. 307–312, September 1994.

[37] V. Capellano, G. Loubet, G. Jourdain, “Adaptive Multichannel Equalizer for Underwater Communications,” *MTS/IEEE Proceedings Oceans 96*, Vol. 2, pp. 994–999, September 1996.

[38] S. M. Jarvis, N. A. Pendergrass, “Implementation of a Multichannel Decision Feedback Equalizer for Shallow Water Acoustic Telemetry Using a Stabilized Fast Transversal Filters Algorithm,” *MTS/IEEE Proceedings Oceans 95,* Vol. 2, pp. 787–796, October 1995.

[39] S. Jarvis, R. Janiesch, K. Fitzpatrick, R. Morrissey, “Results from Recent Sea Trials of the Underwater Digital Acoustic Telemetry System,” *MTS/IEEE Proceedings Oceans 97*, Vol. 1, pp. 702–708, October 1997.

[40] T. H. Eggen, “Underwater Acoustic Communication Over Doppler Spread Channels,” Ph.D. dissertation, MIT/WHOI, Boston, Massachusetts, June 1997.

[41] M. Johnson, L. Freitag, M. Stojanovic, “Improved Doppler Tracking and Correction for Underwater Acoustic Communication,” *presented at the ICASSP 97*, Munich, Germany, 1997.

[42] M. Johnson, D. Brady, M. Grund, “Reducing the Computational Requirements of Adaptive Equalization in Underwater Acoustic Communications,” *MTS/IEEE Proceedings Oceans 95*, Vol. 3, pp. 1405–1410, October 1995.

[43] M. Kocic, D. Brady, M. Stojanovic, “Sparse Equalization for Real-Time Digital Underwater Acoustic Communications,” *MTS/IEEE Proceedings Oceans 95*, Vol. 3, pp. 1417–1422, October 1995.

[44] J. Gomes, V. Barroso, “Blind Equalization Using a Radial basis Function Neural Network,” *MTS/IEEE Oceans 95 Conference*, Vol. 2, pp. 797–802, October 1995.

[45] J. Labat, O. Macchi, C. Laot, “Adaptive Decision Feedback Equalization: Can You Skip the Training Period?,” *IEEE Transactions on Communications*, Vol. 46, No 7, pp. 921–930, July 1998

[46] J. Labat, J. Trubuil, M. Nicot, “Blind Decision Feedback Equalization Application to Underwater Communication Systems,” *Proceedings Oceans 98,* Vol. 2, pp. 805–809, September 1998.

[47] J. Labat, C. Laot, “Blind Adaptive Multiple-Input Decision-Feedback Equalizer with Self-Optimized Configuration,” *IEEE Transactions on Communications*, Vol. 49, No 4, pp. 646–654, April 2001.

[48] R. Weber, A. Waldhorst, F. Schulz, J. F. Bohme, “Blind Receivers for MSK Signals Transmitted Through Shallow Water,” *MTS/IEEE Oceans '01 Conference*, Vol. 4, pp. 2183–2190, November 2001.

[49] T. C. Yang, “A study of multiplicity and diversity in MIMO underwater acoustic communications,” Conference Record of the Forty-Third *Asilomar Conference on Signals Systems and Computers*, Vol. 1,pp. 595–599, November 2009.

[50] D. B. Kilfoyle, J. C. Preisig, A. B. Baggeroer, “Spatial modulation experiments in the underwater acoustic channel,” *IEEE Journal of oceanic engineering,* Vol. 30, No 2, pp. 406–415, April 2005.

[51] M. Chitre, S. Shahabudeen, L. Freitag, M. Stojanovic, “Recent advances in underwater acoustic communications & networking,” *Proceedings Oceans 2008*, Vol. 2008 supplement, pp. 1–10, October 2008.

[52] H. C. Song, P. Roux, W. S. Hodgkiss, W. A. Kuperman, T. Akal, M. Stevenson, “Multiple-input multiple-output coherent time reversal communications in a shallow water acoustic channel,” *IEEE Journal of oceanic engineering,* Vol. 31, No1, pp. 170–178, January 2006.

[53] A. Song, M. Badiey, H. C. Song, W. S. Hodgkiss, M. B. Porter, and KauaiEx-Group, "Impact of ocean variability on coherent underwater acoustic communications during the Kauai experiment (KauaiEx)," *The Journal of the Acoustical Society of America*, Vol. 123, pp. 856–865, February 2008.

[54] E. M. Sozer, J. G. Proakis, M. Stojanovic, J. A. Rice, A. Benson, M. Hatch, “Direct Sequence Spread Spectrum Based Modem for Underwater Acoustic Communication and Channel Measurements,” *MTS/IEEE Proceedings Oceans 99*, Vol. 1, pp. 228–233, September 1999.

[55] M. Stojanovic, L. Freitag, “Hypothesis-Feedback Equalization for Direct-Sequence Spread-Spectrum Underwater Communications,” *MTS/IEEE Proceedings Oceans 2000*, Vol. 1, pp. 123–128, September 2000.

[56] F. Blackmon, E. Sozer, M. Stojanovic and J. Proakis, “Performance Comparison of RAKE and Hypothesis Feedback Direct Spread Spectrum Techniques for Underwater Communications Applications,” *MTS/IEEE Oceans '02 Conference*, Vol. 1, pp. 594–603, October 2002.

[57] J. E. Hakegard, K. Grythe, “Effects of channel estimation errors in OFDM-MIMO based underwater communications,” *International Conference on Advanced Information Networking and Applications Workshops (WAINA '09),* Vol. 1, pp. 1130–1135, May 2009.

[58] M. Stojanovic, “MIMO OFDM over underwater acoustic channels,” *Conference Record of the Forty-Third Asilomar Conference on Signals Systems and Computers*, Vol. 1,pp. 605–609, November 2009.

[59] L. E. Kinsler, A. R. Frey, A. B. Coppens and J. V. Sanders, *Fundamendals of Acoustics*, fourth edition, John Wiley & Sons, New York, 2000.

[60] F. B. Jensen, W. A. Kuperman and M. B. Porter, H. Schmidt, *Computational Ocean Acoustics*, first edition, Springer-Verlag, New York, 2000.

[61] J. T. Hansen, “Link Budget Analysis for Undersea Acoustic Signaling,” M.S. Thesis, Naval Postgraduate School, Monterey, California, 2002.

[62] P. Duke, “Direct-sequence spread-spectrum modulation for utility packet transmission in underwater acoustic communication networks,” M.S. Thesis, Naval Postgraduate School, Monterey, California, 2002.

[63] R. S. Kennedy, *Fading Dispersive Communications Channels*, first edition, Wiley-Interscience, New York, 1969.

[64] J. A. Rice, “Acoustic Signal Dispersion and Distortion by Shallow Undersea Transmission Channels,” *High Frequency Acoustics in Shallow Water*, Lerici, Italy, 1997.

[65] T. S. Rappaport, *Wireless Communications—Principles and Practice*, second edition, Prentice Hall, New Jersey, 2002.

[66] M. Siderius, M. B. Porter and V. K. McDonald, “Experiments Study Underwater Acoustic Communications,” *Sea Technology*, Vol. 45, Issue 5, pp. 42–47, May 2004.

[67] M. Stojanovic, “Underwater Acoustic Communications: Design Considerations on the Physical Layer,” *Fifth Annual Conference on Wireless on Demand Network Systems and Services*, pp. 1–10, January 2008.

[68] L. Freitag, M. Stojanovic, “MMSE acquisition of DSSS acoustic communications signals,” *Proceedings IEEE Oceans 04*, Vol. 1, pp. 14–19, November 2004.

[69] E. M. Sozer, “Reliable Communications over Frequency-Selective Rapidly Fading Channels,” Ph.D. dissertation, Northeastern University, Boston, Massachusetts, May 2003.

[70] R. L. Peterson, R. E. Ziemer and D. E. Borth, *Introduction to Spread Spectrum Communications*, first edition, Prentice Hall, New Jersey, 1995.

[71] K. Karkkainen, Optimized PN Sequences Available for Simulation of CDMA Systems, [Online], Available: http://www.ee.oulu.fi/~kk/, last accessed February 2010.

[72] D. Green and J. Rice, “Synthetic Undersea Acoustic Transmission Channels,” *High Frequency Ocean Acoustics*, pp. 73–81, September 2004.

[73] O. B. Wilson, *Introduction to theory and design of Sonar transducers,* first edition, Peninsula Publishing, Los Altos, 1988.

[74] M. B. Porter, V. K. McDonald, P. A. Baxley and J. A. Rice, “SignalEx: Linking Environmental Acoustics with the Signaling Schemes,” *OCEANS 2000 MTS/IEEE Conference and Exhibition*, Vol. 1,pp. 595–600, September 2000.

[75] P. Hursky, M. B. Porter and M. Siderius, “High-frequency (8-16 KHZ) Model-based Source Localization,” *Journal of the Acoustical Society of America,* Vol. 115, issue 6, pp. 3021–3032, 2004.

[76] SignalEx Web site, [Online], Available: http://hlsresearch.com/signalex (password protected), last accessed July 2009.

[77] BELLHOP ray/beam model web site, [Online], Available: http://www.hlsresearch.com/oalib/ Modes/AcousticsToolbox/ manual_html/node60.html, last accessed July 2009.

[78] Delphi Communication Systems, “Underwater Acoustic Communications Channel and Network Optimization,*”* Maynard, Technical Report, 1999–2000.

[79] M. Stojanovic, J. G. Proakis, James B. Bowlin and J. A. Catipovic, “Performance of a high-rate communication link on a shallow water acoustic channel,” *Journal of the Acoustical Society of America*, Vol. 95, Issue 5, pp. 2809–2810, 1994.

[80] F. Blackmon, E. Sozer and J. Proakis, “Iterative Equalization, Decoding, and Soft Diversity Combining for Underwater Acoustic Channels,” *MTS/IEEE Oceans '02 Conference*, Vol. 4,pp. 2425–2428, October 2002.

[81] A. Song, M. Badiey, “Ocean Variability Effects on Underwater Acoustic Communications,” ONR, Technical Report, pp. 1–8, 2009.

[82] A. Song, M. Badiey, V. K. McDonald, “Multichannel combining and equalization for underwater acoustic MIMO channels,” *Oceans 2008*, pp. 1–6, September 2008.

[83] M. Stojanovic, L. Freitag, “Multiuser undersea acoustic communications in the presence of multipath propagation,” *Proceedings Oceans 2001*, Vol. 1, pp 2165–2169, November 2001.

[84] M. Stojanovic, L. Freitag, “Multichannel detection for wideband underwater acoustic CDMA communications,” *IEEE Journal of Oceanic Engineering*, Vol. 31, No 3, pp. 685–695, July 2006.

[85] M. Stojanovic, L. Freitag, “Acquisition of direct sequence spread spectrum acoustic communication signals,” *Proceedings Oceans 2003*, Vol. 1, pp 279–286, September 2003.

[86] B. Sklar, *Digital Communications*, second edition, Prentice Hall, New Jersey, July 2003.

[87] M. Stojanovic, “Direct Sequence Spread Spectrum Packet Acquisition and Synchronization for Underwater Acoustic Modems,” Technical Report, September 2003.

[88] C. W. Therrien, *Discrete Random Signals and Statistical Signal Processing,* first edition, Prentice Hall, New Jersey, 1992.

[89] G. N. Pelekanos, **“**Performance of acoustic spread-spectrum signaling in simulated ocean channels,” M.S. Thesis, Naval Postgraduate School, Monterey, California, 2003.

[90] M. Abdulrahman, A.U.H. Sheikh, D.D. Falconer, “Decision feedback equalization for CDMA in indoor wireless communications,” *IEEE Journal on selected areas in communications,* Vol. 12, No 4, pp. 698–706, May 1994.

[91] M. Stojanovic, “An adaptive algorithm for differentially coherent detection in the presence of intersymbol interference,” *IEEE Journal on selected areas in communications,* Vol. 23, No 9, pp. 1884–1890, September 2005.

[92] L. Freitag, M. Stojanovic, S. Singh, M. Johnson, “Analysis of channel effects on Direct-Sequence and Frequency-hopped spread spectrum acoustic communication,” *IEEE journal of oceanic engineering*, Vol. 26, No 4, pp 586–593, October 2001.

[93] B. Geller, V. Capellano, J. Brossier, A. Essebbar, G. Jourdain, “Equalizer for video rate transmission in multipath underwater communications,” *IEEE journal of oceanic engineering*, Vol. 21, No 2, pp 150–155, April 1996.

[94] B. S. Sharif, J. Neasham, O. R. Hinton, A. E. Adams, J. Davies, “Adaptive Doppler compensation for coherent acoustic communication,” *IEEE proceedings Radar, Sonar, Navigation*, Vol. 147, No , pp 239–246, October 2000.

[95] L. Freitag, M. Grund, S. Singh, M. Johnson, “Acoustic communication in very shallow water: Results from the 1999 AUV fest,” *Proceedings Oceans 2000*, Vol. 3, pp 2155–2160, September 2000.

[96] R. Weber, F. Schulz, J. F. Bohme, “Blind adaptive equalization of underwater acoustic channels using second order statistics,” *Proceedings Oceans 2002*, Vol. 4, pp 2444–2452, October 2002.

[97] J. Labat, G. Lapierre, J. Trubuil, “Iterative equalization for underwater acoustic channels. Potentially for the TRIDENT system,” *Proceedings Oceans 2003*, Vol. 3, pp 1547–1553, September 2003.

[98] C. C. Tsimenidis, O. R. Sharif, O. R. Hinton, A. E. Adams, “Analysis and modeling of experimental doubly-spread shallow-water acoustic channels,” *Proceedings Oceans 2005 – Europe*, Vol. 2, pp 854–858, June 2005.

[99] A. Song, M. Badiey, “Generalized equalization for underwater acoustic communications,” *Proceedings Oceans 2005*, Vol. 2, pp 1522–1527, September 2005.

[100] T. C. Yang, “Correlation based decision feedback equalizer for underwater acoustic communications,” IEEE journal of oceanic engineering, Vol. 30, No 4, pp 865–880, October 2005.

[101] S. Roy, T. Duman, V. McDonald, J. G. Proakis, “High-rate communication for underwater acoustic channels using multiple transmitters and space-time coding: Receiver structures and experimental results,” *IEEE journal of oceanic engineering*, Vol. 32, No 3, pp. 663–688, July 2007.

[102] E. Calvo, M. Stojanovic, “Efficient channel estimation-based multiuser detection for underwater CDMA systems,” *IEEE journal of oceanic engineering*, Vol. 33, No4, pp 502–512, October 2008.

[103] S. Mason, S. Zhou, W. Yang, P. Gendron, “A comparative study of differential and noncoherent direct sequence spread spectrum over underwater acoustic channels with multiuser interference,” *Oceans 2008*, pp 1–5, September 2008.

[104] D. Johnson, S. R. Degraaf, “Improving the Resolution of Bearing in Passive Sonar Arrays by Eigenvalue Analysis,” *IEEE transactions on acoustics speech and signal processing*, Vol. ASSP-30, No 4, pp. 638–647, August 1982.

[105] M. J. Hinich, “Frequency-wavenumber array processing,” *Journal of Acoustical Society of America*, Vol. 69, No3, pp. 732–737, March 1981.

[106] M. Stojanovic, J. A. Catipovic, J. G. Proakis, “Reduced-complexity spatial and temporal processing of underwater acoustic communication signals,” *The Journal of the Acoustical Society of America*, Vol. 98, Issue 2, pp.961–972, August 1995.

[107] M. Stojanovic, Z. Zvonar, “Multichannel processing of broad-band multiuser communication signals in shallow water acoustic channels,” *IEEE Journal of Oceanic Engineering*, Vol. 21, No 2, pp. 156–166, April 1996.

THIS PAGE INTENTIONALLY LEFT BLANK

INITIAL DISTRIBUTION LIST

[1] Defense Technical Information Center
Ft. Belvoir, VA

[2] Dudley Knox Library
Naval Postgraduate School
Monterey, CA

[3] Roberto Cristi, PhD
Department of Electrical and Computer Engineering
Naval Postgraduate School
Monterey, CA

[4] Murali Tummala, PhD
Department of Electrical and Computer Engineering
Naval Postgraduate School
Monterey, CA

[5] Kevin Smith, PhD
Department of Physics
Naval Postgraduate School
Monterey, CA

[6] Steven Baker, PhD
Department of Physics
Naval Postgraduate School
Monterey, CA

[7] John Proakis, PhD
Department of Electrical and Computer Engineering
Northeastern University
Boston, MA

[8] Joseph Rice, MS
Department of Physics
Naval Postgraduate School
Monterey, CA

[9] Ralph Clark Robertson, PhD
Department of Electrical and Computer Engineering
Naval Postgraduate School
Monterey, CA

[10] Andres Larraza, PhD
Department of Physics
Naval Postgraduate School
Monterey, CA

[11] Naval Attaché
Embassy of Greece,
Washington, DC

[12] Spyridon Dessalermos
Markou Botsari 18
Lykovrisi, Attiki, 14123
Greece